SYNTHESIS, CHARACTERIZATION AND CATALYTIC ACTIVITY OF Al-Mg MIXED OXIDE CATALYSTS FOR BIODIESEL PRODUCTION

PANNAPAT CHOTMONGKOLSAP

A THESIS SUBMITTED IN PARTIAL FULFILLMENT OF THE REQUIREMENTS FOR
THE DEGREE OF MASTER OF SCIENCE
(APPLIED ANALYTICAL AND INORGANIC CHEMISTRY)
FACULTY OF GRADUATE STUDIES
MAHIDOL UNIVERSITY
2008

Thesis
entitled

SYNTHESIS, CHARACTERIZATION AND CATALYTIC ACTIVITY OF Al-Mg MIXED OXIDE CATALYSTS FOR BIODIESEL PRODUCTION

…….....
Mr. Pannapat Chotmongkolsap
Candidate

…….....
Lect. Jonnggol Tantirungrotechai,
Ph.D. (Chemistry)
Major-advisor

…….....
Asst. Prof. Ekasith Somsook,
Ph.D. (Chemistry)
Co-advisor

…….....
Asst. Prof. Laddawan Pdungsap,
Ph.D. (Inorganic Chemistry)
Co-advisor

……..
Prof. Banchong Mahaisavariya
M.D.
Dean
Faculty of Graduate Studies

…….....
Asst. Prof. Duanjai Nacapricha,
Ph.D. (Analytical Chemistry)
Chair
Master of Science Programme in Applied Analytical and Inorganic Chemistry
Faculty of Science

Thesis
entitled

SYNTHESIS AND CHARACTERIZATION OF Al-Mg MIXED OXIDE CATALYSTS FOR TRANSESTERIFICATION

was submitted to the Faculty of Graduate Studies, Mahidol University
for the degree of Master of Science
(Applied Analytical and Inorganic Chemistry)
on
May 29, 2008

…….....
Mr. Pannapat Chotmongkolsap
Candidate

…….
Asst. Prof. Ekasith Somsook,
Ph.D. (Chemistry)
Member

…….....
Asst. Prof. Piboon Pantu,
Ph.D. (Chemical Engineering)
Chair

……..
Asst. Prof. Laddawan Pdungsap,
Ph.D. (Inorganic Chemistry)
Member

…….....
Lect. Jonggol Tantirungrotechai,
Ph.D. (Chemistry)
Member

……..
Prof. Banchong Mahaisavariya
M.D.
Dean
Faculty of Graduate Studies
Mhidol University

…….....
Prof. Skorn Mongkolsuk,
Ph.D. (Biological Science)
Dean
Faculty of Science
Mahidol University

ACKNOWLEDGEMENTS

I would like to express my deepest faithful gratitude to my advisor, Dr. Jonggol Tantirungrotechai who has given me support, guidance, and encouragement throughout my graduate study. Sincere appreciation goes to the thesis examination committee members, Asst. Prof. Ekasith Soomsook, Asst. Prof. Laddawan Pdungsap, and Asst. Prof. Piboon Puntu for their guidance and valuable comments and suggestions.

I am also thankful to Chularat Wattanakit at Department of Chemitry, Faculty of Science, Kasetsart University for their assistance with N_2 adsorpton-desorption analyses; to Mananya Panyadhira and Pungpit Komprapun at the Central Instrument Facility, Research Division, Faculty of Science, Mahidol University for their assistance with TEM observation and DTA-TGA analyses; to Suttipornn Chaichana at Department of Chemitry, Faculty of Science, Mahidol University for their assistance with ^1H NMR analyses.

I would like to thank the Center of Innovation in Chemistry: Postgraduate Education and Research Program in Chemistry (PERCH-CIC) and The Thailand Research Fund (TRF) for scholarship and funding.

I will always cherish the many friends I have made during my time at Mahidol. My thanks also go to all the staff members of the Department of Chemistry for their generous help.

Last but not least, special thanks are expressed to my parents and my brother for their unending love, understanding, and encouragement. They have always believed in my ability which has inspired me to reach the goal.

Pannapat Chotmongkolsap

SYNTHESIS, CHARACTERIZATION AND CATALYTIC ACTIVITY OF Al-Mg MIXED OXIDE CATALYSTS FOR BIODIESEL PRODUCTION

PANNAPAT CHOTMONGKOLSAP 4836435 SCAI/M
M.Sc. (APPLIED ANALYTICAL AND INORGANIC CHEMISTRY)

THESIS ADVISORS: JONGGOL TANTIRUNGROTECHAI, Ph.D. (CHEMISTRY), EKASITH SOMSOOK, Ph.D. (CHEMISTRY), LADDAWAN PDUNGSAP, Ph.D. (INORGANIC CHEMISTRY)

ABSTRACT

The use of biodiesel has rapidly increased in recent years because it is renewable, non toxic, and biodegradable. Transesterification of vegetable oils with methanol using solid acids or solid bases as heterogeneous catalysts is a suitable method for biodiesel production since reaction temperature is low and the catalysts can be easily separated from the reaction mixture.

Both alumina (Al_2O_3) and magnesia (MgO) are commonly used in the chemical industry as catalysts, catalyst supports, and adsorbents. Since alumina is amphoteric while magnesia is basic, the Al-Mg mixed oxides are interesting as bifunctional acid-base catalysts. Moreover, porous materials are important for catalytic reaction because the diffusion property of these materials enhances interaction between the substrates and the surface of the materials due to higher surface area and greater accessibility of the pores. Cetyltrimethylammonium bromide (CTAB) is one of the structure-directing agents for synthesizing several porous materials. In this work, alumina, magnesia and Al-Mg mixed oxides were prepared from aluminum isopropoxide and magnesium nitrate in the presence of CTAB in an acidic media to compare their properties as catalysts. The oxide samples were also doped with KI or KNO_3 to increase the base strength. The synthesized materials were characterized by PXRD, IR, DTA-TGA, TEM, N_2 adsorption-desorption measurement, XRF, and acid-base strength measurement. All samples were tested for activities in transesterification of soybean oil with methanol at 80 ^{o}C. Percentage yields of fatty acid methyl ester (FAME) were characterized by ^{1}H NMR. The phases of the Al-Mg mixed oxides are the mixture of γ-Al_2O_3 and periclase (MgO) or the mixture of hydrotalcite ($Mg_6Al_2CO_3(OH)_{16}\cdot 4H_2O$) and periclase depending on the Al:Mg ratio. The Al-Mg mixed oxides have mesoporous structure with surface areas of 96-266 m^2g^{-1}. The calcined KI doped Al-Mg mixed oxide at Al:Mg ratio of 1:4 has base strength in the range of $9.8 \leq pK_{BH^+} \leq 15$ and has the highest catalytic activity in transesterification of approximately 90 % yield of FAME after 8 h. This suggest that of the catalyst tested the calcined KI doped Al-Mg mixed oxide at Al:Mg ratio of 1:4 is the most efficient catalyst for use in biodiesel production.

KEY WORDS: MESOPOROUS METERIAL/ HETEROGENEOUS CATALYST/ TRANSESTERIFICATION

108 pp.

การสังเคราะห์ ศึกษาคุณลักษณะ และประสิทธิภาพการเร่งปฏิกิริยาของตัวเร่งปฏิกิริยาอลูมิเนียม-แมกนีเซียมมิกซ์ออกไซด์ สำหรับการผลิตไบโอดีเซล

(SYNTHESIS, CHARACTERIZATION AND CATALYTIC ACTIVITY OF Al-Mg MIXED OXIDE CATALYSTS FOR BIODIESEL PRODUCTION)

ปัณณพัฒน์ โชติมงคลทรัพย์ 4836435 SCAI/M

วท.ม. (เคมีวิเคราะห์และเคมีอินทรีย์ประยุกต์)

คณะกรรมการควบคุมวิทยานิพนธ์: จงกล ตันติรุ่งโรจน์ชัย Ph.D (CHEMISTRY),

เอกสิทธิ์ สมสุข, Ph.D. (CHEMISTRY), ลัดดาวัลย์ ผดุงทรัพย์ Ph.D. (INORGANIC CHEMISTRY)

บทคัดย่อ

ในปัจจุบันนี้ ไบโอดีเซลได้มีการนำมาใช้มากขึ้นเรื่อยๆ เนื่องจากเป็นเชื้อเพลิงที่สามารถหมุนเวียนกลับมาใช้ใหม่ได้ ไม่เป็นพิษ และสามารถย่อยสลายได้ในธรรมชาติ ปฏิกิริยาทรานสเอสเทอริฟิเคชั่นของน้ำมันพืชกับเมทานอลโดยใช้ตัวเร่งปฏิกิริยาแบบวิวิธพันธ์ เป็นวิธีหนึ่งที่เหมาะสมสำหรับการผลิตไบโอดีเซล เนื่องจากอุณหภูมิที่ใช้ในปฏิกิริยาต่ำ และสามารถแยกตัวเร่งปฏิกิริยาออกจากปฏิกิริยาได้โดยง่าย ทั้งอลูมินาและแมกนีเซียได้ถูกนำไปใช้ในอุตสาหกรรม เป็นทั้งตัวเร่งปฏิกิริยา, ตัวรองรับสำหรับตัวเร่งปฏิกิริยา และตัวดูดซับ อลูมินามีคุณสมบัติปีนได้ทั้งกรดและเบส ในขณะที่แมกนีเซียมีคุณสมบัติเป็นเบส อลูมิเนียม -แมกนีเซียมมิกซ์ออกไซด์จึงมีความน่าสนใจในการใช้เป็นตัวเร่งปฏิกิริยากรด-เบส นอกจากนี้ วัสดุที่ความพรุนสูงมีความสำคัญในการเร่งปฏิกิริยา เนื่องจากเพิ่มประสิทธิภาพในการแพร่ผ่านของสารที่เข้ามาทำปฏิกิริยากับพื้นผิวของตัวเร่งปฏิกิริยา และถ้ายิ่งมีพื้นผิวที่สูงทำให้สามารถเพิ่มการสัมผัสของสารได้มากยิ่งขึ้นด้วย Cetyltrimethyl ammonium bromide (CTAB) เป็น structure-directing agent ที่นิยมใช้สำหรับการสังเคราะห์วัสดุที่มีรูพรุน ในงานวิจัยนี้ได้ใช้ aluminum isopropoxide และ magnesium nitrate เป็นสารตั้งต้นผสมกับ CTAB ในสภาวะที่เป็นกรด เพื่อเตรียม อลูมินา แมกนีเซีย และอลูมิเนียม-แมกนีเซียมมิกซ์ออกไซด์ และเปรียบเทียบคุณสมบัติของสารที่เตรียมได้ในการเป็นตัวเร่งปฏิกิริยา จากนั้นตัวอย่างออกไซด์ที่ได้มาจะนำไปโดปด้วย KI หรือ KNO_3 เพื่อเพิ่มความเป็นเบส เทคนิคที่ใช้ในการวิเคราะห์สารที่สังเคราะห์ได้ได้แก่ PXRD, IR, DTA-TGA, TEM, N_2 adsorption-desorption measurement, XRF และ acid-base strength measurement สารทุกตัวอย่างได้ถูกนำไปทดสอบประสิทธิภาพในการเร่งปฏิกิริยาทรานสเอสเทอริฟิเคชั่นของน้ำมันถั่วเหลืองกับเมทานอลที่อุณหภูมิ 80 องศาเซลเซียส สำหรับร้อยละของผลิตภัณฑ์สามารถหาได้โดยใช้เทคนิค ^1H NMR โดยเฟสของอลูมิเนียม-แมกนีเซียม มิกซ์ออกไซด์เป็นเฟสผสมของ γ-Al_2O_3 และ periclase (MgO) หรือเฟสผสมของ hydrotcite ($Mg_6Al_2CO_3(OH)_{16}{\cdot}4H_2O$) และ periclase ขึ้นอยู่กับอัตราส่วนของอลูมินัมและแมกนีเซียม อลูมิเนียม-แมกนีเซียมมิกซ์ออกไซด์ที่สังเคราะห์ได้มีโครงสร้างรูพรุนในลักษณะของ mesoporous และมีพื้นที่ผิวแบบ BET อยู่ในช่วง 96-266 m^2g^{-1} อลูมิเนียม-แมกนีเซียมมิกซ์ออกไซด์ที่อัตราส่วนโดยโมลของอลูมินัมต่อแมกนีเซียมเท่ากับ 1:4 และโดปด้วย KI จะมีความแรงของเบสอยู่ในช่วง $9.8 \leq pK_{BH^+} \leq 15$ และมีประสิทธิภาพในการเร่งปฏิกิริยาทรานสเอสเทอริฟิเคชั่นสูงสุด โดยให้ร้อยละผลิตภัณฑ์สูงถึงร้อยละ 90 ภายหลังจากการเร่งปฏิกิริยา 8 ชั่วโมง ในการศึกษานี้พบว่า KI โดปอลูมิเนียม-แมกนีเซียมมิกซ์ออกไซด์ที่อัตราส่วนโดยโมลของอลูมินัมต่อแมกนีเซียมเท่ากับ 1:4 เป็นตัวเร่งปฏิกิริยาที่มีประสิทธิภาพมากที่สุด สำหรับการผลิตไบโอดีเซล

108 หน้า

CONTENTS

CONTENTS (cont.)

Page

LIST OF TABLE

Table **Page**

LIST OF FIGURES

Figure **Page**

LIST OF FIGURES (cont.)

Figure **Page**

LIST OF FIGURES (cont.)

Figure **Page**

LIST OF ABBREVIATIONS

Å	Angstrom
A.U.	Arbitrary unit
BET	Brunauer-Emmett-Teller
°C	Degree Celsius
cm	Centimeter
DTA	Differential thermal analysis
FAME	Fatty acid methyl ester
FT-IR	Fourier transform infrared spectroscopy
g	Gram
h	Hour
Hz	Hertz
kcal	Kilo calories
kDa	Kilodalton
kV	Kilovoltage
mA	Miliampare
min	Minute
mL	Milliter
mmol	Milimole
nm	Nanometer
NMR	Nuclear Magnetic Resonance
PXRD	Powder x-ray diffraction
s	Second
TEM	Transmission electron microscopy
TGA	Thermal gravimetric analysis
WDXRF	Wavelength dispersive x-ray fluorescence spectroscopy

THE RELEVANCE OF THE RESEARCH WORK TO THAILAND

Biodiesel is a popular alternative fuel because of its many advantages over petroleum diesel, such as renewability, non-toxicity, biodegradability, and no sulfur content. Due to the current fossil fuel crisis, the Thai Government has formulated a strategy to ensure that the demand of 10 % biodiesel blended diesel (B10) increase from 0.7 to 8.5 million litres per day by 2012. Currently, the most economical process for biodiesel manufacture is transesterificaion of vegetable oils by an alcohol, usually methanol. The most commonly used catalyst is an alkali base, such as NaOH and KOH. However, this method has downstream purification cost because a large amount of water is required to wash out the alkali base from the biodiesel, and this waste water is needed to be neutralized before discard. The use of heterogeneous catalysts can be an attractive solution. As a matter of fact, heterogeneous catalysts can be separated more easily from reaction products. In my work, The mesoporous Al-Mg mixed oxides as solid base catalysts were synthesized and used to catalyze methanolysis of soybean oil. These novel heterogeneous catalysts should be benefitial to Thailand.

CHAPTER 1
INTRODUCTION

1.1 DIESEL

Diesel or diesel fuel is used in diesel engine invented in 1892 by Rundolf Diesel in cooperation with the German conglomerate MAN AG. Diesel is produced from petroleum, obtained in the fractional distillation of crude oil between 200 and 350 ^{o}C at atmospheric pressure [1]. The compositions of diesel fuel are 75% saturated hydrocarbons (primarily paraffins including *n*, *iso*, and cycloparaffins) and 25% aromatic hydrocarbons (including naphthalenes and alkylbenzenes) [2]. The average chemical formula for common diesel fuel is $C_{12}H_{23}$ (ranging from $C_{10}H_{20}$ to $C_{15}H_{28}$).

1.2 BIODIESEL

Diesel fuels are commonly used in many types of vehicles including automobiles, aircrafts, and etc. However, petroleum diesels are non-renewable fuels, produce pollutants such as oxides of nitrogen, oxides of sulphur, carbon dioxide, carbon monoxide, lead, and hydrocarbons. Hence, biodiesel is a good alternative because it is renewable, biodegradable, and nontoxic. The combustion of biodiesel will release carbon dioxide which can be fixed through photosynthesis. Biodiesel is derived from vegetable oils or animal fats. The direct use of the oils and fats or blending them with petroleum diesel is possible. However, the better quality biodiesel can be produced through the microemulsion, thermal cracking or transesterification method [2].

1.2.1 Production of biodiesel

1.2.1.1 Direct use and blending

The vegetable oils have free fatty acid composition, low volatility, high viscosity and polyunsaturated character [3] causing inefficient fuel atomization, incomplete combustion, carbon deposit, oil ring sticking, lubricating oil thickening, gum formation due to oxidation and polymerization during combustion. So the vegetable oils are impractical for direct use in diesel engines. In addition, the blending between vegetable oils and conventional diesel fuels in a suitable ratio produces biodiesels that are stable for only short term usages [4].

1.2.1.2 Microemulsions

Microemusions comprise of diesel fuel, vegetable oil, alcohol, surfactant, and cetane improver. The use of microemusions can solve the problem of high viscosity of vegetable oil, increase cetane number, and improve spray characteristics [5]. Although microemusions can be used as diesel fuel, many problems were encounterd: irregular injector needle sticking, heavy carbon deposit, incomplete combustion, and an increase of lubricating oil viscosity [6].

1.2.1.3 Thermal cracking or pyrolysis

Thermal cracking or pyrolysis is defined as the conversion of one substance into another by means of heat or by heat with the aid of a catalyst. It involves heating in the absence of air or oxygen [7]. Any triglycerides from vegetable oils can be pyrolyzed to lighter hydrocarbons. The distribution of cracking products depends on pyrolysis temperature, residence time, dilution rate of gas and feedstock, and type of vegetable oils [8]. The mechanism of thermal decomposition of triglyceride is shown in Figure 1.1. The products of this process are alkanes, alkenes, aromatics, and carboxylic acids that have low viscosity and a high cetane number which are similar to diesel from fossil fuel except they have high pour point. Although this process produces accepted amount of sulphur, water, sediments, and copper corrosion values, it gives unaccepted amount of ash contents and carbon residues. In

addition, thermal cracking process has high cost for the distilled equipment to separate various fractions.

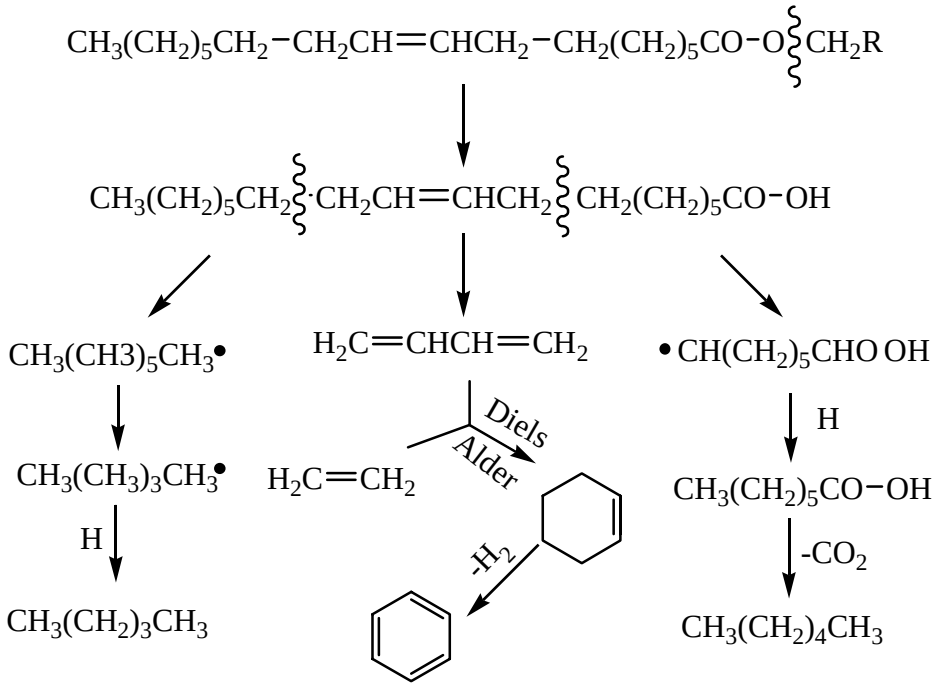

Figure 1.1 The mechanism of thermal decomposition of glycerides.

1.2.1.4 Transesterification of vegetable oil

Transesterification or alcoholysis is the reaction between triglyceride of fat or oil and alcohol to form ester and glycerol (Figure 1.2). This reaction occurs by the replacement of alcohol from an ester by another alcohol.

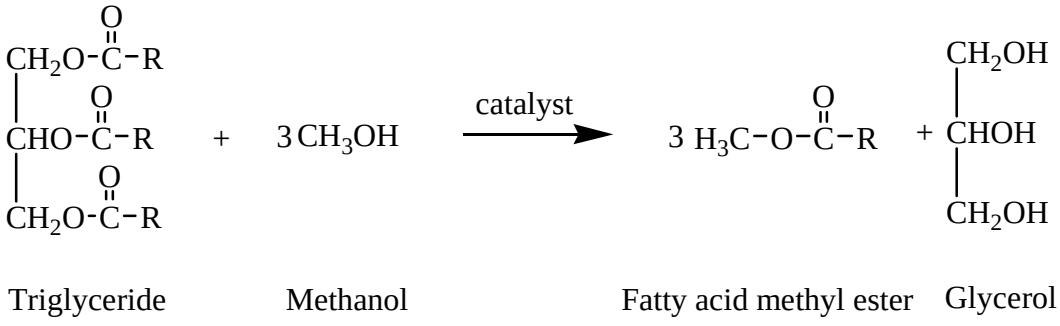

Figure 1.2 Transesterification of triglyceride with alcohol.

Glycerol is the main byproduct that can be separated and purified for a commercial value. Methanol is preferred over other alcohols due to its low cost and its physical and chemical characters. Stoichiometrically, one equivalent of triglyceride reacts with three equivalents of alcohol, but practically a large excess amount of methanol is needed to drive the reaction equilibrium to maximize percentage yield of fatty acid methyl ester (FAME). FAME has low volumetric heating value but it has high cetane number, high flash point, and low viscosity. These characters are close to the diesel from fossil fuel. The type of oils has been used for biodiesel production depends on available raw materials of each country, for instance, in the United States soybean oil is usually used, in European countries rapeseed oil is commonly used, in Malaysia coconut oil and palm oil are used [9-12]. However, alcoholysis of animal fats produces turbid ester products that raise the cloud and pour points [8].

Transesterification consists of a number of consecutive and reversible reaction as shown in Figure 1.3. The first step is the conversion of triglyceride to diglyceride, then diglyceride to monoglyceride, and followed by the conversion to monoglyceride and glycerol, respectively. In an overall reaction, one mole of triglyceride produces three moles of fatty acid alkyl esters and one mole of glycerol.

1. Triglyceride (TG) + R'OH $\overset{\text{Catalyst}}{\rightleftharpoons}$ Diglyceride (DG) + R^1COOR'

2. Diglyceride (DG) + R'OH $\overset{\text{Catalyst}}{\rightleftharpoons}$ Monoglyceride (MG) + R^2COOR'

3.Monoglyceride (MG) + R'OH $\overset{\text{Catalyst}}{\rightleftharpoons}$ Glyerol (GL) + R^3COOR'

Figure 1.3 The transesterification of triglyceride, diglyceride, and monoglyceride with alcohols.

A catalyst can be used in the transesterification to increase the rate of reaction and yield. Several types of catalysts have been used for transesterification such as acid catalysts, alkali catalysts, and lipases (biocatalysts). The acid catalysts,

such as H_2SO_4 and HCl, are common catalysts suitable for catalyzing triglyceride with high free fatty acids (> 3 %) and water contents because esterification of free fatty acids by acid catalysts can reduce acid value of triglycerides [13]. The mechanism for the acid-catalyzed esterification is shown in Figure 1.4. The initial step is the protonation of the acid to give an oxonium ion, which can undergo an exchange reaction with an alcohol to give the intermediate and loses a proton to become an ester [14]. The acid catalyzed transesterification of triglyceride and alcohol occurs in a similar manner. The mechanism is shown in Figure 1.5. The initial step is the protonation of the ester and then the addition of the exchanging alcohol gives the intermediate, which can dissociate via the transition state to give the ester [15]. NaOH, KOH, $NaOCH_3$, $KOCH_3$, and carbonates are common alkali catalysts for the transesterification of triglyceride, which proceeds at a faster rate than that of the acid catalyzed reaction. However, the presence of water can cause hydrolysis of triglyceride and lead to the saponification reaction as shown in Figure 1.6. The mechanism of transesterification using alkali as catalysts is shown in Figure 1.7. The first step is the reaction of the base with alcohol, producing an alkoxide and the protonated catalyst. The nucleophilic attack of the alkoxide at the carbonyl group of the triglyceride generates a tetrahedral intermediate, from which the alkyl ester and the corresponding anion of the diglyceride are formed. The latter deprotonates the catalyst or alcohol can react with a second molecule of alcohol and starts another catalytic cycle. Diglycerides and monoglycerides are converted by the same mechanism to the mixture of alkyl esters and glycerol [16]. Lipases have been used as a biocatalyst in biodiesel production with high yield under a mild condition, but the enzymes are expensive and not suitable for a large scale reaction [17]. Thus, it is unsuitable for industrial usage. In addition, transesterifications of triglyceride using supercritical fluid of alcohol without catalyst produce high yield in a short period of time, and easy-to-purify product [16], but this process has high cost to carry out because the process requires high temperature and high pressure, as well as a large amount of alcohol.

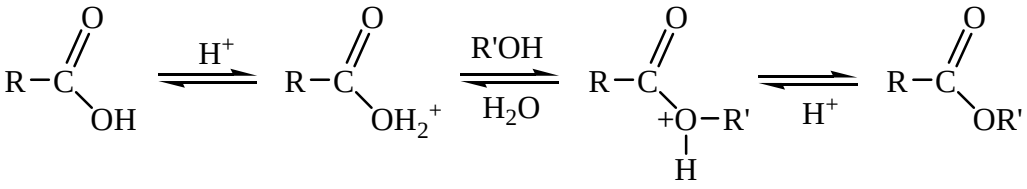

Figure 1.4 The mechanism of acid catalyzed esterification of fatty acids.

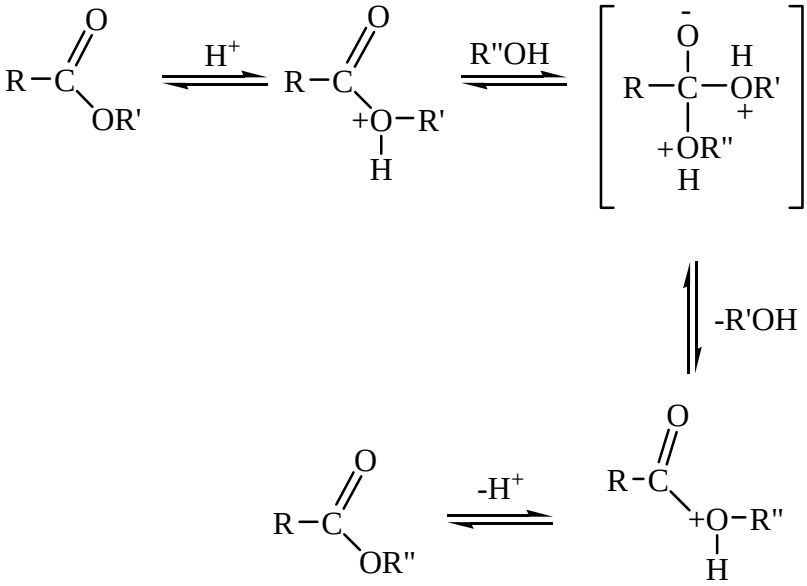

Figure 1.5 The mechanism of acid catalyzed transesterification.

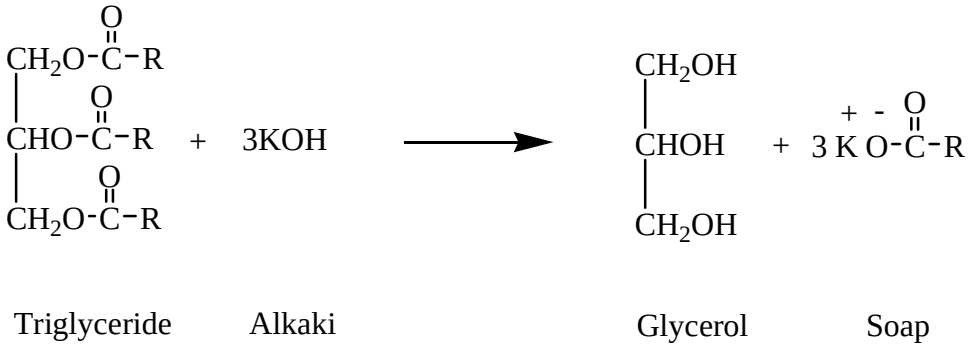

Figure 1.6 The saponification of triglycerides with alkali.

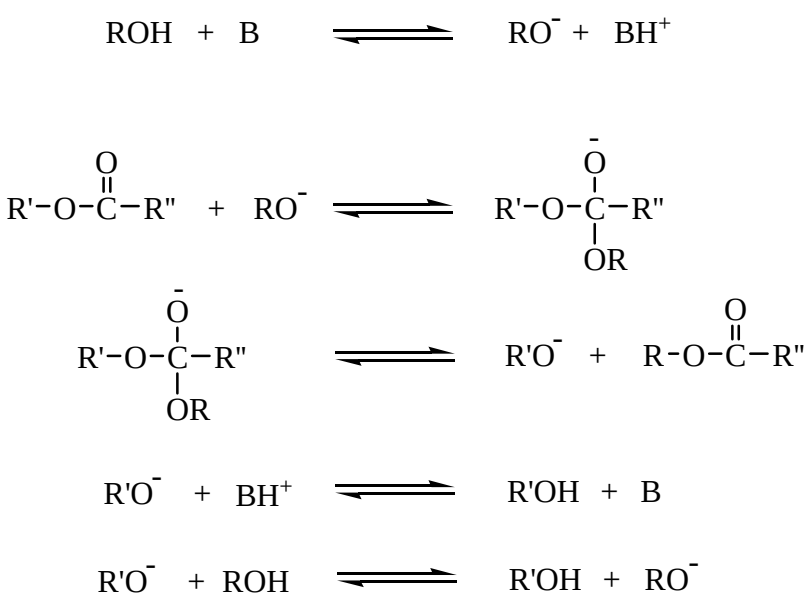

Figure 1.7 The mechanism of alkali catalyzed transesterification.

1.3 HETEROGENEOUS CATALYSTS

Heterogeneous catalysis is made to influence substances on the rates of chemical reactions. The catalyst is in a different phase from the reactants and usually a solid [18]. In order for the reaction to occur, one or more of the reactants must diffuse to the catalyst surface and adsorb onto it. After reaction, the products must desorb from the surface and diffuse away from the solid surface. Frequently, this transport of reactants and products from one phase to another plays a dominant role in limiting the reaction rate [18]. Use of an insoluble, nonvolatile solid as catalyt for a fluid-phase reaction has major advantages: loss of the catalyst is minimized, it dose not significantly contaminate the reaction products, and it stays physically in place in the reaction chamber [19].

Al_2O_3 is an heterogeneous catalyst and it can catalyze dehydraion reaction, such as the conversion of alcohol to olefins at elevated temperatures. The Al_2O_3 probably functions as a Lewis acid since alcohol usually dehydrate via formation of a carbocation, $R\text{-}CH_2\text{-}CH_2^+$. Zeolites, which are aluminosilicates that can be regarded as being derived from Al_2O_3 and SiO_2, function as acidic catalysts. In addition, Both Al_2O_3 and zeolites can catalyze isomerization, cracking, alkylation, and other organic

reactions. A structure related class of microporous materials based on aluminum phosphate ($AlPO_4$) has also been developed; like zeolite, they have cavities and channels at the molecular level and can function as sharp-selective catalysts [19].

MgO is another interesting heterogeneous catalyst. The basic oxide favors anionic reaction mechanisms on its surface. The lattice oxide ions on the surface can abstract protons from adsorbates, forming OH^-. For example, in the production of acrylonitrile (CH_2=CH-CN) for the synthesis fibers industry, acetonitrile (CH_3CN) and methanol (CH_3OH) adsorb on MgO and each loses H^+ to form $^-CH_2CN$ and CH_3O^-; then attack of the anion end of the former on the C atom of the latter leads to CH_2=CH-CN, and finally, the protons are redistributed in H_2, H_2O, and unchanged MgO. It may be noted that the catalyst is acting in part as a dehydrating agent [19].

1.4 ALUMINUM OXIDE OR ALUMINA (Al_2O_3)

Alumina is formed by the combustion of aluminum and by igniting aluminum hydroxide or aluminum salts of volatile acid. It is a white amorphous powder, which is insoluble in water and (if ignited at a high temperature) insoluble in acids also. A cubic modification of aluminum oxide (γ-Al_2O_3), density 3.4 g mL^{-1}, is obtained by the dehydration of hydragillite (gibbsite) or of bauxite, or by gentle heating of the amorphous oxide hydrate [20]. According to the mode of preparation, γ-Al_2O_3 may be obtained with very different particle sizes and, in some cases, with considerable lattice distortion. These differences may give rise to differences of up to 10 kcal $mole^{-1}$ in the heat of solution. Above 1000 ^oC, γ-Al_2O_3 changes irreversibly into α-Al_2O_3 or corundum (heat of transformation of 20.6 kcal $mole^{-1}$). There are also other unstable modifications such as δ-Al_2O_3 and ζ-Al_2O_3. γ-Al_2O_3 has a structure like that of the magnesium spinel ($MgAl_2O_4$). The spinel has 24 cations and 32 anions in a cubic unit cell as shown in Figure 1.8. The oxygen atoms are close-packed, with the magnesium atoms occupying tetrahedral sites and the aluminum atoms occupying octahedral sites [21]. In γ-Al_2O_3, as shown in Figure 1.9, the oxygen atoms occupy the positions of the spinel lattice, but 1/9 of the places belonging to the metal atoms are left unoccupied. The vacant positions are distributed essentially over those sites which, in the structure of spinel itself, are occupied by Al atoms [20, 22]. The transformation of aluminum

oxide hydrate into aluminum oxide may produce not only the modification properly known as γ-Al_2O_3, as a metastable phase, but possibly five unstable varieties which change successively and ultimately into α-Al_2O_3 as shown in Figure 1.10 [20].

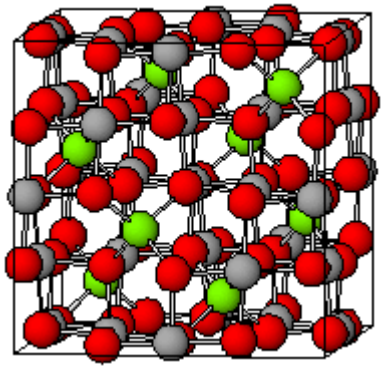

Figure 1.8 Arrangement of atoms within the $MgAl_2O_4$ spinel unit cell, Mg is in green, Al is in grey, and O is in red.

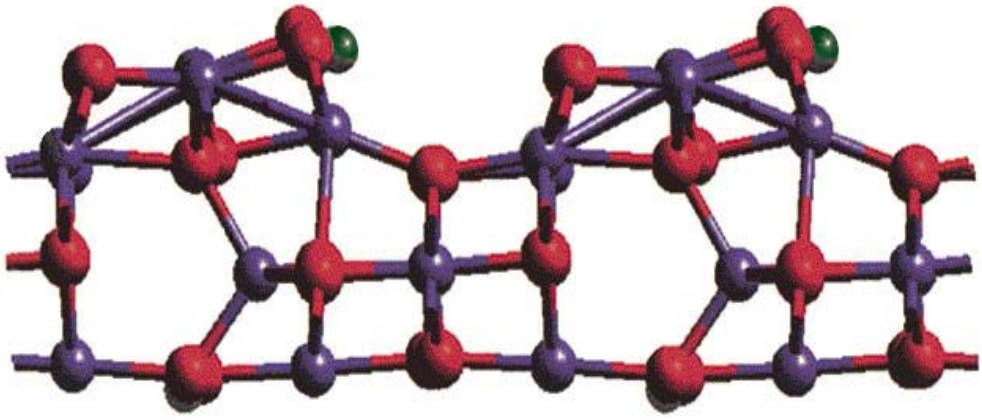

Figure 1.9 Arrangement of atoms of γ-Al_2O_3, Al is in red, O is in blue, and vacant atoms is in green.

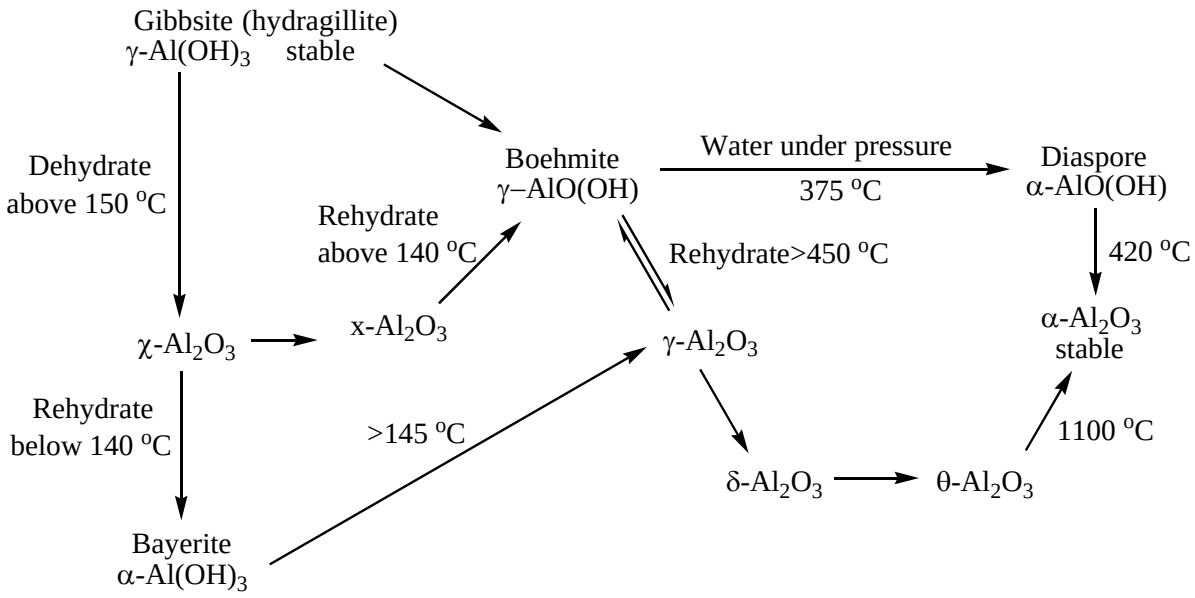

Figure 1.10 The transformation of various crystalline modifications of the aluminum oxides and hydroxides.

1.5 MAGNESIUM OXIDE OR MAGNESIA (MgO)

Magnesia is formed when magnesium burns in air, or by the ignition of the hydroxide carbonate, nitrate, and other oxyacid salts of magnesium. It is a loose, white, very infusible powder (magnesia usta, burned magnesia, etc.). In the electric furnace it sublimes, and condenses in the crystalline form. This latter may more readily be obtained by heating it with mineralizing agents such as with calcium borate, or by strongly heating it in a current of hydrogen chloride. Crystalline magnesium oxide is found in nature, in the form of very small regular octohedra and cubes, as periclase (hardness 6, density 3.7 g mL^{-1}) [20]. The crystal structure of periclase is that of halite (rocksalt) and is composed of two interpenetrating face centerd cubic (FCC) lattices of cation and oxygen. Both cations and anions are in octahedral coordination as shown in Figure 1.11 [23]. Whereas crystallized magnesium oxide is hardly attacked by water, and attacked only with difficulty by acids, the finely divided material dissolves readily in acids and is slowly converted by water into the hydroxide [20].

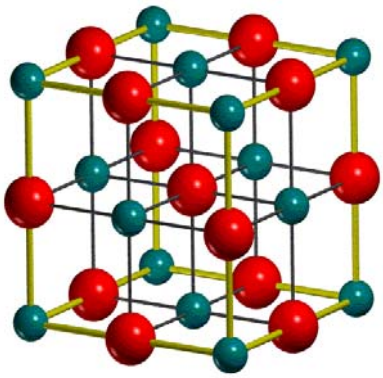

Figure 1.11 Arrangement of atoms within the periclase (MgO) unit cell, Mg is in blue, O is in red.

CHAPTER 2
LITERATURE REVIEW

The biodiesel fuel can be produced by many methods to replace fossil fuel. The direct usage of vegetable oils as biodiesel is impractical because of the high viscosity and volatility. The transesterification process is the most suitable way for large scale production of biodiesel. Here, the transesterification processes with biocatalysts (enzymes), heterogeneous catalysts, and supercritical methanol method will be described.

2.1 BIOCATALYSTS

The enzymes used for the reaction can be categorized according to their preparation methods as the extracellular enzymes (immobilized enzymes) and the intracellular enzymes (immobilized whole cells). The preparation of the intracellular enzyme is simpler and more efficient than that of the extracellular enzymes. Both preparation methods are compared in Figure 2.1

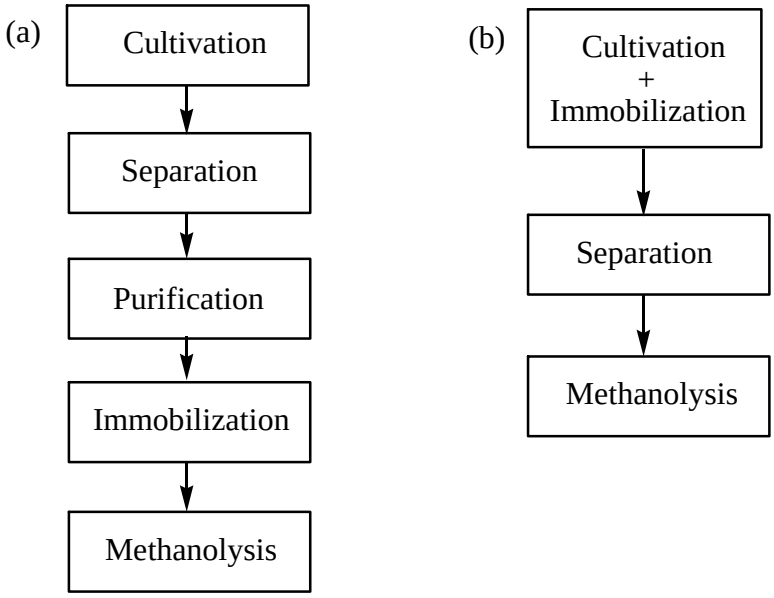

Figure 2.1 A comparison of preparation method of (a) extracellular enzyme and (b) intracellular enzyme.

2.1.1 Extracellular enzymes

Many enzymes have been used to catalyze transesterification of various oils with primary short chain alcohols, but these alcohols deactivate the enzymes. For example, transesterification of sunflower oil with methanol, ethanol, or buthanol using *M. miehei* and *C. antartica* (Novozym 435) as catalysts yields only a trace of the fatty acid alkyl esters [24]. To overcome this problem the stepwise addition of methanol was introduced, and 97 % yield of FAME was obtained with Novozyme 435 the catalyst [25]. *C. antartica* was suitable for the reaction in the mixture of *t*-butanol and methanol. It can catalyze the transesterification of cottonseed oil with 97% yield of FAME. The *t*-butanol in the mixture acts as a solvent and solubilizes both methanol and glycerol, but the *t*-butanol is not a substrate for the enzyme [26]. Du et al. [27] reported that different acyl acceptors, such as methyl acetates and ethyl acetate, with Novozyme 435 can catalyze the reaction of soybean oil to produce 92% yield of FAMEs via interesterification or ester-ester interchange reaction as shown in Figure 2.2. In this reaction, there is no glycerol as a by-product, and triacetylglycerol or triacetin is easy to be separated from the biodiesel. The triacetin can be used as an antifungal agent, a fixative in perfurmery, or a solvent for basic dyes.

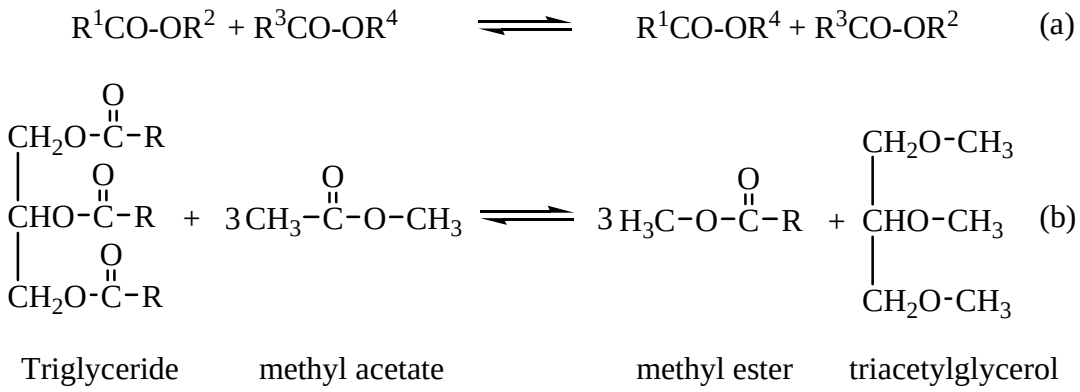

Figure 2.2 Interesterification reaction (a) general reaction, (b) interesterification reaction of triglyceride and methyl acetate.

Pretreatment of the immobilized enzymes can minimize the deactivation of the enzymes. For instance, the pretreatment of the immobilized Novozyme 435 by washing with 2-butanol or *t*-butanol to regenerate deactivated enzymes resulted in the increase in activity by 10-fold compared to the untreated enzymes. The 2-butanol and *t*-butanol can restore enzyme activity to 56 and 75 % of the original, respectively [28]. Preincubation of the immobilized *C. antartica* in methyl oleate for 0.5 h and subsequently in soybean oil for 12 h resulted in 97% yield of FAMEs [25]. To decrease the solidification point, cloud point, and pour point of the biodiesel, fuel additives such as butyl oleate and isoamyl alcohol, are used as the acyl acceptor [29]. A suitable amount water can reduce enzyme inactivation by methanol; for example, *R. oryzae* can catalyze the methanolysis of soybean oil with 4-30 wt % water and produce 80-90 % yield of FAME [30].

2.1.2 Intracellular enzymes

R. oryzae cells can be stabilized by cross-linking treatment with 0.1% glutaraldehydrate, and catalyzed ethanolysis of soybean oil with stepwise addition of ethanol to produce 72-83 % yield of FAME after sixth batch cycle, but the methanolysis without stabilizing *R. oryzae cells* can produce only 50% yield after sixth bath cycle [31]. The pretreat cells with lower alcohol, e.g. methanol, ethanol, propanol, before usage can improve yield of FAME to 350-600 times compared with the untreated cells [32]. Enzyme can also be stabilized by the addition of various fatty

acids to the cells. Oleic acid and linoleic acid enriched cells enchanced activity more than saturated fatty acid enriched cells, and palmitic acid enriched cells had higher stability than unsaturated fatty acid enriched cells. The optimum ratio of unsaturated fatty acid to total fatty acids (oleic acid/ oleic acid + palmitic acid) for optimum activity and stability is 0.67 [33]. The lipase localization of *P. oryzae* cells has two different molecular masses of 34 and 31 kDa, which are labeled ROL34 and ROL31, respectively. ROL34 was bound to the cell wall and ROL31 was mainly bound to the cell membrane. When cells were cultivated with olive oil or oleic acid, the methanolysis activity correlated with the relative amount of ROL31. Hence, ROL31 localized in the cell membrane plays a crucial role in the methanolysis acitivity [34]. In addition, the intracellular lipase can catalyze waste oil efficiently in the presence of water without solvent [32].

2.2 SUPERCRITICAL ALCOHOLS

A non-catalytic biodiesel production route with supercritical alcohol has been developed that allows a simple process and high yield because of simultaneous transesterification of triglyceride and alkyl esterification of fatty acids and the dielectric constant of alcohol such as methanol dramatically changes from liquid to supercritical state that close to vegetable oil allowing a homogeneous mixture in supercritical condition [35]. A reaction mechanism of vegetable oil in supercritical methanol is shown in Figure 2.3. An alcohol molecule directly attacks the carbonyl atom of the triglyceride because in the supercritical state, hydrogen bonding would be significantly decreased, which would allow methanol to be a free monomer and produce methyl ester and diglyceride, consequently. Saka et al [36]. Compared the supercritical alcohol types that catalyzed rapeseed oil at 300 ^{o}C and 43 MPa with alcohol:oil ratio of 42:1. They found that alcohol with the shorter alkyl chain gave better conversion. Almost 100 % conversion was obtained in 15 min by methanol, while ethanol and 1-propanol required 45 min. 1-butanol and 1-octanol produced about 85 and 62 % conversion, respectively. They also compared the reaction rate of the methanolysis of rapeseed oil with that of the methyl esterification of oleic acid. Methyl esterification proceeds faster since fatty acids, especially unsaturated fatty acids, are more soluble than triglycerides so that the reaction can proceed easier and

the transesrerification of triglyceride consists of three steps as shown in Figure 1.3. The formation of alkyl ester from monoglyceride determines the reaction rate because monoglycerides are the most stable intermediate compound. On the contrary, alkyl esterification is only a one-step reaction. The effect of water content in the reaction was studied [37]. When rapeseed oil was mixed with methanol containing 10 %, 18 %, 25 %, and 36 % of water in supercritical condition, rapeseed oil completely converted to methyl ester within 4 min. But, when the addition of various water content in oleic acid and supercritical methanol, the conversion of oleic acid to methyl ester was somewhat reduced with increasing of the water content, since methyl oleate may be hydrolyzed to oleic acid over a prolonged treatment. However, an addition of 50 % water with the water:rapseed oil molar ratio of 26:1 under supercritical methanol at 350 ^{o}C for 4 min led to hydrolysis products. Since the amount of water is large enough for the hydrolysis reaction to occur and the hydrolysis reaction is much faster than transesterification, fatty acids can be produced from methyl esters as shown in Figure 2.4. At supercritical condition, water is rich with ionic products and can mix with polar methanol, the mixture will have both strong hydrophilic and hydrophobic properties that can improve reaction rate. Moreover, the separation of methyl ester and glycerol from the reaction mixture become easy because glycerol will be in the water layer (lower layer), while methyl esters are in the upper layer.

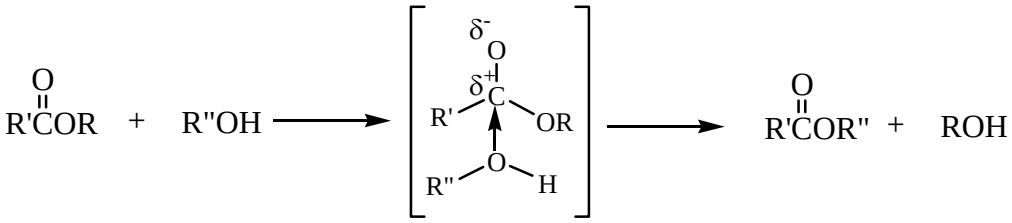

R : alkyl group
R' : long chain hydrocarbon
R'' : alkyl group

Figure 2.3 A proposed reaction mechanism of transesterification in supercritical methanol.

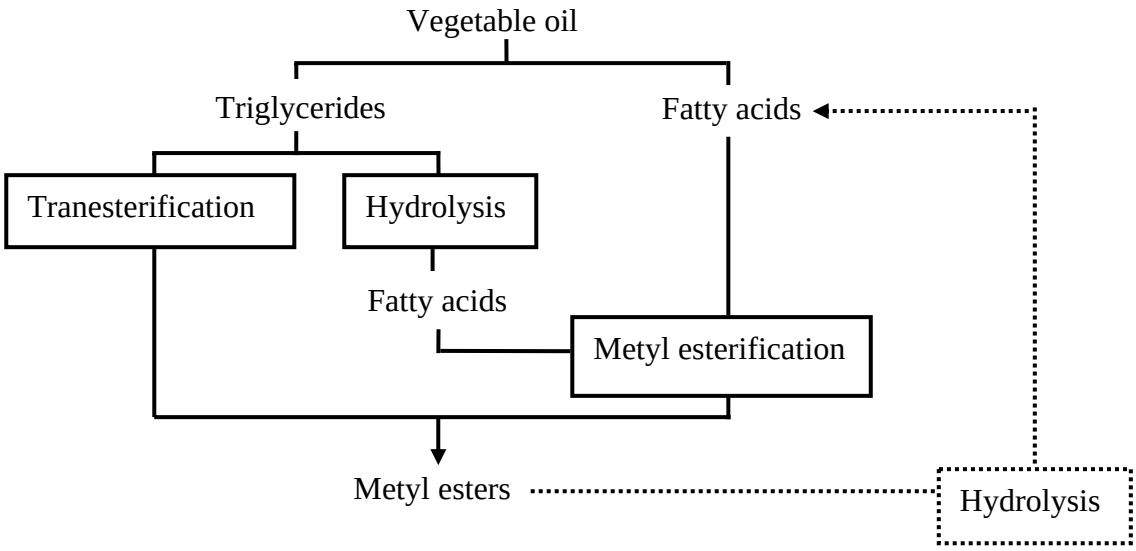

Figure 2.4 Reactions involved in the treatment of rapeseed oil by supercritical methanol in the presence of water.

Madras et al. [38] reported the rate constants for the formation of methyl ester from various oils. The transesterification reaction rate is the highest for the triglyceride of saturated fatty acid followed by triglycerides of unsaturated acids. The reaction rate of triglycerides of tri-unsaturaed fatty acid is the slowest compared to triglycerides of di-unsaturaed and mono-unsaturaed fatty acid. The co-solvent for supercritical methnolysis can increase solubility of methanol and vegetable oil at low reaction temperature and pressure because it can decrease the critical point of methanol, and allow the supercritical reaction to be carried out under milder condition. Supercritical CO_2 and supercritical propane are good solvents for vegetable oil and methanol. Supercritical CO_2 can be used as a co-solvent to catalyze soybean oil with supercritical methanol to produce 98.5 % yield of FAME at 10 min under optimum condition (280 ^oC, 14.3 MPa, methanol:soybean oil = 24:1, CO_2: methanol ratio = 0.1). When supercritical propane was used as a co-solvent, the percentage yield of FAME at 10 min is 98% under similar condition (280 ^oC, 12.8 MPa, methanol:soybean oil = 24:1, propane: methanol = 0.05) [39, 40].

2.3 HETEROGENEOUS CATALYSTS

The cost of transesterification of vegetable oils involves two main factors, the cost of raw materials and the cost of processing. The biocatalysts have high cost of materials, supercritical alcohols require high temperature and high pressure that led to high capital cost of processing, and homogeneous catalysts have the cost of eliminating waste streams. Hence, heterogeneous catalysts can be an attractive solution, since they can be separated more easily from reaction products and the raction conditions could be less drastic than supercritical alcohol process. The heterogeneous catalysts for transesterification reaction are categorized into acid catalysts and base catalysts.

2.3.1 Acid catalysts

Acid catalysts can catalyze both esterification of free fatty acids and transesterification of triglycerides. Brönsted acid catalysts are active mainly in esterification reactions, while Lewis acid catalysts are more active in transesterification reaction (39). The acid catalysts can catalyze even the low quality oils which have high free fatty acid content. The reaction mechanism of Lewis acid catalysts is shown in Figure 2.5. The formation of electrophilic species occurs from the Lewis acid catalysts in the first step. The rate determiaton depends on the Lewis acid strength. After the Lewis complex formation (step1), the alcohol forms a nucleophilic bond with the carbonyl carbon (step 2). Subsequently, the new ester forms (step 3) and desorbs from the Lewis site (step 4). And then the cycle is repeated. If the strength of acidic sites is too high, the desorption of the product is not favored, leading to a slow reaction rate. Thus, very strong Lewis acid catalysts are less active in transesterification reactions [42].

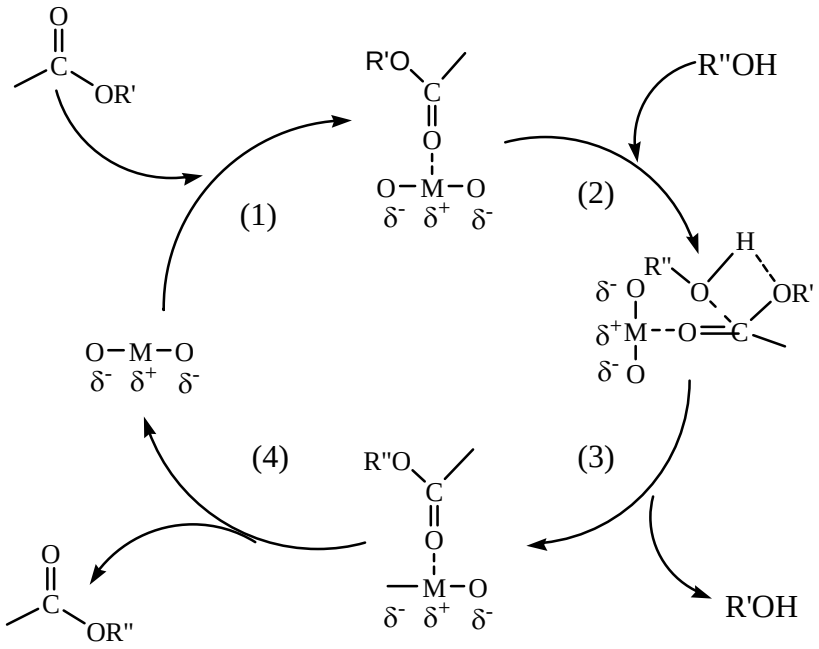

Figure 2.5 A proposed reaction mechanism of Lewis acid catalyzed transesterification of triglycerides.

The catalytic activities of several acid catalysts in transesterification of triacetin with methanol at 60 °C using methanol:triacetin ratio of 6:1 and 2 wt% solid acid was reported as follow: Amberlyst-15 (sulfonated polystyrene) > SZ (sulfate modified zirconia) > Nafion NR50 (perfluorinated resin sulfonic acid) > WS (tungsta modified zirconia) > SPA (supported phosphoric acid) > zeolite β (alumino silicate) > ETS-10(H) (titanosilicate). Amberlyst-15, SZ, and WS exhibited decrease activity due to the blockage of the sites by adsorbed intermediates or product species. Zeolite β revealed low activity because of diffusion limitations in the micropores of bulky triacetin molecules and ETS-10(H) has low acid strength [43]. Tungstated zirconia-alumina (WZA), sulfated zirconia (SZA), sulfated tin oxide (STO), TiO_2-ZrO_2, and Al_2O_3-ZrO_2 can catalyze transterification of soybean oil at 200-300 ^oC. The activities of the catalysts at 4h are WZA > TiO_2-ZrO_2 > Al_2O_3-ZrO_2 > SZA > STO [44, 45], Jitputti et al. [46] tested the transesterification of crude palm kernel oil (1.05 % free fatty acid, 0.09% moisture content) and crude coconut oil (2.25% free fatty acid, 0.17% moisture content) with 3 wt% SZ, STO, ZnO, and ZrO_2 , methanol: oil ratio of 6:1, reaction temperature 200 ^oC, reaction time 4 h. They found that SZ (90.3 % yield

of FAME from palm kernel oil, 86.3 % yield of FAME from coconut oil) had the highest activity, followed by STO, ZnO, and ZrO_2, respectively, but SZ was deactivated after the first use. Vanadyl phosphate ($VOPO_4 \cdot 2H_2O$) can catalyze the reaction of soybean oil with methanol, when the methanol: soybean oil ratio is 12:1, the catalyst loading was 5 wt%, and the reaction temperature was 180 ^oC. The fresh catalyst produced 78 % yield of FAME at 1 h and the used catalyst produced only 35 % yield of FAME after the same amount of time. The deactivation of the catalyst is due to the reduction of the surface vanadium species from V^{5+} to V^{3+} by methanol. However, the vanadium catalyst can be reactivated by calcinations in air. 78 % yield of FAME at 1 h was obtained for the regenerated catalyst [47]. In addition, Sreeprasanth et al. [48] reported that double-metal cyanide Fe-Zn are active in transesterification and esterification of various oils. These catalysts are Lewis acidic, hydrophobic, and insoluble. The reaction condition is 3 wt% catalyst, methanol: oil ratio of 15:1, reaction temperature 170 ^oC, and 8 h reaction time. The catalyst can be reused without any purification (98.3 % conversion for fresh catalyst, 98.1 % conversion for third reused catalyst) and no leaching nor dissolution was detected.

2.3.2 Base catalysts

Transesterification of vegetable oil using base catalysts requires lower reaction temperature than transesterification using acid catalysts. The reaction mechanism of Lewis base catalyzed transesterification is shown in Figure 2.6. In the first step, surface oxygen react with H^+ from CH_3OH to form surface CH_3O^-, which is strongly basic and has high catalytic activity in transesterification reaction [16]. The carbonyl carbon atom of the triglyceride molecule was attacked by a methoxide anion from the surface of the metal oxide to form a tetrahedral intermediate, from which the alkyl ester and the corresponding anion of the diglyceride are formed. The latter deprotonates the catalyst or reacts with a second molecule of alcohol and starts another catalytic cycle. Diglycerides and monoglycerides are converted by the same mechanism to the mixture of alkyl esters and glycerol [16].

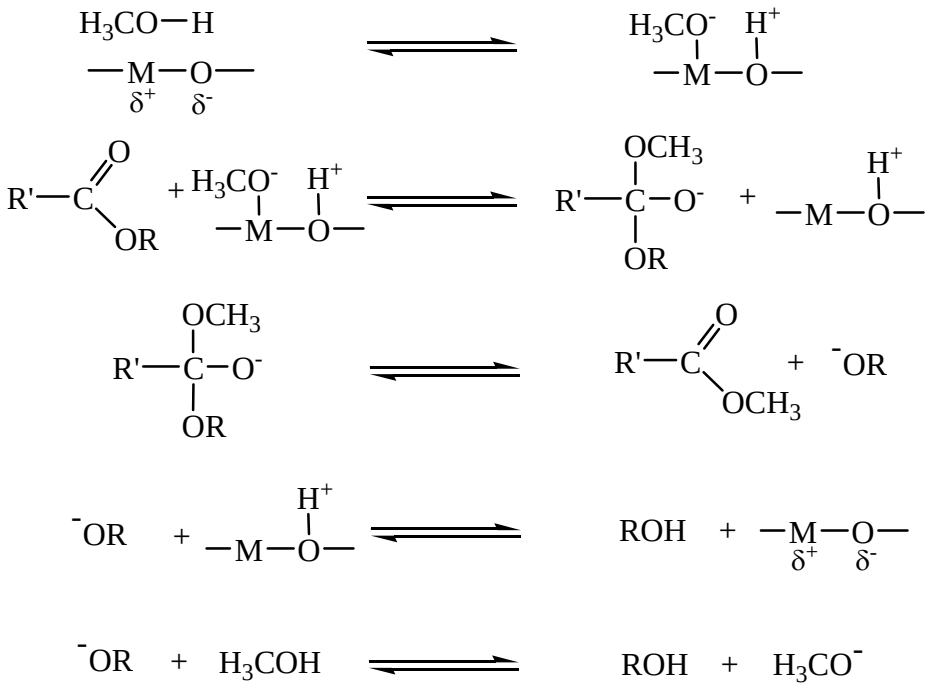

Figure 2.6 A proposed reaction mechanism of Lewis base catalyzed transesterification of triglycerides.

$Ca(OH)_2$, CaO, and $Ca(OCH_3)_2$ can catalyze transesterification of rapeseed oil at methanol reflux temperature with methanol:rapeseed oil ratio of 4.5:1 and 0.8 wt% catalyst. Percentage of the solubility of $Ca(OH)_2$, CaO, and $Ca(CH_3O)_2$ in methanol are 0.010, 0.035, and 0.040, respectively, so that they are heterogeneous catalysts. The reactivity order is $Ca(OCH_3)_2$ > CaO > $Ca(OH)_2$, which agrees with the Lewis basic theory. The methoxides of alkaline earth metals are more basic than their oxides which are more basic than their hydroxides. Their acitivities were higher than 90 % yield of FAME at 2.5 h [49]. Nanocrystalline CaO with crystal size of 20 nm and specific surface area of 90 m^2g^{-1} has high activity (>99 % conversion at 24 h) for methanolysis of soybean oil at room temperature with methanol:soybean oil ratio of 27:1 and 1.27 wt% catalyst, while commercial CaO with crystal size of 43 nm and specific surface area of 1 m^2g^{-1} has only 2 % conversion at 6 h. The nanocrystalline CaO can be reused without calcinations. The reused catalyst exhibited activity for the reaction without deactivation until fourth and fifth cycles, when the activity decreased from 96 to 74 % conversion. The authers suggested that the catalyst may be deactivated by impurity [50]. Gelbard et al. [51] investigated polystyrene supported biguanide and

guanidine as strong base catalysts because their basicities are in the range of common inorganic bases such as alkalines, hydroxides, and carbonates. The activity of the polystyrene supported biguanide and guanidine in the transesterification of oil at 70 ^{o}C and methanol:oil:catayst molar ratio of 69:1:0.02 are 94 and 63 % yield of FAME, respectively. Anionic resins (PA308, PA306, PA306s, HPA25) were studied for the transesterification of triolein at 50 ^{o}C with ethanol:triolein molar ratio of 10:1. The PA306s was the most active catalyst that produced more than 80 % ethyl ester at 4 h but the reused PA306s was deactivated by the ion-exchange reaction of the resin's hydroxyl ion with the oleic acid group of triolein, diolein, or monolein. However, PA306s can easily be regenerated by washing the resin with citric acid in ethanol solution following by NaOH solution and ethanol. The regenerated PA306s has no loss of activity (>80 % at 4 h) [52]. Liu et. al. [53] tested polymeric resin (A26) with quaternary ammonium functional groups ($QN^{+}OH^{-}$) to be active in methanolysis of triacetin at 60 ^{o}C, methanol:triacetin ratio of 6:1, 1.67 wt% A26 relative to the mass of the reaction mixture (90 % conversion at 240 min). The A26 can be reused by washing with methanol to exchange most OH^{-} groups of the resin with MeO^{-}. The A26 can be reused for more than four reaction cycles with the same conversion. Suppes et al. [54] studied basic zeolites, such as NaX, KX, CsX, and ETS-10. The methanolysis of soybean oil using basic zeolites as catalysts with methanol:oil ratio of 6:1 at 60 ^{o}C and 10 wt% catalyst showed low acitivity (2-10 % yield of FAME at 24 h). Although, ETO has higher activity under the same condition except the reaction temperature was 100 ^{o}C. 92 % methyl ester was obtained with ETO at only 3 h, but the activity decreased to 28% yield in the fifth reaction cycle due to the leaching of sodium and potassium ions. Likewise, KOH doped NaX (10 wt% KOH) studied by Xie et al. [55] was active in the methanolysis of soybean oil with methanol:oil ratio of 10:1, 3 wt% catalyst, reaction temperature of 65 ^{o}C to give 85.2 % yield of methyl ester and only 48.7 % yield in the second reaction cycle because of the leaching of potassium. $Sr(NO_3)_2$ doped ZnO with (2.5 mmol $SrNO_3$ g^{-1}) by impregnation method is active in the transesterification of soybean oil with methanol:oil ratio of 12:1, 5 wt% catalyst. 94.7 and 15.4 % yield of FAME were obtained from fresh and first reused catalysts, respectively. This catalyst was deactivated by the deposition of reactants and products on the active sites and/or by transformation of the active sites during the reaction [56].

Cantrell et al. [57] reported catalytic activity of alumina, MgAl hydrotalcite, and magnesia for the transesterification of glyceryl tributyrate with methanol:glyceryl tributyrae ratio of 30:1. MgAl hydrotalcite at Mg:Al ratio of 3:1 has higher activity at 3 h (74.8 % conversion) than those of the magnesia (11% conversion) and the alumina (no activity). Reusability and leaching of their catalysts were not reported. Potassium salts doped alumina catalysts were reported by Xie et al. [58] The transesterification of soybean oil using calcined KI doped alumina has high activity of 87.4 % conversion. Reusability and leaching of their catalysts were not stated.

2.4 MESOPOROUS ALUMINA

Mesoporous materials are important for catalytic reaction because the diffusion property of these materials enhances the better interaction between the substrates and the surface of the materials due to higher surface area and accessibility of the pores [59]. The mesoporous materials are synthesized via electrostatic interaction between surfactant and precursor mechanism such as S^+I^- or S^-I^+ (S = surfactant, I = precursor) and interaction between neutral surfactant and neutral precursor mechanism as N^oI^o (N = surfactant, I = precursor) [60]. γ-Al_2O_3 phase is metastable and can be transformed into δ-Al_2O_3 phase at roughly 800 ^oC and the most stable α-Al_2O_3 phase is finally obtained [61]. However, γ-Al_2O_3 has highest surface area. Hence, γ-Al_2O_3 phase is the most important phase for catalysis [60]. The synthesis of porous alumina is complex due to its susceptibility for hydrolysis as well as to the phase transitions accompanying the thermal breakdown of the ordered structure. The hydrolysis behavior of the alumina is very complicated and it is strongly affected by pH, water, temperature, relative humidity, and other factors so that the synthesis of mesoporous alumina is rather difficult and strict conditions are required [62]. Vaudry et al. [63] first investigated the mesoporous alumina with pore size of about 2 nm and surface area of 710 m^2g^{-1}. These mesoporous alumina materials were synthesized using lauric acid as a template and aluminum *sec*-butoxide as an aluminum precursor. Thermally unstable formation of alumina takes place through an S-I mechanism (S = acid, I = alkoixde). Hexagonal mesoporous alumina samples were obtained by precipitation method using $Al(NO_3)_2$ as an aluminum source, urea as a pH adjustor, and sodium dodecyl sulphate

as a template with electrostatic mechanism (S^+I^-). This mesoporous alumina became disorder upon calcinations at 300 ^oC [64]. Pseudo lamellar mesostrucured γ-Al_2O_3 with crystalline framework walls (MSU-γ) was synthesized by Zhang et al. [65] using aluminum tri-*tert*-butoxide as a precursor, anhydrous aluminum chloride as a pH adjustor and hydrolysis-condensation controller, nonionic triblock copolymer Pluronic L64 $(EO)_{13}(PO)_{30}(EO)_{13}$) as a template and employing pseudoboehmite nanoparticles intermediate as building blocks. The MSU-γ has surface area of 346 m^2g^{-1} and pore volume of 0.46 cm^3g^{-1}. Somorjai et al. [66] first investigated the synthesis of ordered mesoporous alumina with amorphous walls under strict condition using aluminum triisopropoxide (I^o) as a precursor, Pluronic P123 ($(EO)_{20}(PO)_{70}(EO)_{20}$) as a template ($N^o$), and HCl as a pH adjustor through N^oI^o mechanism. The ordered mesoporous alumina has surface area of 410 m^2g^{-1}, and pore volume of 0.80 cm^3g^{-1}. Cabrera et al. [67] studied mesoporous alumina using aluminum *sec*-butoxide as a precursor, cetyltrimethyl ammonium bromide (CTAB) as a cationic surfactant, triethanolamine as a hydrolysis delaying agent. The calcined mesoporous alumina has surface area of 340 m^2g^{-1}. The high surface area mesostructured γ-alumina was obtained by Aguado et al. [68] The mesoporous γ-alumina was synthesized by sol-gel method employing aluminum triisopropoxide as a precursor, CTAB as a template, and HCl as a pH adjustor without hydrolysis retarding agent. The calcined alumina has high surface area (626 m^2g^{-1}) with γ-Al_2O_3 phase at calcination temperature of 550 ^oC.

CHAPTER 3
OBJECTIVES

Even though biodiesel can be produced by several methods, transesterification vegetable oil or animal fats with alcohol is the most avialable one. As the quality of biodiesel produced from transesterification is close to these of prteoleum diesel and can be used in diesel engines without any modification.

In transesterification reaction, a catalyst is needed to achieve a good yield in a short period of time, and the common catalyst used for the reaction is a homogeneous base. However, the drawback of a homogeneous catalyst in the seperation process has led to many research in the development of solid base catalyst. With the acid-base properties of aluminum oxide and magnesium oxide, being amphoteric and basic, we proposed that the Al-Mg mixed oxide will offer an interesting acid-base properties. In addition, an incorporation of an alkali species like potassium into the mixed oxide may increase the basic strength, leading to a more active solid base for the transesterification. Furthermore, in an heterogeneous system, the textural structure of the catalyst plays an important role in raising the catalytic activity. Mesoporous structured solids provide better interaction between substrates and the active sites due to the large suface area. Hence, the mesoporous alkali metal doped Al-Mg mixed oxides are interesting to catalyze methanolysis of soybean oil. The objectives in this research are:

1. To synthesize and characterize mesoporous Al-Mg mixed oxides.
2. To study their catalytic activity in transesterification of soybean oil.

CHAPTER 4
MATERIALS AND METHODS

4.1 MATERIAL AND CHEMICALS

Chemicals and reagents obtained commercially are shown in Table 4.1 All chemicals were used as received.

Table 4.1 List of chemicals.

Chemicals	Chemical formula or Abbreviation	Manufacturer
Aluminum tri-isopropoxide, 98 %	$Al(O^iPr)_3$	Merck
Magnesium nitrate hexahydrate, 99 %	$Mg(NO_3)_2 \cdot 6H_2O$	Unilab
Cetyltrimethylammonium bromide 99 %	$CH_3(CH_2)_{15}N(CH_3)_3NBr$, CTAB	Merck
Potassium iodide, 99.9 %	KI	J.T. Baker
Potassium nitrate, 99 %	KNO_3	Riedel-de Haën
Potassium hydroxide, 99 %	KOH	Ajax Finechem
Sodium sulfate anhydrous, 99 %	Na_2SO_4	Fischer Chemicals
n-Butylamine, 99 %	$CH_3(CH_2)_3NH_2$	Merck
2-Propanol, 99.99 %	$CH_3CHOHCH_3$, ^iPrOH	Fischer Chemicals
Ethanol, 99.9 %	CH_3CH_2OH, EtOH	Merck
Methanol, 99.9 %	CH_3OH, MeOH	Fischer Chemicals

Table 4.1 List of chemicals (cont.).

Chemicals	Chemical formula or Abbreviation	Manufacturer
Methanol, 99.9 %	CH_3OH, MeOH	Fischer Chemicals
Toluene, 99.97 %	$C_6H_5CH_3$	Fischer Chemicals
Cyclohexane, 99.99 %	C_6H_{14}	Lab Scan
Hydrochloric acid, 37 % w/w	HCl	Lab Scan
Bromothymol blue	$C_{27}H_{28}Br_2O_5S$	Merck
Phenolphthalein	$C_{20}H_{14}O_4$	BDH Chemicals
4-nitroaniline	$C_6H_4NH_2NO_2$	Aldrich
2,4-dinitroaniline, 98 %	$C_6H_3(NH_2)(NO_2)_2$	Aldrich
Soybean oil (anjoon brand)	-	Thai Vegetable Oil Public Company Limited

4.2 INSTRUMENT AND APPARATUS

Powder x-ray diffraction (PXRD) measurements were carried out on a Bruker D8 ADVANCE diffractometer using a high-power CuK_α source focusing Ge-crystal (Johansson type) monochromator (λ = 1.540619 Å) operating at 40 kV and 40 mA. The diffraction patterns over the 2θ range of 0.5-5 and 8-100^o were recorded at a scan rate of 2 s/step, step size 0.015 2θ/s and a scan rate of 1 s/step, step size 0.037 2θ/s respectively[a].

The Crystalline size of KI, KIO_3, KNO_3, and K_2O by Scherrer equation

$$t = \frac{K\lambda}{B\cos\theta}$$

Where t is the crystalline size

K is the Scherrer constant (0.9)

λ is the wavelength of X-rays

B is the full width half maximum of the peak (FWHM)

θ is the angle corresponding to the peak

The infrared (IR) spectra of compounds were recorded on a FT-IR system 2000 (Perkin-Elmer) spectrometer (KBr pellets)[a].

The differential thermal analysis (DTA) and the thermal gravimetric analysis (TGA) (TA instrument STD 2690 simultaneous DTA-TGA) were used to study the thermal property of samples. Data were analyzed by TA Universal Analysis computer program. Samples were placed in an alumina cup and heated from 10 ^{o}C to 1000 ^{o}C at a heating rate of 10 ^{o}C min^{-1} in air with a flow rate of 100 mL min^{-1}[b].

Transmission electron microscopy (TEM) images were recorded using a Philips Tecnai-20 operating at 25 and 50 kV[b].

N_2 adsorption-desorption experiments were carried out using a Micromeritics 2020 ASAP equipment and pore size distributions were calculated using the Barret-Joyner-Halenda (BJH) model on the desorption branch. The surface area values were obtained by application of Brunauer-Emmett-Teller (BET) equation. The out gass temperature operated at 90 ^{o}C for 60 min and 350 ^{o}C for 240 min[c].

^{1}H NMR results were analyzed by 300 MHz Bruker NMR spectrometer at room temperature[a].

Wavelength dispersive x-ray fluorescence spectrometer (WDXRF), Bruker AXS Model S4 EXPLORER equipped with Rh*K* radiation operation at 50 kV and 20 mA with scintillation detector and sealed proportional counter, was employed to analyze chemical composition. Each bulk powder sample was placed in a sample cup with Mylar sheet 6 μm for measurement. The method for analysis was Fast-He34[a].

a = Department of Chemistry, Mahidol University

b = Central Instrument Facility (CIF), Mahidol University

c = Department of Chemistry, Kasetsart University

4.3 METHOD OF CATALYST SYNTHESIS

4.3.1 Al-Mg mixed oxide catalysts

The synthesis of the alumina, the Al-Mg mixed oxides, and the magnesia can be performed as follow: $xAl(O^iPr)_3$:$yMg(NO_3)_2$:0.8CTAB:$22H_2O$:17^iPrOH, where x + y = 1 and x:y ratio is 1:0, 8:1, 4:1, 2:1, 1:1, 1:2, 1:3, 1:4, 1:8, or 0:1. In the typical synthesis, CTAB was dissloved with 2-propanol and water the metal precursor was added to the CTAB solution and stirred for 4 h. The reaction mixture was heated in oil bath at 80 ^oC for 2 h and subsequently dried at 100 ^oC. The organic portion of the materials was extracted with 0.5 M n-butylamine in ethanol solution (100 mL g^{-1} of sample) at 80 ^oC. After extraction, the solid sample was calcined at 550 ^oC for 5 h at a heating rate of 1 ^oC/min to preserve under O_2 flow (flow rate of 80 mL min^{-1}). A slow heating rate was used during calcination to preserve mesoporous structure of the Al-Mg mixed oxides.

4.3.2 Alkali doped Al-Mg mixed oxide catalysts

1 g of the alumina, the Al-Mg mixed oxides, or the magnesia was ground with 2.1 mmol KI or KNO_3 and a small amount of water in the mortar for 30 min. The mixture was heated at 120 ^oC in an oven overnight and then calcined in air at 550 ^oC for 5 h (a heating rate of 1 ^oC min^{-1}).

4.4 ACID AND BASE STRENGTH MEASUREMENTS

Acid-base strength of the catalysts was measured by Hammett indicator method [68]. The indicators used in the study were bromothylmol blue, phenolthalein, 2,4-dinitroanline, and 4-nitroaniline with pK_a of 7.2, 9.8, 15, and 18.4, respectively. Color tests were made by transferring 0.1 g of dried catalyst to a test tube, and then adding three drops of a 10% v/v methanol solution of the indicator. After one day of equilibration, the colors of the indicators were recorded. The base strength was reported as being stronger than the weakest indicator which exhibits a color change, but weaker than the strongest indicator that produces no change.

4.5 TRANSESTERIFICATION OF SOYBEAN OIL

Commercial edible grade soybean oil (anjoon brand) was obtained from local market. The acid value of the soybean oil was determined to be 0.4 mg KOH g^{-1}, and the average molecular weight was 909 g mol^{-1}, calculated from the saponification index (SV = 185.6 mg KOH g^{-1}) [69, 70].

Transesterification of the soybean oil was performed by refluxing 10 mL of methanol (247 mmol) with 11.23 g of soybean oil (12.3 mmol) and 0.5615 g of the catalyst (5 wt%) at 70 ^{o}C. The catalyst was dried at 120 ^{o}C in an oven overnight prior to use. A 0.5 mL aliquot was taken from the reaction mixture at various times in order to follow the product yield. Each aliquot was extracted in a hexane/water system. The hexane layer was then dried with anhydrous Na_2SO_4 and was purged with N_2 to remove hexane.

The percentage yield of the fatty acid methyl ester (FAME) can be determined by the integration ratio of the ^{1}H NMR signal of the methoxy protons of FAME (A_1) and the signal of the metylene protons of the triglyeride and FAME (A_2), as shown in scheme 4.1 [71].

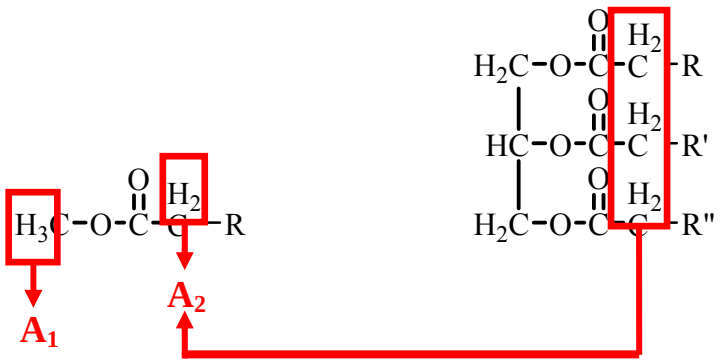

Fatty acid methyl ester **Triglyceride**

$$\% \text{ yield of FAME} = \left(\frac{A_1 / 3}{A_2 / 2} \right) \times 100$$

Scheme 4.1

CHAPTER 5
RESULTS AND DISCUSSION

The structure of all samples was characterized by powder X-ray diffraction and fourier-transform infrared spectroscopy. The thermal property of all samples was characterized by the differential thermal analysis and the thermal gravimetric analysis. The textural property of calcined samples was characterized by transmission electron microscopy and N_2 adsorption-desorption measurement and the ratio between Al and Mg of calcined samples was characterized by X-ray fluorescence spectrometry.

5.1 POWDER X-RAY DIFFRACTION (PXRD)

5.1.1 Al-Mg mixed oxides

The powder X-ray diffraction (PXRD) patterns of all as-synthesized samples exhibited CTAB pattern as shown in Figure 5.1. The CTAB template was removed by extraction with butylamine in ethanol solution followed by calcination at 550 ^{o}C. After the extraction, the pattern of the alumina samples showed the phases of aluminum oxide chloride (AlOCl) and aluminum oxide chloride hydroxide ($Al_{17}O_{16}(OH)_{16}Cl_{13}$). The extraction samples of the Al-Mg mixed oxides at the Al:Mg ratios of 8:1, 4:1, and 2:1 were amorphous as evident from PXRD patterns in Figure 5.2. The extraction samples of the Al-Mg mixed oxides at Al:Mg ratios of 1:1, 1:2, 1:3, 1:4, and 1:8 were the mixture of hydrotalcite ($Mg_6Al_2CO_3(OH)_{16}\cdot 4H_2O$), brucite ($Mg(OH)_2$), and magnesium chloride hydroxide hydrate ($Mg_3(OH)_5Cl\cdot 4H_2O$, $Mg_3(OH)_5Cl\cdot 3H_2O$, and $Mg_2(OH)_3Cl\cdot 4H_2O$). The magnesia sample consisted of the same phases, except that the hydrotalcite phase was absent. The relative amounts of the brucite and magnesium chloride hydroxide hydrate increased with the increase of the magnesia content as shown in Figure 5.3.

The calcined products of the alumina and the magnesia were γ-Al_2O_3 and periclase (MgO), respectively. The PXRD patterns of the calcined products of the Al-Mg mixed oxides at Al:Mg ratios of 8:1, 4:1, and 2:1 showed mixed phases between γ-Al_2O_3 and periclase. The relative amount of the periclase phase in the Al-Mg mixed oxides increased with the increase of the magnesium content as seen in Figure 5.4. The Al-Mg mixed oxides at Al:Mg ratios of 1:1, 1:2, 1:3, 1:4, and 1:8 were the mixture between hydrotalcite ($Mg_6Al_2CO_3(OH)_{16}\cdot 4H_2O$) and periclase. The amount of the hydrotalcite phase in the Al-Mg mixed oxides was the highest at the Al:Mg ratio of 1:3 which was the exact ratio of Al:Mg in the hydrotalcite. The relative hydrotalcite content decreased as the Al:Mg ratio deviated from 1:3. In addition, the Al-Mg mixed oxides had higher relative amount of periclase phase with the increase of the magnesia content as seen in Figure 5.5. The change in the relative amount of each phase was consistent with the molar ratio of Al:Mg in the samples.

The PXRD results suggested that the Al_2O_3 and MgO phases of Al-Mg mixed oxides did not mix as a homogeneous solid solution and only hydrotalcite had the atomic mixture of Al-Mg. This was attributed to the differences in the hydrolysis rate of $Al(O^iPr)_3$ and $Mg(NO_3)_2$, as well as the condensation rate of Al and Mg intermediates during the synthesis of the as-synthesized Al-Mg mixed oxides. The appearance of chloride in some of the phases might be due to the chloride ions from HCl which incorporated into the solid structure after the extraction of the template because chloride compounds were less soluble in ethanol extraction solvent and chloride ions could strongly coordinate with aluminum ions [65].

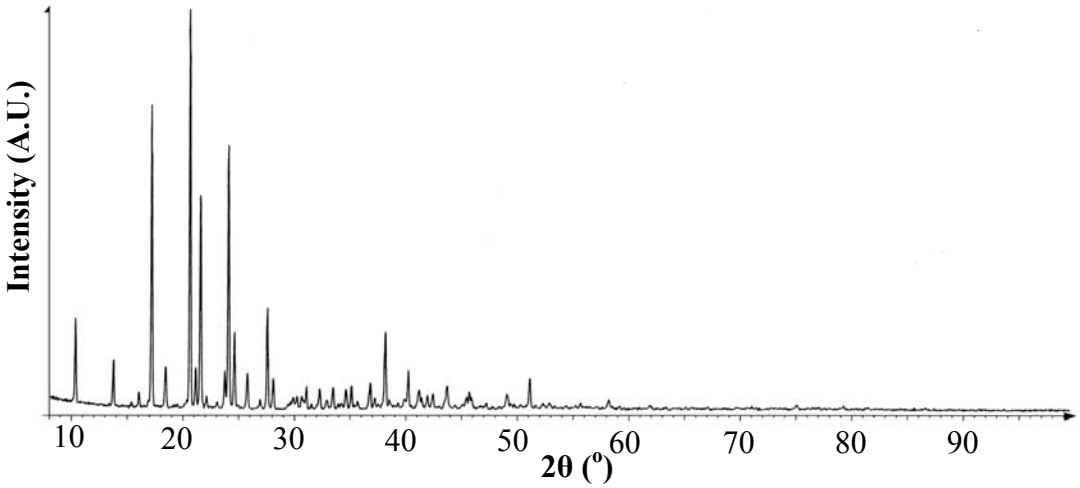

Figure 5.1 PXRD pattern of CTAB.

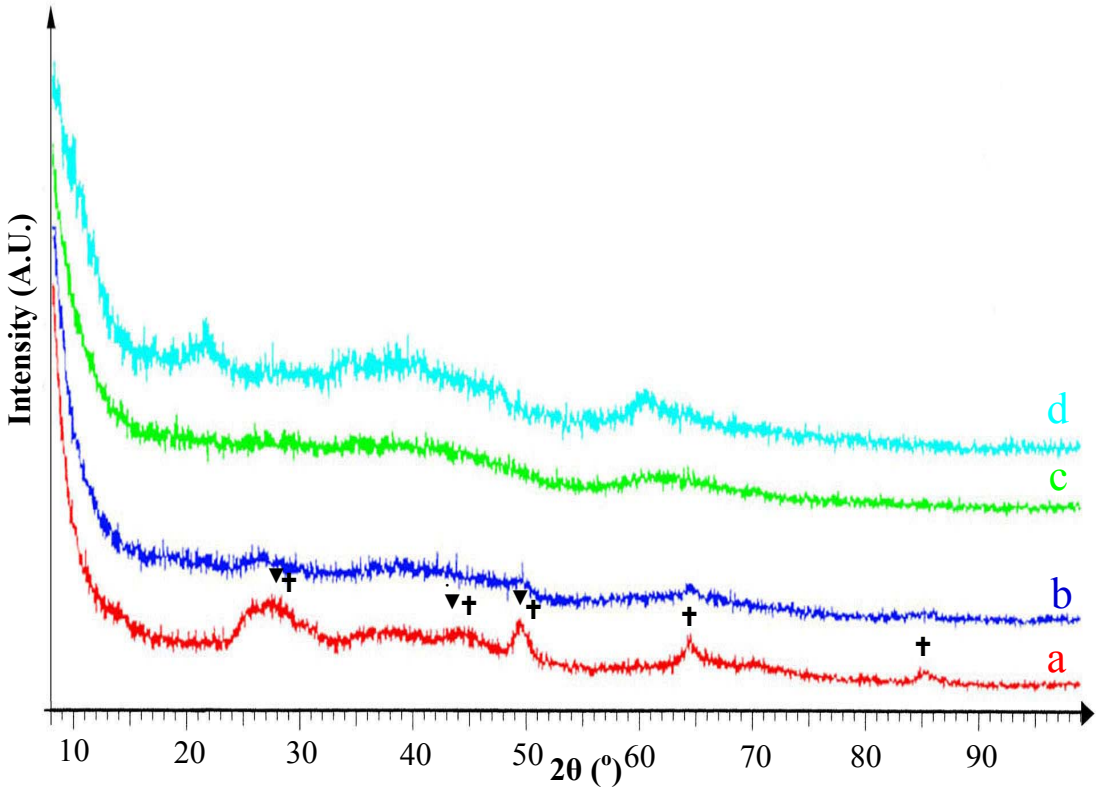

Figure 5.2 PXRD patterns of extraction samples of (a) the alumina, the Al-Mg mixed oxide at Al:Mg ratios of (b) 8:1, (c) 4:1, and (d) 2:1. (▼) aluminum oxide chloride (AlOCl), (✝) aluminum oxide chloride hydroxide ($Al_{17}O_{16}(OH)_{16}Cl_3$).

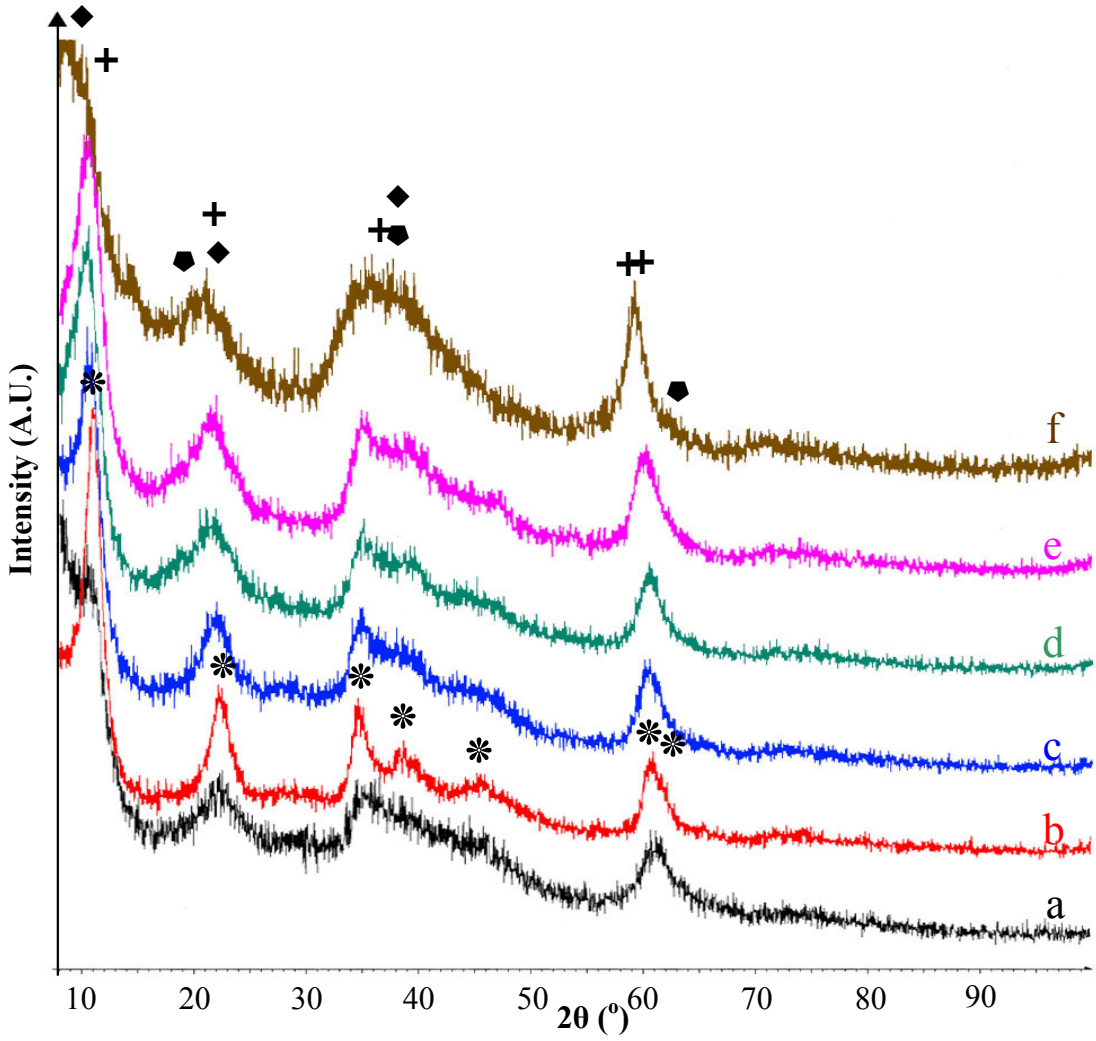

Figure 5.3 PXRD patterns of extraction samples of the Al-Mg mixed oxide at Al:Mg ratios of (a) 1:1, (b) 1:2, (c) 1:3, (d) 1:4, (e) 1:8, and (f) the magnesia. (*) hydrotalcite ($Mg_6Al_2CO_3(OH)_{16}\cdot 4H_2O$), (⬟) brucite ($Mg(OH)_2$), (+) magnesium chloride hydroxide hydrate ($Mg_3(OH)_5Cl$), (◆) magnesium chloride hydroxide hydrate ($Mg(OH)_3Cl\cdot 4H_2O$).

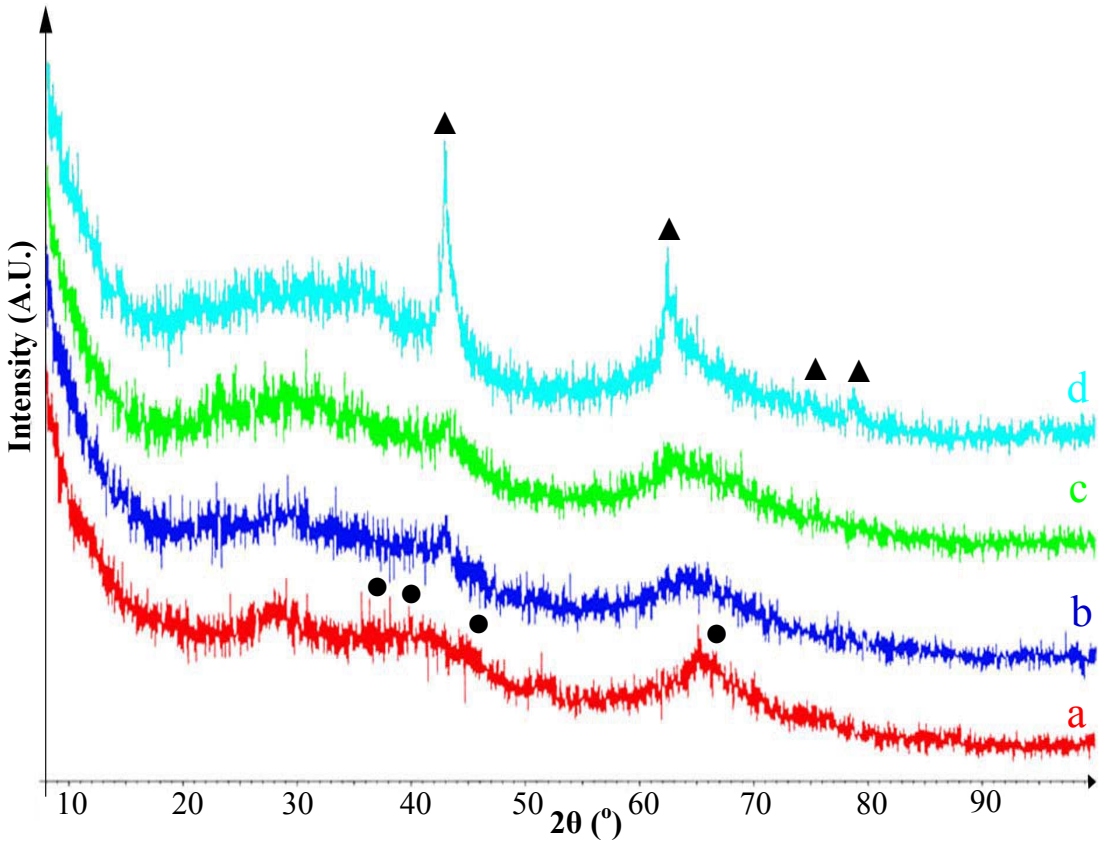

Figure 5.4 PXRD patterns of calcined products of (a) the alumina, the Al-Mg mixed oxide at Al:Mg ratios of (b) 8:1, (c) 4:1, and (d) 2:1. (●) γ-Al_2O_3, (▲) periclase (MgO).

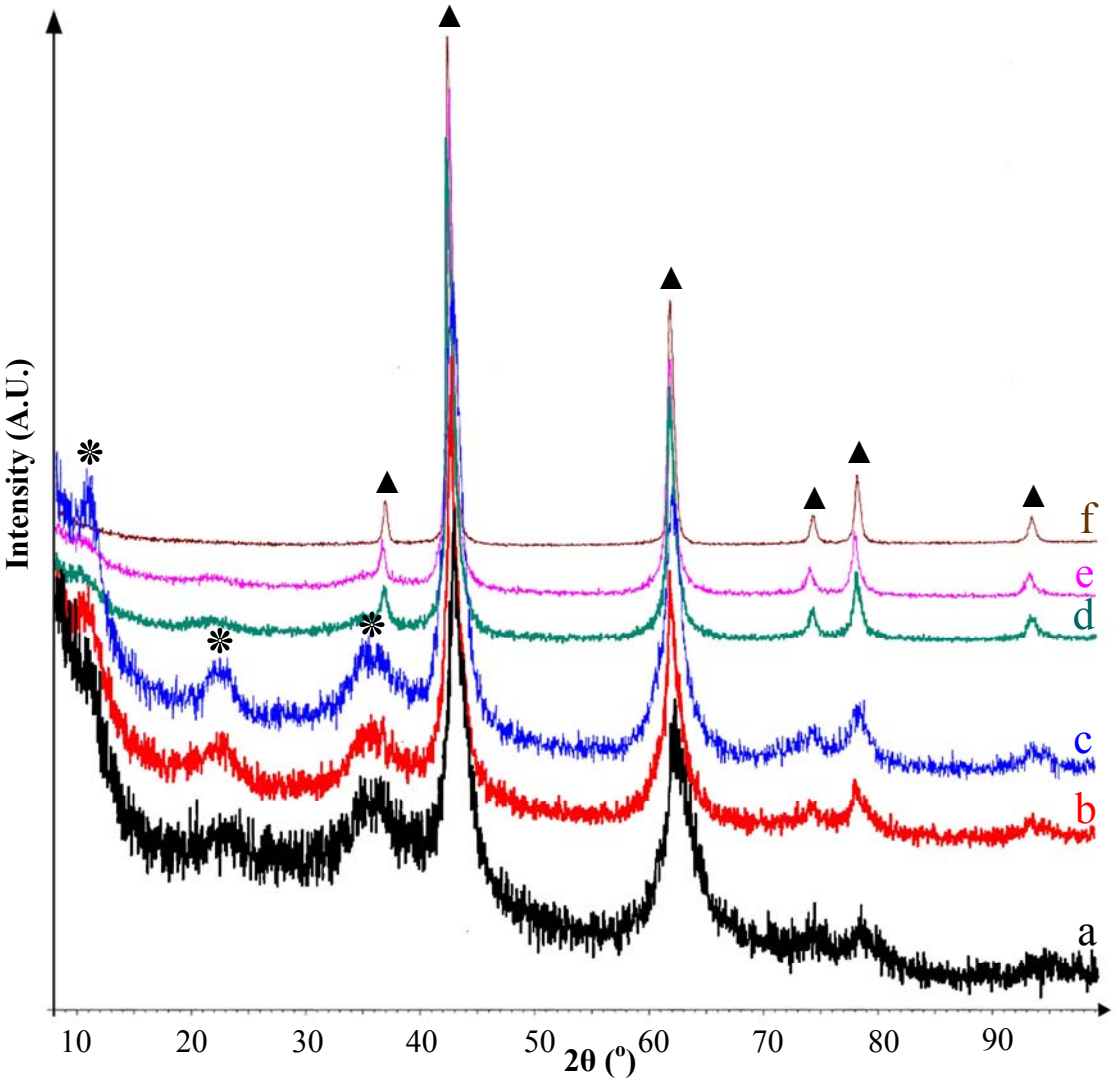

Figure 5.5 PXRD patterns of calcined products of the Al-Mg mixed oxide at Al:Mg ratios of (a) 1:1, (b) 1:2, (c) 1:3, (d) 1:4, (e) 1:8, and (f) the magnesia. (▲) periclase (MgO), (*) hydrotalcite ($Mg_6Al_2CO_3(OH)_{16}\cdot 4H_2O$).

5.1.2 Alkali doped Al-Mg mixed oxides

The PXRD patterns of the as-synthesized KI doped alumina and Al-Mg mixed oxides at Al:Mg ratios of 8:1, 4:1, and 2:1 showed the mixture of phases: aluminum oxide chloride hydroxide ($Al_{17}O_{16}(OH)_{16}Cl_3$), nordstrandite ($Al(OH)_3$), potassium iodide (KI), and potassium iodate (KIO_3). The relative amount of the nordstrandite in the as-synthesized KI doped Al-Mg mixed oxide increased with the increase of magnesium content but this phase was not found in the as-synthesized KI doped alumina as shown in Figure 5.6. In addition, the PXRD patterns of the as-synthesized KI doped Al-Mg mixed oxides at Al:Mg ratios of 1:1, 1:2, 1:3, 1:4, 1:8, and the as-synthesized KI doped magnesia showed the mixed phases of hydrotalcite, potassium iodide, and potassium iodate. The brucite was found in the as-synthesized KI doped magnesia instead of hydrotalcite as shown if Figure 5.7. The presence of potassium iodate in the as-synthesized KI doped samples indicated the partial oxidation of potassium iodide to potassium iodate during impregnation procedure. The calcined product of the KI doped alumina only had γ-Al_2O_3 phase and no appearance of potassium species, suggesting the well-dispersed potassium species on the alumina. The calcined products of the KI doped Al-Mg mixed oxides at Al:Mg ratios of 8:1, 4:1, and 2:1 had the same phases as the undoped KI samples, beside the additional appearance of potassium iodate, as shown in Figure 5.8. The PXRD patterns of the calcined products of the KI doped Al-Mg mixed oxides at Al:Mg ratios of 1:1, 1:2, 1:3, 1:4, 1:8, and the magnesia showed mixed phases of periclase, KI and KIO_3. The Al-Mg mixed oxide at Al:Mg ratio of 1:1 had the highest relative amount of KI phase. The Al-Mg mixed oxide at Al:Mg ratio of 1:2 had the highest relative amount of KIO_3. However, no regular trend was observed as shown in Figure 5.9. The average crystalline sizes of KI (200) and KIO_3 (220) of the calcined KI doped Al-Mg mixed oxides and magnesia were 2.20-96.57 and 2.69-151.11 nm, respectively. The PXRD pattern of the as-synthesized KNO_3 doped Al-Mg mixed oxide at Al:Mg ratio of 1:4 showed the mixed phases between hydrotalcite and niter (KNO_3). Its calcined product had mixed phases of periclase, potassium aluminum chloride oxide ($KAlCl_2O$), niter, and potassium oxide (K_2O). The results suggested that KNO_3 partially decomposed to K_2O upon calcinations at 550 ^oC as shown in Figure 5.10. The average crystalline size

of KNO_3 (111) and K_2O (200) of the calcined KNO_3 doped Al-Mg mixed oxide at Al:Mg of 1:4 were 31.95 and 38.89 nm, respectively.

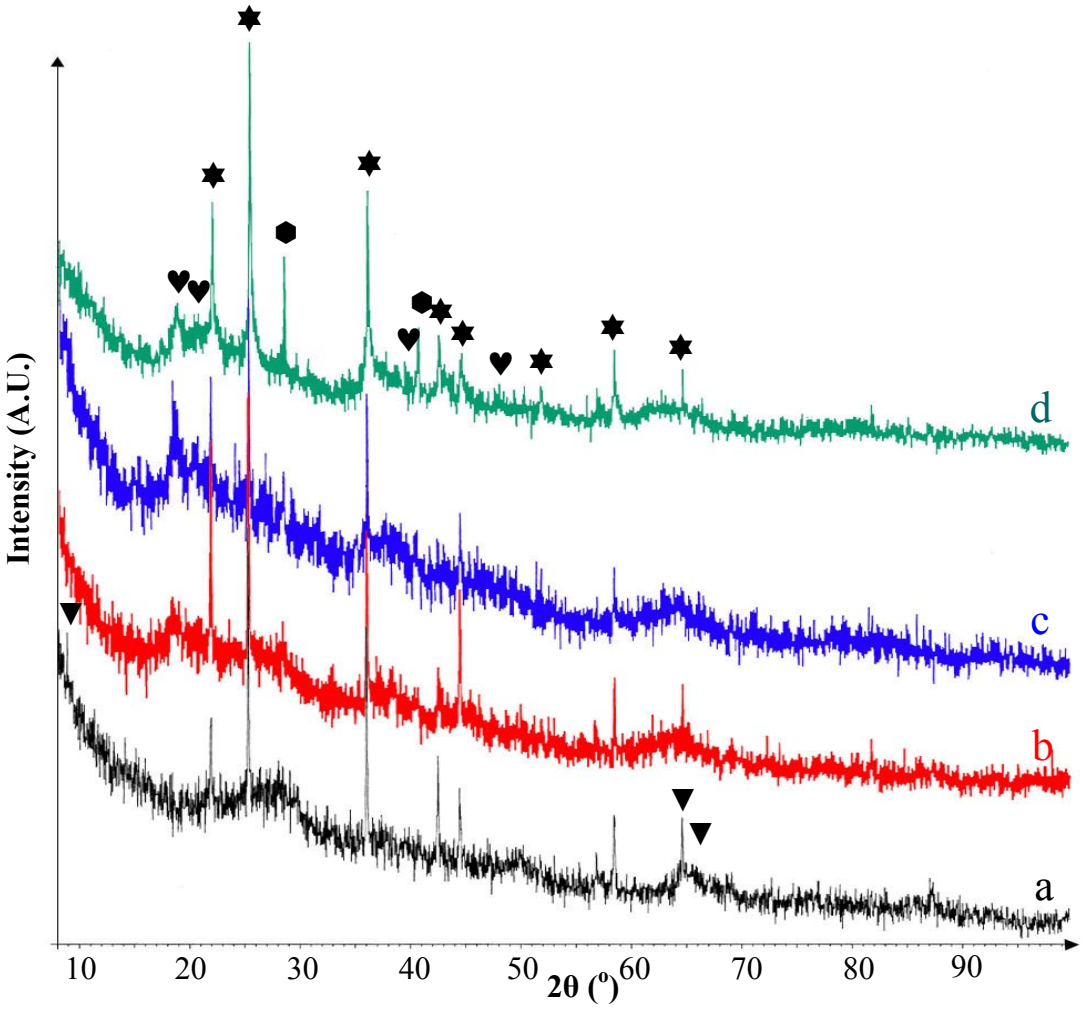

Figure 5.6 PXRD patterns of the as-synthesized KI doped (a) alumina, Al-Mg mixed oxides at Al:Mg ratios of (b) 8:1, (c) 4:1, and (d) 2:1. (▼) aluminum oxide chloride hydroxide ($Al_{17}O_{16}(OH)_{16}Cl_3$), (♥) nordstrandite ($Al(OH)_3$) (★) potassium iodide (KI), (⬢) potassium iodate (KIO_3).

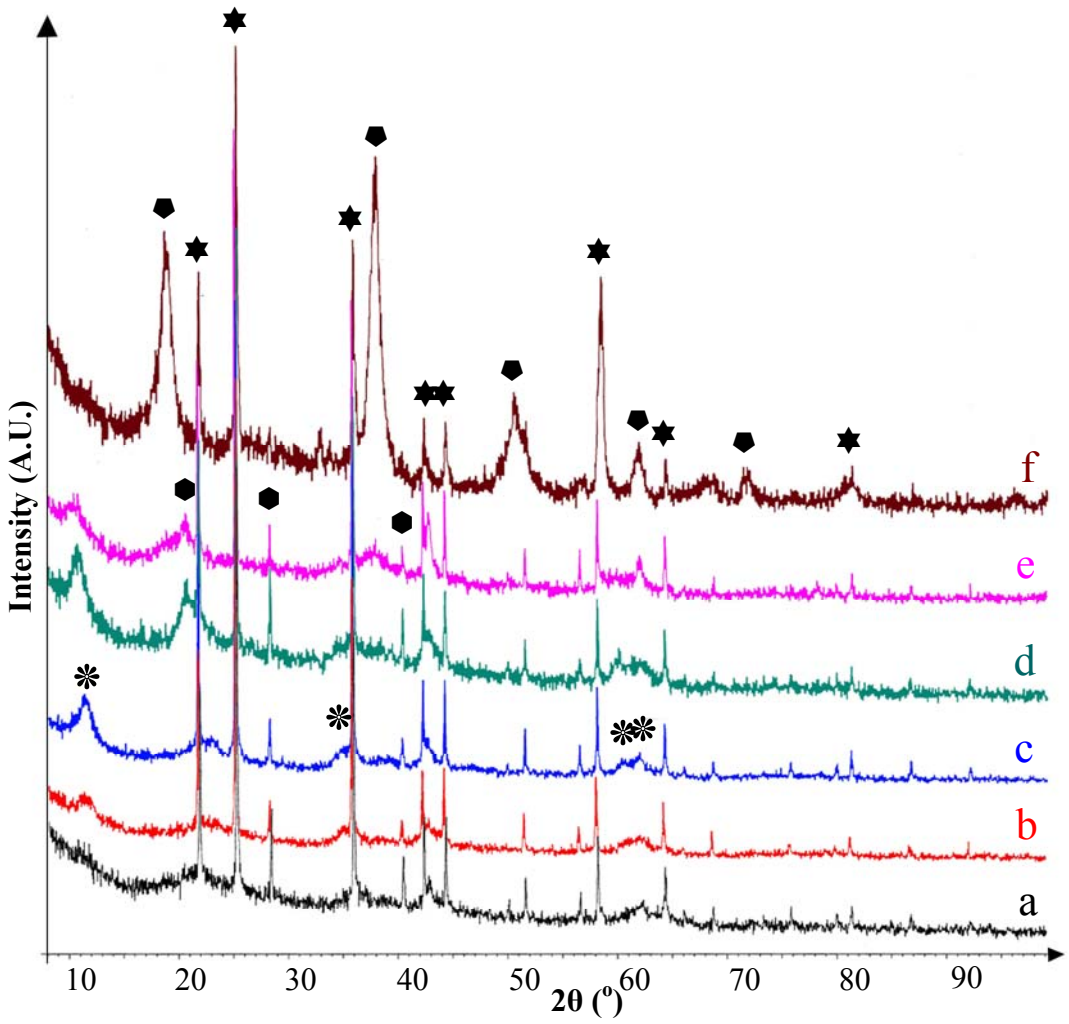

Figure 5.7 PXRD patterns of the as-synthesized KI doped Al-Mg mixed oxides at Al:Mg ratios of (a) 1:1, (b) 1:2, (c) 1:3, (d) 1:4, (e) 1:8, and (f) the magnesia. (*) hydrotalcite ($Mg_6Al_2CO_3(OH)_{16}\cdot 4H_2O$), (⬟) brucite, (★) potassium iodide, (⬢) potassium iodate.

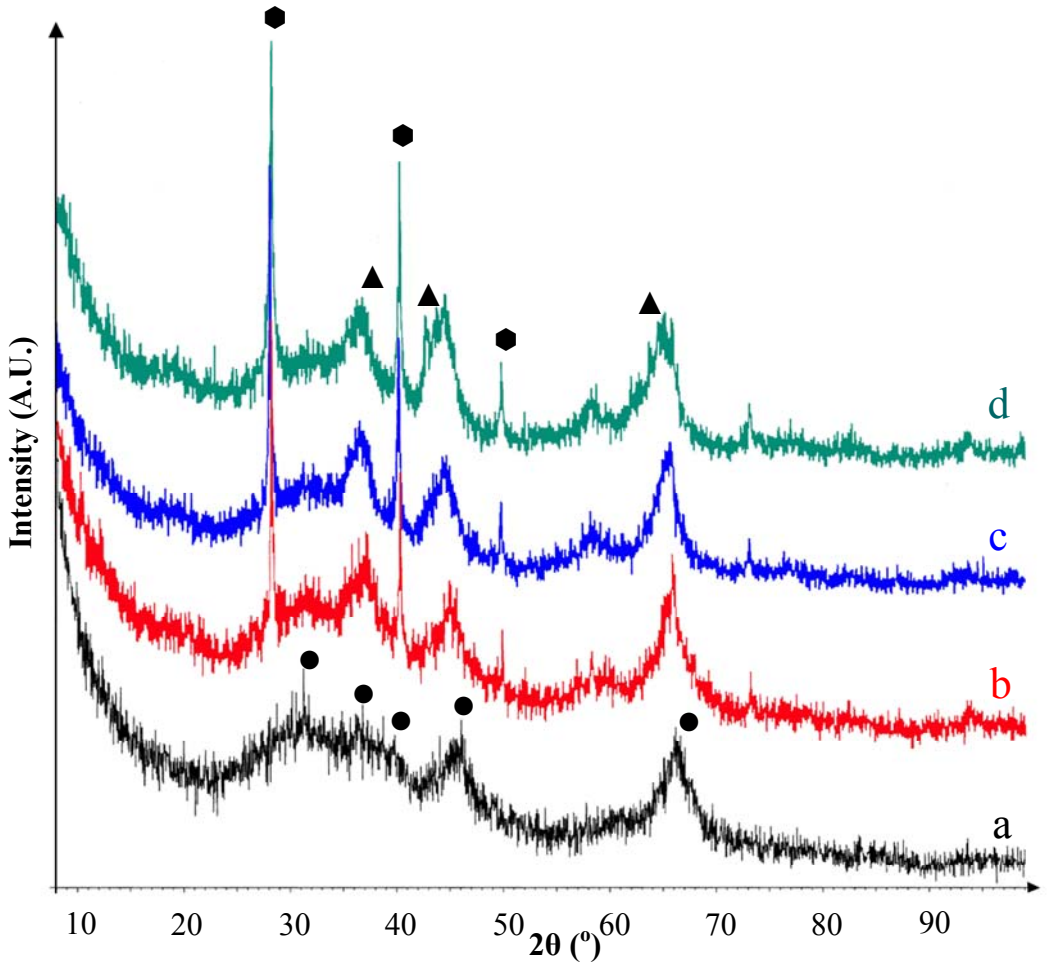

Figure 5.8 PXRD of patterns of the calcined products of the KI doped (a) alumina, Al-Mg mixed oxides at Al:Mg ratios of (b) 8:1, (c) 4:1, and (d) 2:1. (●) γ-Al_2O_3, (▲) periclase, (⬢) potassium iodate**.**

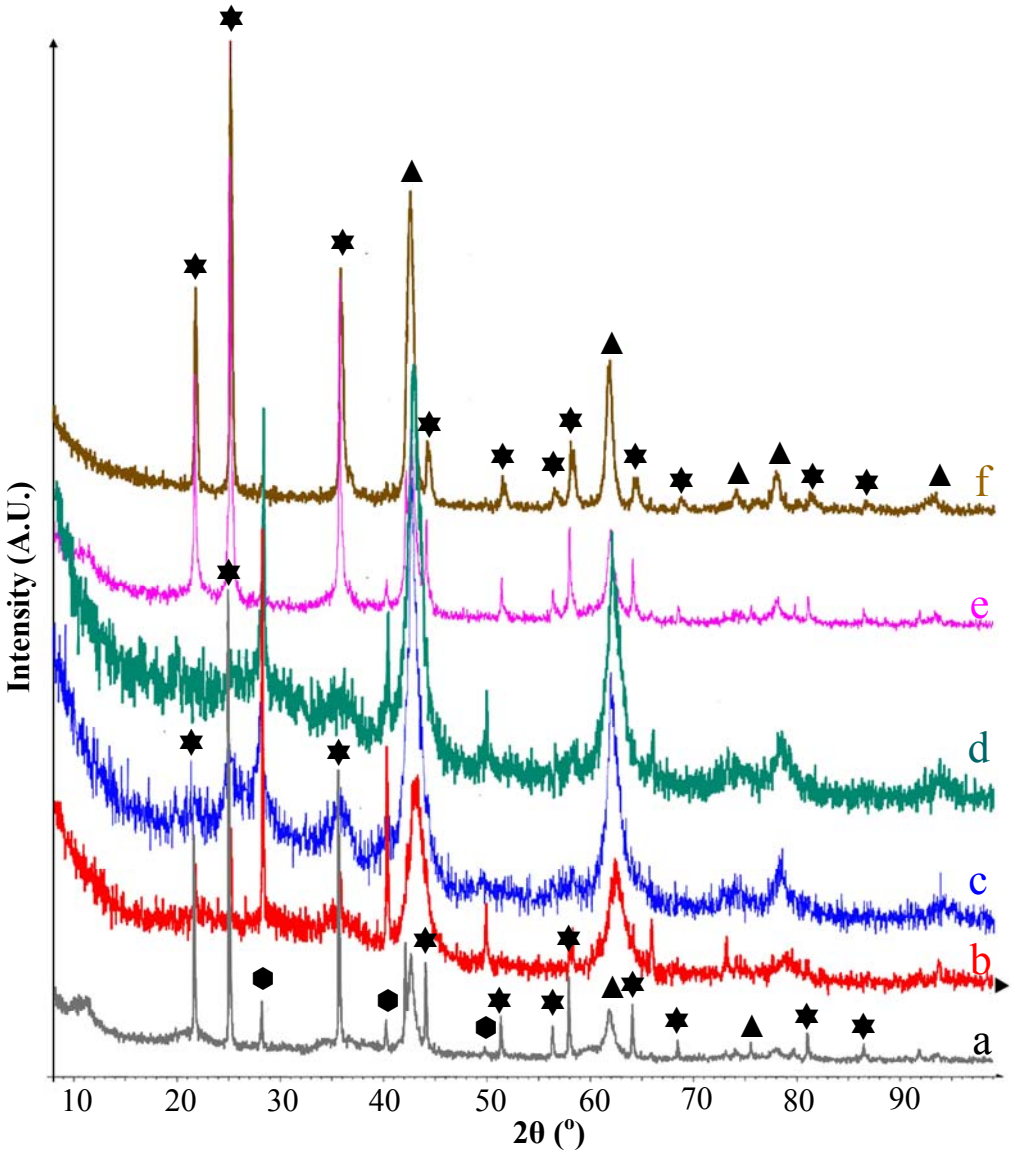

Figure 5.9 PXRD patterns of the calcined products of the KI doped Al-Mg mixed oxide at Al:Mg ratios of (a) 1:1, (b) 1:2, (c) 1:3, (d) 1:4, (e) 1:8, and (f) the magnesia. (▲) periclase, (★) potassium iodide, (⬢) potassium iodate.

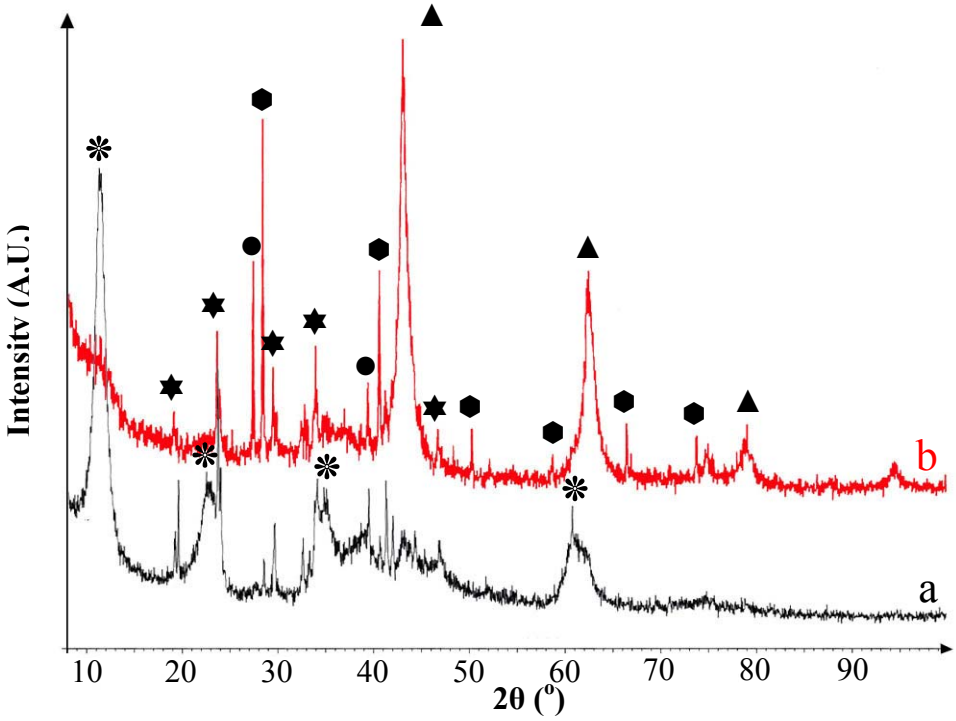

Figure 5.10 PXRD patterns of the KNO_3 doped Al-Mg mixed oxide at Al:Mg ratio of 1:4, (a) the as-synthesized and (b) the calcined products. (▲) periclase, (*) hydrotalcite, (⬢) potassium aluminum chloride oxide ($KAlCl_2O$), (★) niter (KNO_3), (●) potassium oxide (K_2O).

5.2 FOURIER-TRANSFORM INFRARED SPECTROSCOPY (FT-IR)

5.1.1 Al-Mg mixed oxides

The infrared spectra of all the as-synthesized samples showed similar patterns. The infrared spectrum of the as-synthesized Al-Mg mixed oxide at Al:Mg ratio of 1:4 exhibited the broad intense band at 3435 cm^{-1} due to OH stretching of water molecules and the bands at 1638 and 912-964 cm^{-1} were attributed to the in-plane and out-of-plane OH bending, respectively [72]. The bands at 2850 and 2919 cm^{-1} were assigned to C-H stretching of CH_3 and CH_2 of the CTAB [73]. The bands at 1385-1488 cm^{-1} were assigned to N-O stretching of NO_3^- [58]. The bands in the 800-400 cm^{-1} region were assigned to the stretching of Al-O-Mg, Al-O or Mg-O [73]. The infrared spectra of the extraction samples had similar patterns with those of the as-synthesized samples but the intensities decreased and the C-H stretching and bending bands disappeared, indicating the complete decomposition of organic portion. The bands at 1546-1561 cm^{-1} were attributed to C-O stretching of carbonate anions (CO_3^{2-}) that might come from CO_2 in air during the extraction procedure [58]. The infrared spectra of the calcined products exhibited similar patterns with those of the extraction samples However, the C-O stretching bands of carbonate anion disappeared, indicating the decomposition of the carbonate ions during calcination under oxidizing atmosphere. These results were in agreement with the PXRD results, which suggested the presence of hydrotalcite phase, which contained carbonate ions, in the sample after extraction and the relative amount of hydrotalcite decreased upon calcination. The infrared spectra of the Al-Mg mixed oxides with Al:Mg ratio of 1:4 at various preparation steps were shown in Figure 5.11.

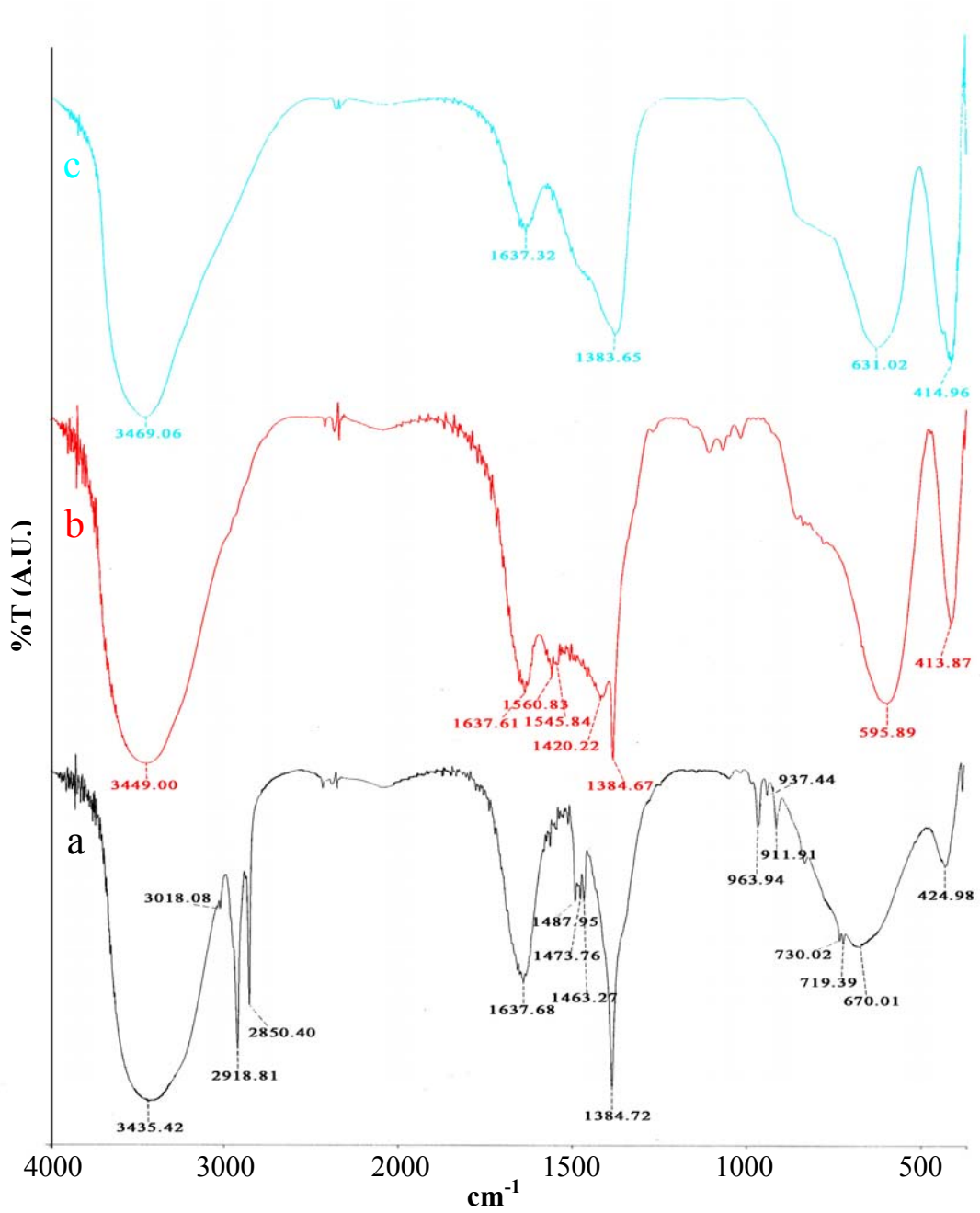

Figure 5.11 FT-IR spectra of the Al-Mg mixed oxides at Al:Mg ratio of 1:4 : (a) the as-synthesized, (b) the extraction, and (c) the calcined samples.

5.1.2 Alkali doped Al-Mg mixed oxides

. The as-synthesized alkali doped catalysts exhibited similar IR spectra to those of the calcined Al-Mg mixed oxides except the presence of C-O stretching band of carbonate anions. The exposure to air and water during alkali impregnation might cause the incorporation of CO_3^{2-} ions into the structure. As the hydrotalcite phase was found in the PXRD experiment. The IR spectra of the calcined products of the alkali doped Al-Mg mixed oxides had similar pattern to those of the as-synthesized alkali doped samples but the intensities at 1540-1560 cm^{-1} decreased a little, indicating that the carbonate ions in the samples partially decomposed. The example of the typical IR spectra of the alkali doped Al-Mg mixed oxide before and after calcination was shown in Figure 5.12.

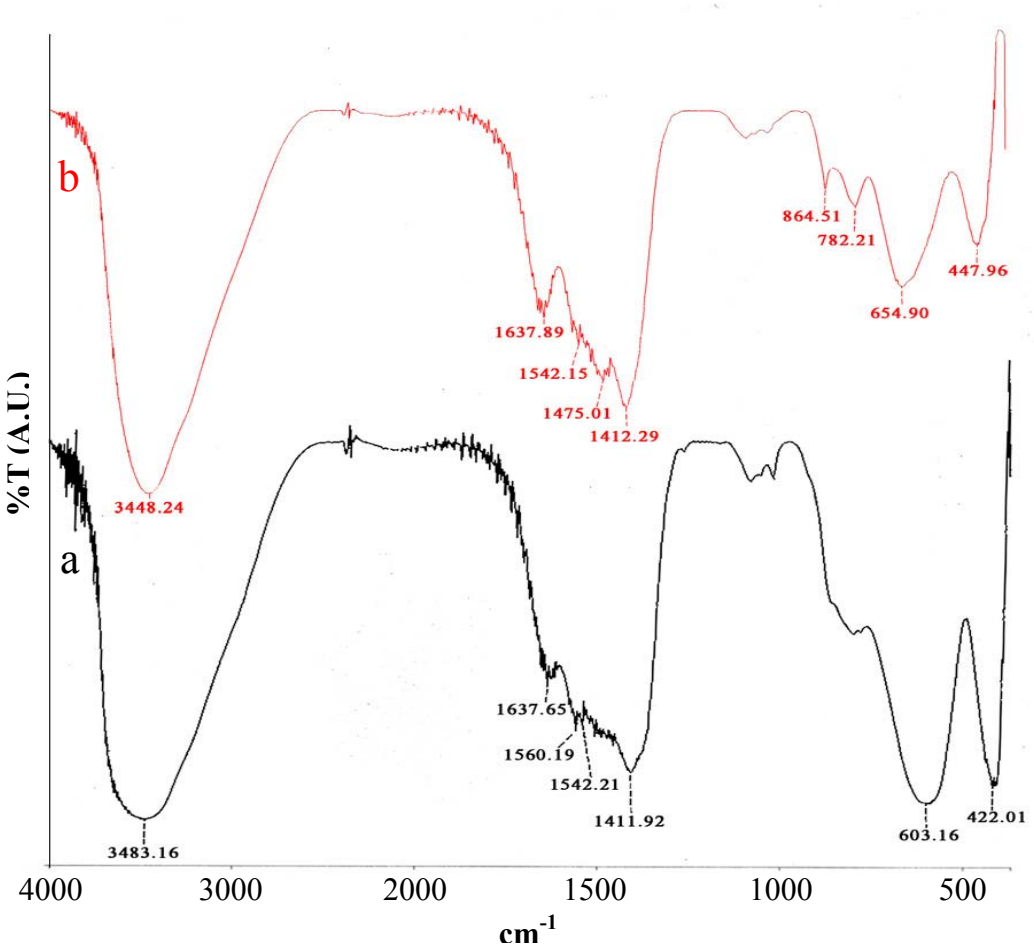

Figure 5.12 FT-IR spectra of the KI doped Al-Mg mixed oxide at Al:Mg ratio of 1:4 (a) the as-synthesized and (b) the calcined samples.

5.3 THERMAL ANALYSIS

Thermogravimetry analysis and differential thermal analysis (TGA-DTA) of the CTAB were shown in Figure 5.13. The TGA result indicated a two-step complete decomposition of CTAB. The first mass change occurred at above 200 ^{o}C with a mass loss of over 90 % and the second mass change at above 400 ^{o}C. The former mass change was attributed to the decomposition of CTAB, and the latter was to the decomposition of carbon residue[74]. The DTA of CTAB (Figure 5.13b) displayed one endothermic peak at 114 ^{o}C and three exothermic peaks at 208, 324, and 492 ^{o}C. The endothermic process was probably due to the desorption of physisorbed water in CTAB. The first two exothermic peaks (at 208, and 324 ^{o}C) were possibly associated with the decomposition of CTAB, as they were in the same temperature vicinity as the major mass loss (90 %). The last exothermic peak at 492 ^{o}C was attributed to the combustion of the carbon residue. The TGA-DTA results of the as-synthesized alumina, Al-Mg mixed oxides at Al:Mg ratios of 2:1 and 1:2, and magnesia showed similar patterns. Nevertheless, the combustion of carbon residue in the as-synthesized Al-Mg mixed oxides took place at higher temperature (526 ^{o}C and 537 ^{o}C for the Al-Mg mixed oxides at Al:Mg ratios of 2:1 and 1:2, respectively) than the as-synthesized alumina (509 ^{o}C) and the as-synthesized magnesia (501 ^{o}C) samples. In addition, the decomposition of CTAB in the as-synthesized samples occurred at higher temperature than that of the CTAB itself. According to Figure 5.13 c-h, the DTA results revealed the exothermic decomposition at 343, 343, 330, and 346 ^{o}C for the as-synthesized alumina, Al-Mg mixed oxides at Al-Mg ratios of 2:1 and 1:2, and magnesia, respectively, indicating the interactions between the oxides and CTAB. Furthermore, the exothermic peak at about 300 ^{o}C in the DTAs of the as-synthesized Al-Mg mixed oxides and that of the as-synthesized magnesia, which was absent in the DTAs of the CTAB and the as-synthesized alumina, was likely due to the dehydroxylation of $Mg(OH)_2$ [75].

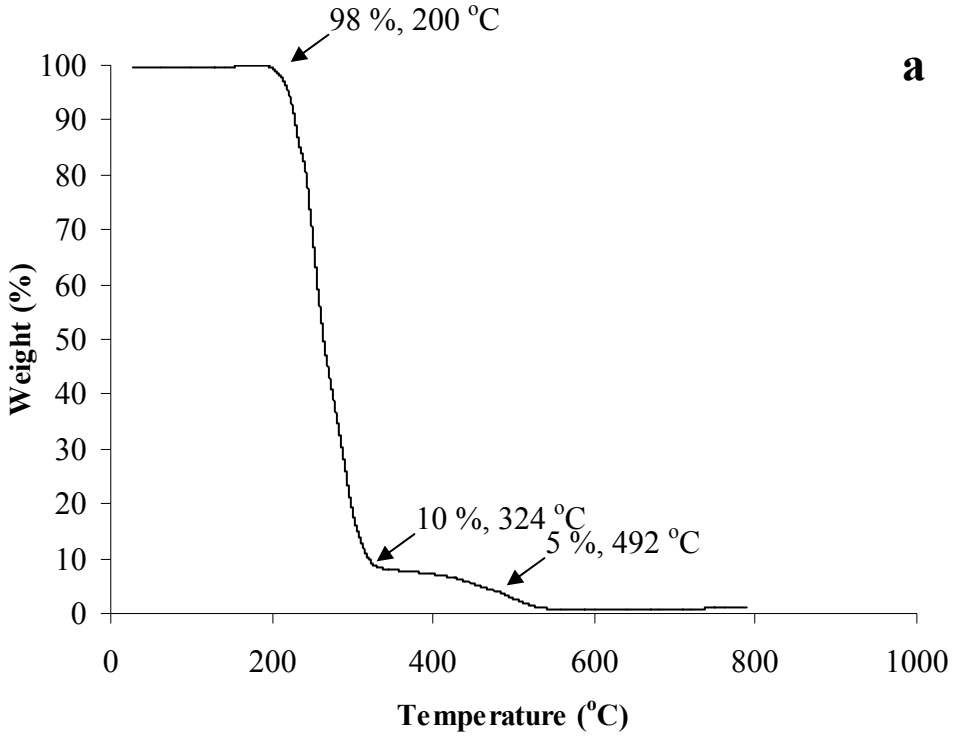
98 %, 200 °C
a
100
90
80
70
60
50
40
30
20
10
0
Weight (%)
10 %, 324 °C
5 %, 492 °C
0
200
400
600
800
1000
Temperature (°C)

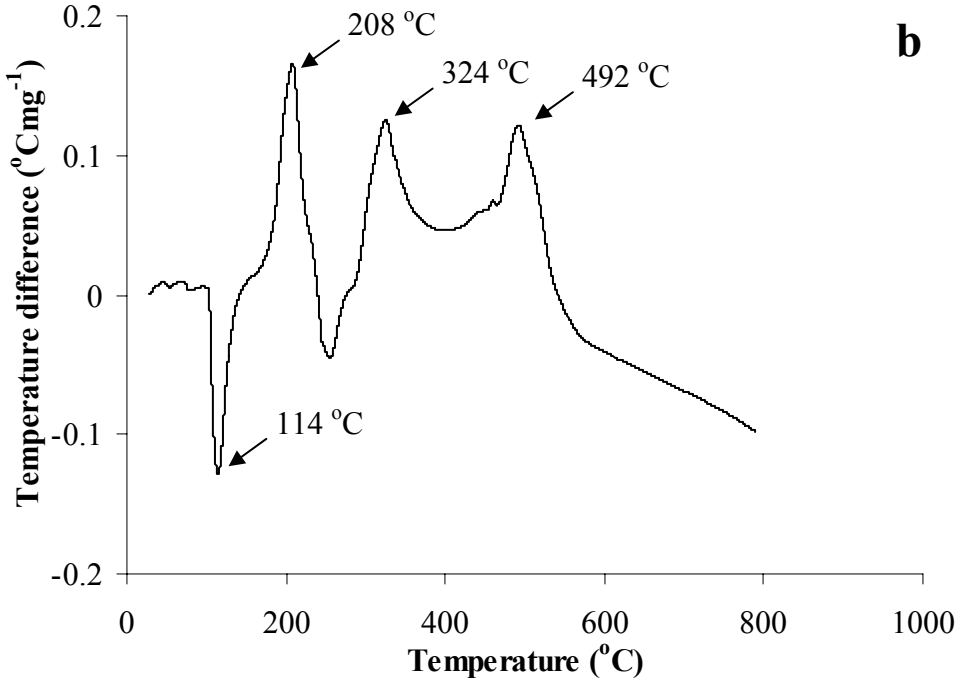
0.2
0.1
0
-0.1
-0.2
Temperature difference (°Cmg-1)
208 °C
324 °C
492 °C
b
114 °C
0
200
400
600
800
1000
Temperature (°C)

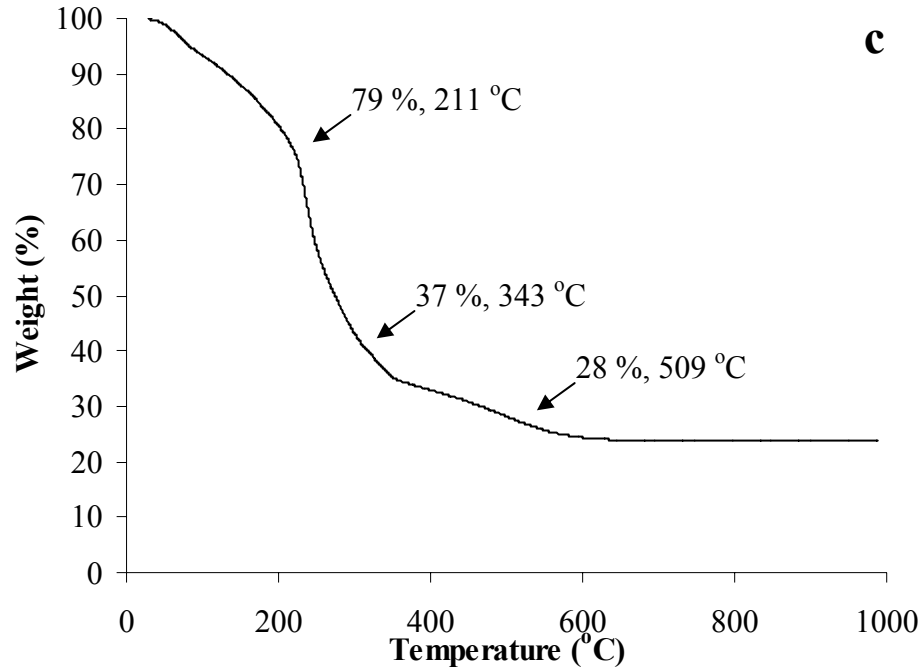
c
79 %, 211 °C
37 %, 343 °C
28 %, 509 °C
Weight (%)
Temperature (°C)
100
90
80
70
60
50
40
30
20
10
0
0
200
400
600
800
1000

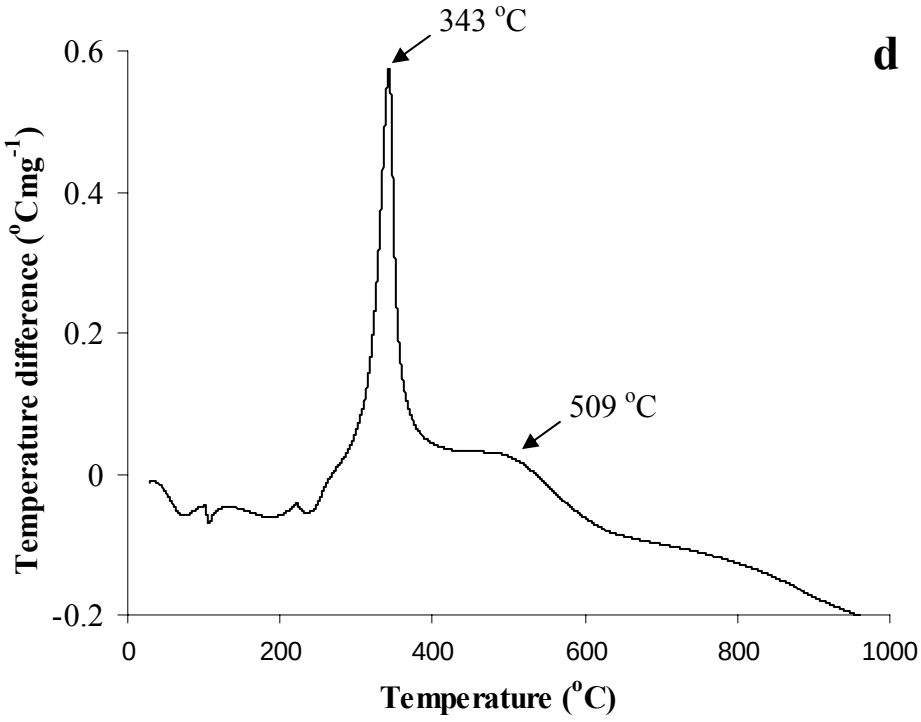
d
343 °C
509 °C
Temperature difference (°Cmg-1)
Temperature (°C)
0.6
0.4
0.2
0
-0.2
0
200
400
600
800
1000

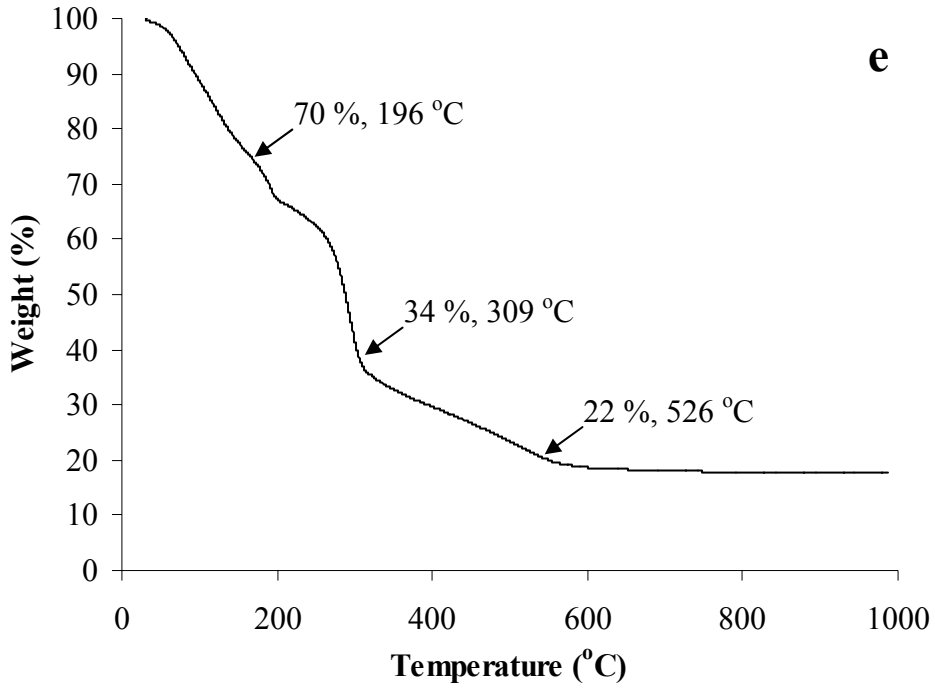
e
70 %, 196 °C
34 %, 309 °C
22 %, 526 °C
Weight (%)
Temperature (°C)
100
90
80
70
60
50
40
30
20
10
0
0
200
400
600
800
1000

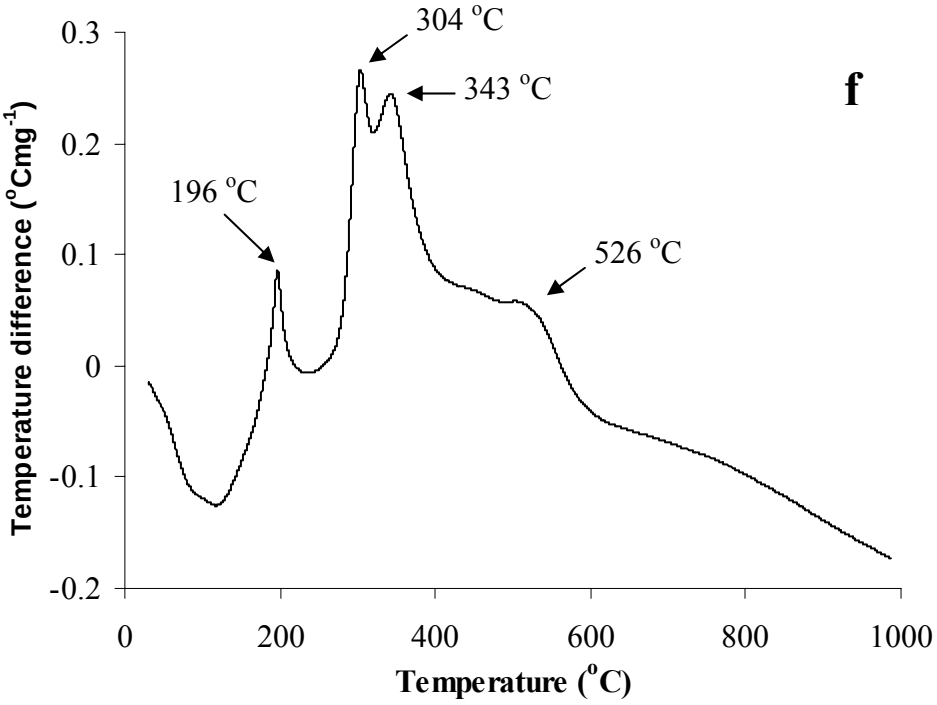
f
304 °C
343 °C
196 °C
526 °C
Temperature difference (°Cmg-1)
0.3
0.2
0.1
0
-0.1
-0.2
0
200
400
600
800
1000
Temperature (°C)

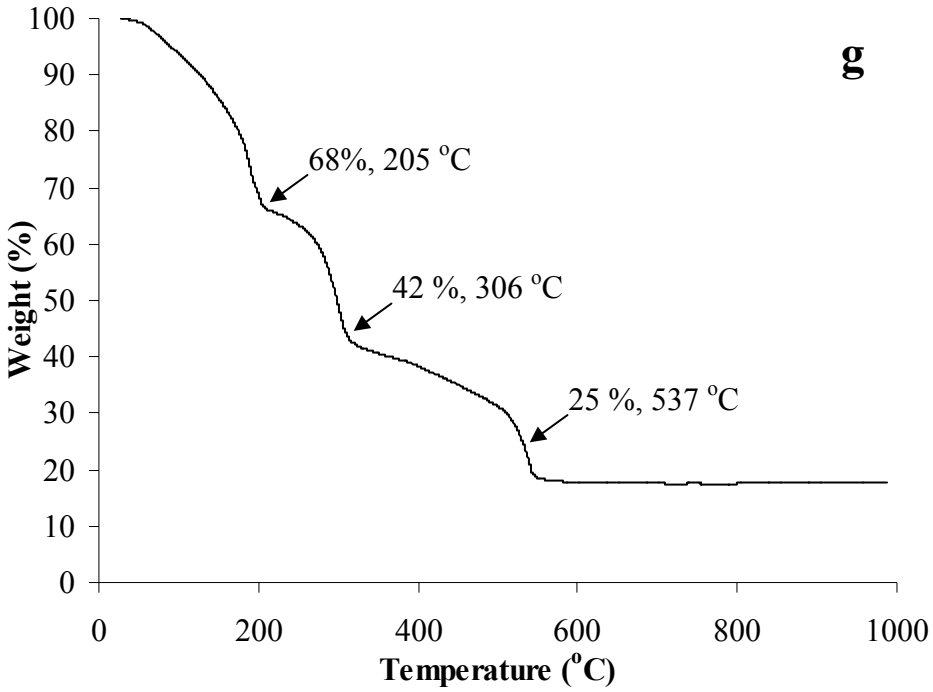
g
68%, 205 °C
42 %, 306 °C
25 %, 537 °C
Weight (%)
Temperature (°C)
100
90
80
70
60
50
40
30
20
10
0
0
200
400
600
800
1000

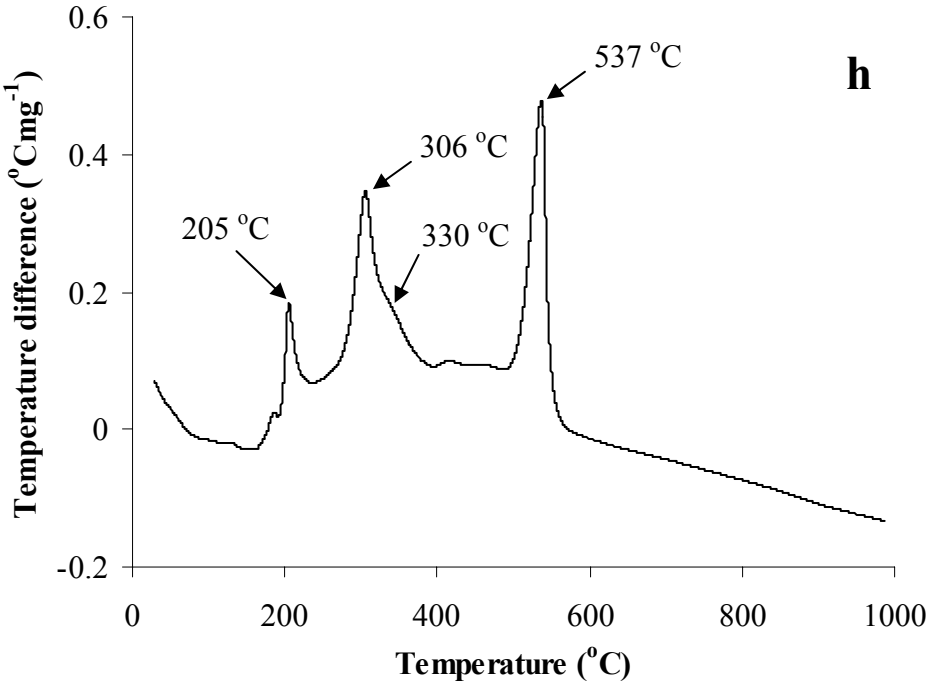
h
537 °C
306 °C
205 °C
330 °C
Temperature difference (°Cmg-1)
Temperature (°C)
0.6
0.4
0.2
0
-0.2
0
200
400
600
800
1000

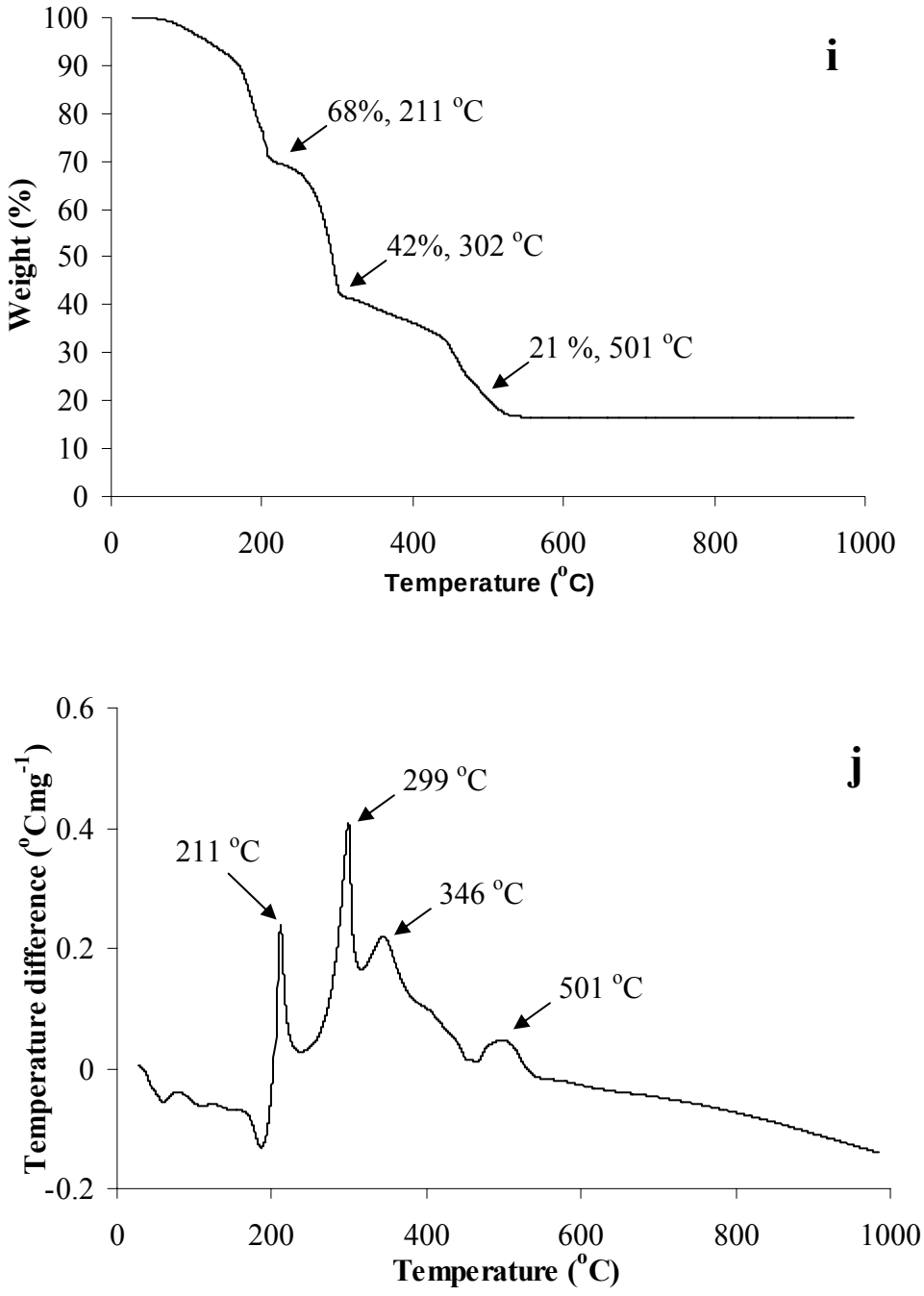

Figure 5.13 TGA curves of (a) CTAB, (c) as-synthesized alumina, (e) as-synthesized Al-Mg mixed oxides at Al:Mg ratios of 2:1, (g) 1:2, and (i) as-synthesized magnesia and DTA curves of (b) CTAB, (d) as-synthesized alumina, as-synthesized Al-Mg mixed oxides at Al:Mg ratios of (f) 2:1, (h) 1:2, and (g)as-synthesized magnesia.

5.4 TRANSMISSION ELECTRON MICROSCOPY (TEM)

TEM images of all calcined products of alumina, Al-Mg mixed oxides, and magnesia (Figure 5.14 a-f) showed worm whole-like structure and they had less porosity with increasing magnesia content. The calcined magnesia sample displayed no feature of mesoporous structure (Figure 5.14 f). Hence, the presence of the magnesia might lead to the collapse of the porous structure.

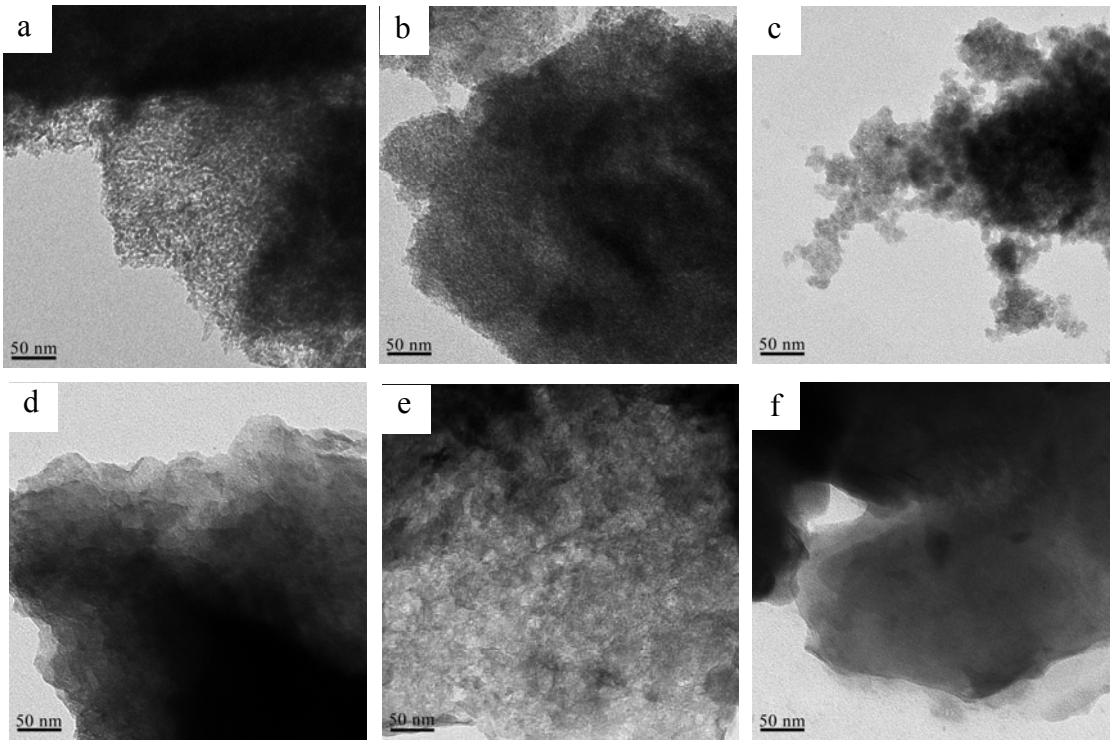

Figure 5.14 TEM images of the calcined products of (a) the alumina, (b) the Al-Mg mixed oxides at Al:Mg ratios of 4:1, (c) 2:1, (d) 1:2 , (e) 1:4, and (f) the magnesia. Bar scales in the images are 50 nm.

5.5 N_2 ADSORPTION-DESORPTION MEASUREMENT

Textural properties of calcined products of the alumina, the Al-Mg mixed oxides, and the magnesia were summarized in Table 5.1. The BET surface areas of the alumina, the Al-Mg mixed oxides at Al:Mg ratios of 8:1, 4:1, and 2:1 were similar (211-230 m^2g^{-1}) and the BET surface areas of the Al-Mg mixed oxides decreased as the Al:Mg ratio changed from 2:1 to 1:1 and increased as the Al:Mg ratio changed from 1:1 to 1:4 and decreased again as the Al:Mg ratio changed from 1:4 to the pure magnesia. Likewise, the total pore volumes decreased as the Al:Mg ratio changed from 8:1 to 1:1 and increased as the Al:Mg ratio changed from 1:1 to the pure magnesia. Nevertheless, the average pore sizes exhibited no correlation with the Al-Mg content.

The average crystalline sizes of KI and KIO_3 of the calcined KI doped Al-Mg mixed oxides and magnesia were larger than average pore diameter of the calcined Al-Mg mixed oxides and magnesia. Likewise, the crystalline size of K_2O of the calcined Al-Mg mixed oxide at Al:Mg ratio of 1:4 was larger than the average pore diameter of the calcined Al-Mg mixed oxide at Al:Mg ratio of 1:4. Hence, the particles of KI, KIO_3, KNO_3, and K_2O were mostly on the external surface of the Al-Mg mixed oxides and magnesia.

The alumina and the Al-Mg mixed oxide at Al:Mg mixed ratio of 1:4 had narrow pore size distributions with average pore size of 4.7 and 3.9 nm, respectively, as shown in Figure 5.15. The other Al-Mg mixed oxides had similar pore size distribution curve, but the magnesia had a broad pore size distribution as shown in Figure 5.15. The N_2 adsorption-desorption isotherms of the alumina, the Al-Mg mixed oxides, and the magnesia (Figure 5.16) were similar and could be classified as the classical shape of type IV isotherm, indicating typical mesoporous solids. The hysteresis loop of the alumina displayed type E characteristic, indicating that the alumina had tubular or ink-bottom pores [76]. All Al-Mg mixed oxide samples had hysteresis loops of type B characteristic, indicating that the Al-Mg mixed oxides had capillary space between parallel plates or open slit-shaped capillary [76]. However, the isotherm of the magnesia indicated that the magnesia had spaces among particles

instead of pores. This result agreed with the TEM image and the BJH pore size distribution, where less pore structure and broad pore size distribution were observed.

Table 5.1 The physico-chemical properties of the alumina, the Al-Mg mixed oxide, and the magnesia.

Al:Mg ratio	BET surface area (m^2g^{-1})	Pore volume (cm^3g^{-1})	Average pore diameter (nm)
1:0	230	0.27	4.7
8:1	216	0.32	5.9
4:1	224	0.32	5.8
2:1	211	0.27	5.1
1:1	127	0.09	4.7
1:2	172	0.13	5.2
1:3	252	0.18	3.8
1:4	266	0.19	3.9
1:8	205	0.25	7.2
0:1	96	0.38	16.3

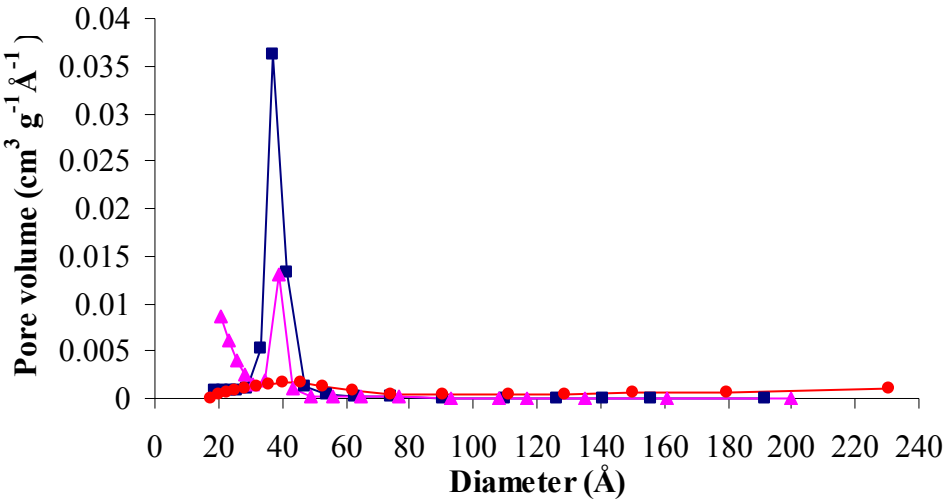

Figure 5.15 BJH pore size dritribution of (■) the calcined alumina, (▲) the calcined Al-Mg mixed oxide at Al:Mg ratio of 1:4, and (●) the calcined magnesia.

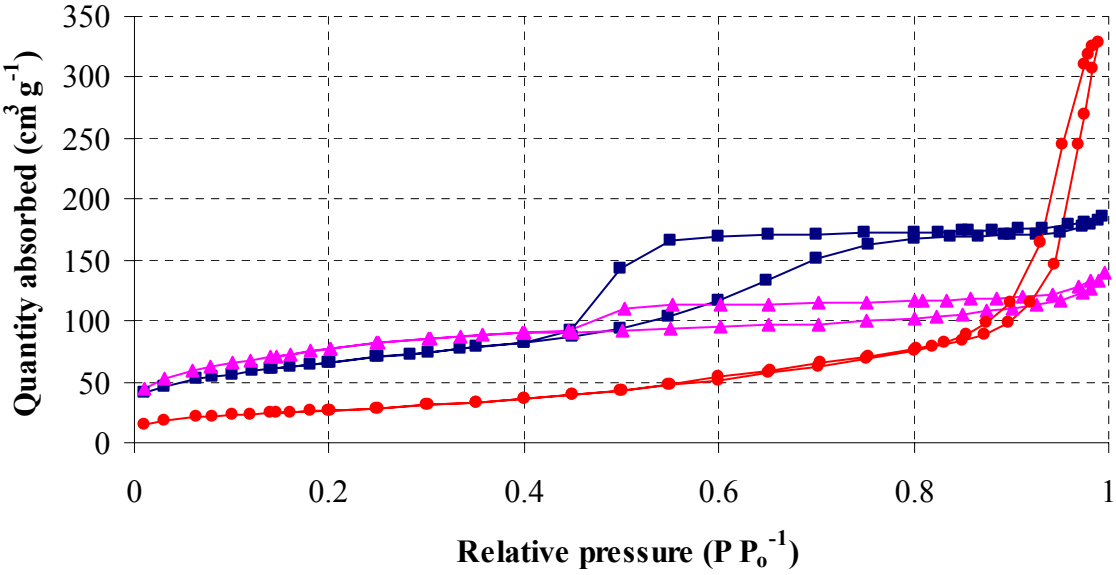

Figure 5.16 N_2 adsorption-desorption isotherms of (■) the calcined alumina, (▲) the calcined Al-Mg mixed oxide at Al:Mg ratio of 1:4, and (●) the calcined magnesia.

5.6 X-RAY FLUORESCENCE SPRCTROMETRY (XRF)

The Al:Mg atomic ratios in the calcined Al-Mg mixed oxides were measured by XRF spectrometry and shown in Table 5.2. The Al:Mg atomic ratio values in all samples were close to the values estimated from the amount of the starting materials. However, the calcined alkali doped samples had 1.55 – 2.00 mmol of potassium atoms per 1 g of catalyst, which was lower than the theoretical value (2.1 mmol per 1g of catalyst).

Table 5.2 The Al:Mg atomic ratio values in the calcined Al-Mg mixed oxides.

Sample	Al:Mg ratio (Theory)	Al:Mg ratio (Experiment)
Al-Mg mixed oxide at Al:Mg ratio of 8:1	1:0.125	1:0.094
Al-Mg mixed oxide at Al:Mg ratio of 4:1	1:0.25	1:0.21
Al-Mg mixed oxide at Al:Mg ratio of 2:1	1:0.5	1:0.47
Al-Mg mixed oxide at Al:Mg ratio of 1:1	1:1	1:1.01
Al-Mg mixed oxide at Al:Mg ratio of 1:2	1:2	1: 2.10
Al-Mg mixed oxide at Al:Mg ratio of 1:3	1:3	1:3.35
Al-Mg mixed oxide at Al:Mg ratio of 1:4	1:4	1:4.15
Al-Mg mixed oxide at Al:Mg ratio of 1:8	1:8	1:8.06

5.7 ACID AND BASE STRENGTH MEASUREMENT

The base strength of the alumina, the Al-Mg mixed oxides, and the magnesia increased with increasing magnesia content. Likewise, alkali doped samples had higher base strength with increasing magnesia content. Moreover, both KI and KNO_3 doped Al-Mg mixed oxides at the same Al:Mg ratio had the same base strength. Hence, the magnesia content could increase the base strength and the presence of alkali species (potassium) could also increase the base strength of the catalysts. The base strength of the alumina, the Al-Mg mixed oxides, the magnesia, and the alkali doped samples were shown in Table 5.3.

Table 5.3 Base strength of the catalysts.

Catalyst	$pK_{BH}+$
alumina	$pK_{BH^+} \leq 7.2$
Al-Mg mixed oxide at Al:Mg ratio of 8:1	$pK_{BH^+} \leq 7.2$
Al-Mg mixed oxide at Al:Mg ratio of 4:1	$pK_{BH^+} \leq 7.2$
Al-Mg mixed oxide at Al:Mg ratio of 2:1	$7.2 \leq pK_{BH^+} \leq 9.8$
Al-Mg mixed oxide at Al:Mg ratio of 1:1	$7.2 \leq pK_{BH^+} \leq 9.8$
Al-Mg mixed oxide at Al:Mg ratio of 1:2	$7.2 \leq pK_{BH^+} \leq 9.8$
Al-Mg mixed oxide at Al:Mg ratio of 1:3	$7.2 \leq pK_{BH^+} \leq 9.8$
Al-Mg mixed oxide at Al:Mg ratio of 1:4	$7.2 \leq pK_{BH^+} \leq 9.8$
Al-Mg mixed oxide at Al:Mg ratio of 1:8	$7.2 \leq pK_{BH^+} \leq 9.8$
magnesia	$7.2 \leq pK_{BH^+} \leq 9.8$
KI doped alumina	$7.2 \leq pK_{BH^+} \leq 9.8$
KI doped Al-Mg mixed oxide at Al:Mg ratio of 8:1	$7.2 \leq pK_{BH^+} \leq 9.8$
KI doped Al-Mg mixed oxide at Al:Mg ratio of 4:1	$7.2 \leq pK_{BH^+} \leq 9.8$
KI doped Al-Mg mixed oxide at Al:Mg ratio of 2:1	$7.2 \leq pK_{BH^+} \leq 9.8$
KI doped Al-Mg mixed oxide at Al:Mg ratio of 1:1	$9.8 \leq pK_{BH^+} \leq 15$
KI doped Al-Mg mixed oxide at Al:Mg ratio of 1:2	$9.8 \leq pK_{BH^+} \leq 15$
KI doped Al-Mg mixed oxide at Al:Mg ratio of 1:3	$9.8 \leq pK_{BH^+} \leq 15$
KI doped Al-Mg mixed oxide at Al:Mg ratio of 1:4	$9.8 \leq pK_{BH^+} \leq 15$
KNO_3 doped Al-Mg mixed oxide at Al:Mg ratio of 1:4	$9.8 \leq pK_{BH^+} \leq 15$
KI doped Al-Mg mixed oxide at Al:Mg ratio of 1:8	$9.8 \leq pK_{BH^+} \leq 15$
KI doped magnesia	$9.8 \leq pK_{BH^+} \leq 15$

5.8 TRANSESTERIFICATION OF SOYBEAN OIL

Percentage yields of fatty acid methyl ester from soybean oil using alkali doped alumina, alkali doped Al-Mg mixed oxides, and alkali doped magnesia were shown in Figure 5.17 and Figure 5.18.

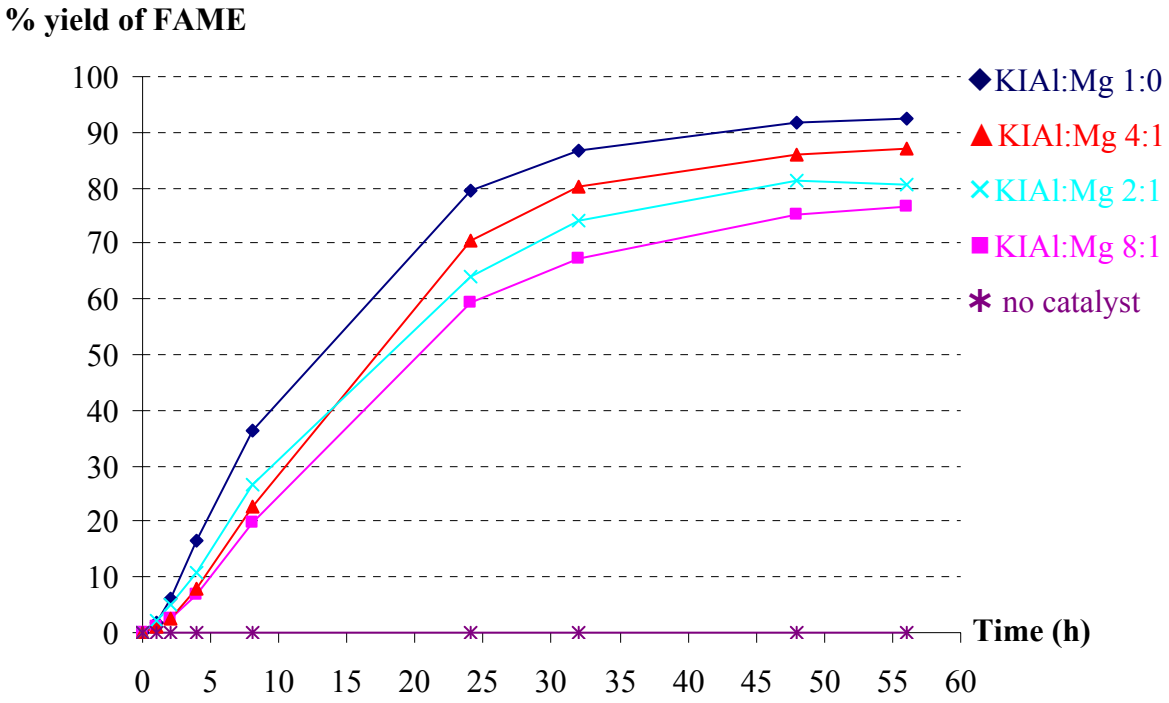

Figure 5.17 Percentage yields of FAME from transesterification of soybean oil using no catalyst, KI doped alumina, and KI doped Al-Mg mixed oxides at Al:Mg ratios of 8:1, 4:1, and 2:1 as catalyst.

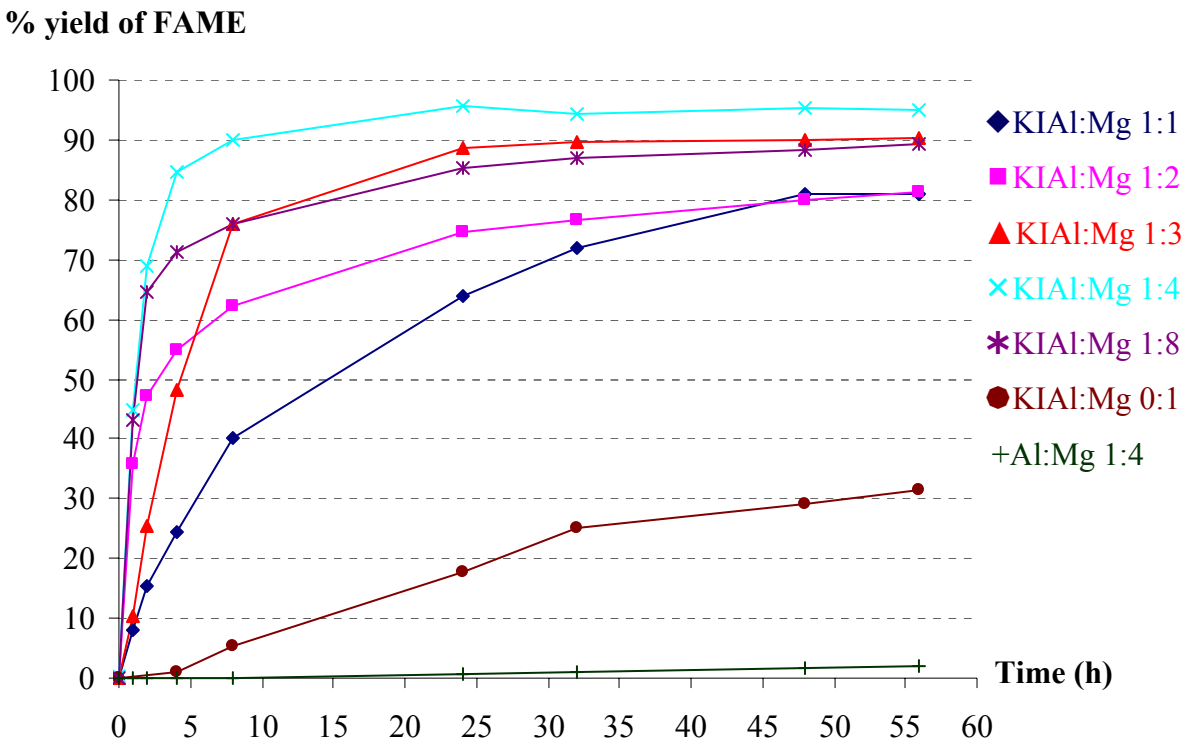

Figure 5.18 Percentage yields of FAME using KI doped Al-Mg mixed oxide at Al:Mg ratios of 1:1, 1:2, 1:3, 1:4, and 1:8, KI doped magnesia, and undoped Al-Mg mixed oxide at Al:Mg 1:4 as catalyst.

The transesterification of soybean oil with methanol in the absence of catalyst essentially produced no fatty acid methyl ester (FAME) under the condition studied, while all KI doped catalysts were active for the reaction as shown in Figure 5.17 and 5.18. The KI doped alumina was more active than the KI doped Al-Mg mixed oxides with high aluminum content at the Al:Mg ratios of 1:2, 1:4, and 1:8. These samples had similar basic strength ($7.2 \leq pK_{BH^+} \leq 9.8$) and similar surface area (211-230 m^2g^{-1}), thus the difference in the transesterification is yet explained and further study is needed. One hypothesis now is the potassium species was better dispersed on the alumina compared to on the mixed oxides, as the XRD results showed no crystalline potassium species on the alumina, but KI and KIO_3 phases were observed on the mixed oxides. However, the KI doped Al-Mg mixed oxides at Al:Mg ratios of 1:1, 1:3 and 1:4 gave higher yield of FAME as the magnesium content increased as shown in

Figure 5.18. The yield of FAME from the reaction with the KI doped Al-Mg mixed oxide at Al:Mg ratio of 1:4 was approximately 90% after 8 h, while the yield from the reaction with the KI doped Al-Mg mixed oxide at Al:Mg ratio of 4:1 was only 20 % after 8 h. The higher activity in this case might be a result of the higher magnesium content which led to the higher basicity of the sample. Figure 5.19 showed the correlation of the magnesia content and the FAME produced from the reaction at 24 h. The undoped Al-Mg mixed oxide at Al:Mg ratio of 1:4 showed no activity after 8 h and has only 2% yield of FAME after 56 h because of low basicity of this catalyst ($7.2 \leq pK_{BH^+} \leq 9.8$) as shown in Figure 5.18. Figure 5.19 also showed that the KI doped magnesia catalyst was not as active as the KI doped Al-Mg mixed oxides. Even though the KI dope magnesia sample had similar base strength to those of the KI doped mixed oxides, the surface area of the magnesia support was much lower (96 m^2g^{-1}). Therefore, the lower activity was obtained. In addition, the KI doped Al-Mg mixed oxide at Al:Mg ratio of 1:4 had higher activity than that of the KNO_3 doped Al-Mg mixed oxide at the same Al:Mg ratio (Figure 5.20). This result was in good agreement with that reported by Xie [58]. Xie reported that the calcined KI doped alumina had higher activity than KNO_3 doped sample, with 87.4 and 67.4 % yield of FAME at 6 h, respectively. However, our KI doped Al:Mg mixed oxide at Al:Mg 1:4 exhibited higher activity (85 % yield at 4 h).

The leaching and reuse ability of the KI doped Al-Mg mixed oxide at Al:Mg ratio of 1:4 were shown in Figure 5.21 and 5.22, respectively. Leaching test for the calcined KI doped Al-Mg mixed oxide at Al:Mg ratio of 1:4 was carried out by filtering out the catalyst from the transesterification reaction mixture after 2 h. The result showed no change in the percentage yield of FAME after the catalyst removal. 10 mL of methanol was added to the reaction at 25 h to ensure that the loss of activity was not caused by methanol evaporation during the catalyst removal. After the addition of methanol, the yield of FAME remained relative unaffected, indicating that the Al-Mg mixed oxide at Al:Mg ratio of 1:4 was a heterogeneous catalyst without any soluble active species in the reaction. To study the reuse ability of the KI doped Al-Mg mixed oxide catalyst, recovered catalysts were washed with acetone and hexane, respectively, and dried at 120 ^oC for 24 h, then either used without further treatment or

treated by calcinations at 550 ^{o}C for 5 h. The recovered catalyst with calcination treatment showed to be only half as active as the first catalyst (47 % vs 95 % yield at 24 h), as shown in Figure 5.22, for the calcined KI doped Al-Mg mixed oxide at Al:Mg ratio of 1:4. The recovered catalyst used without calcinations was even less active (10 % yield at 24 h). These results indicated that the reused catalysts were somehow deactivated or poisoned during the reaction.

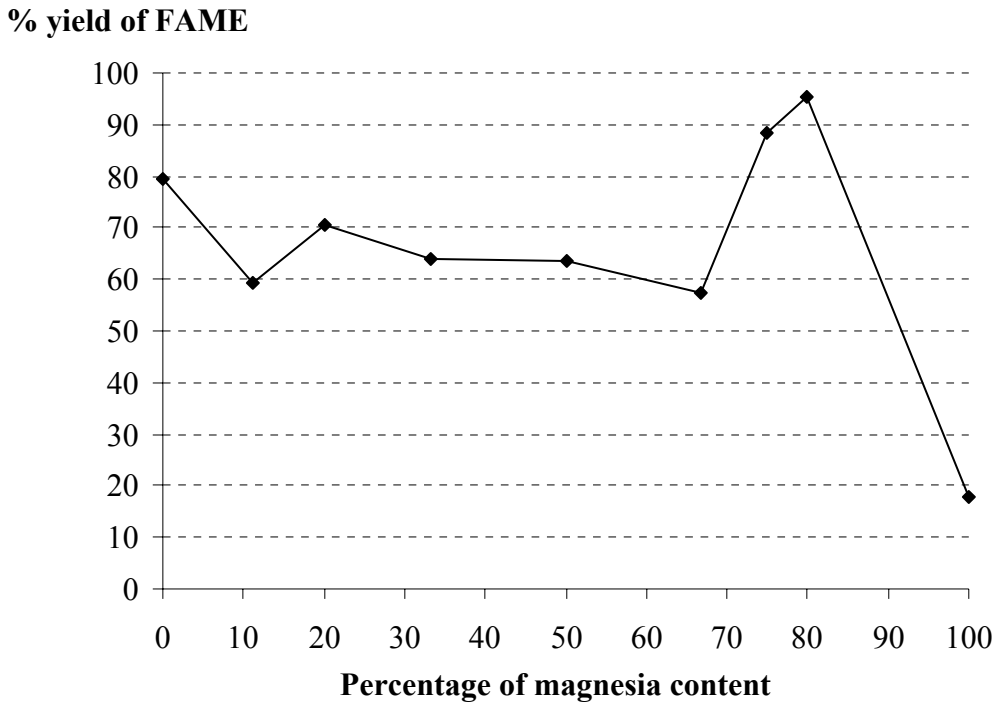

Figure 5.19 Correlation of the magnesia content in the KI doped Al-Mg mixed oxide catalysts and the percentage yield of FAME produced from the transesterification of soybean oil with methanol at 24 h.

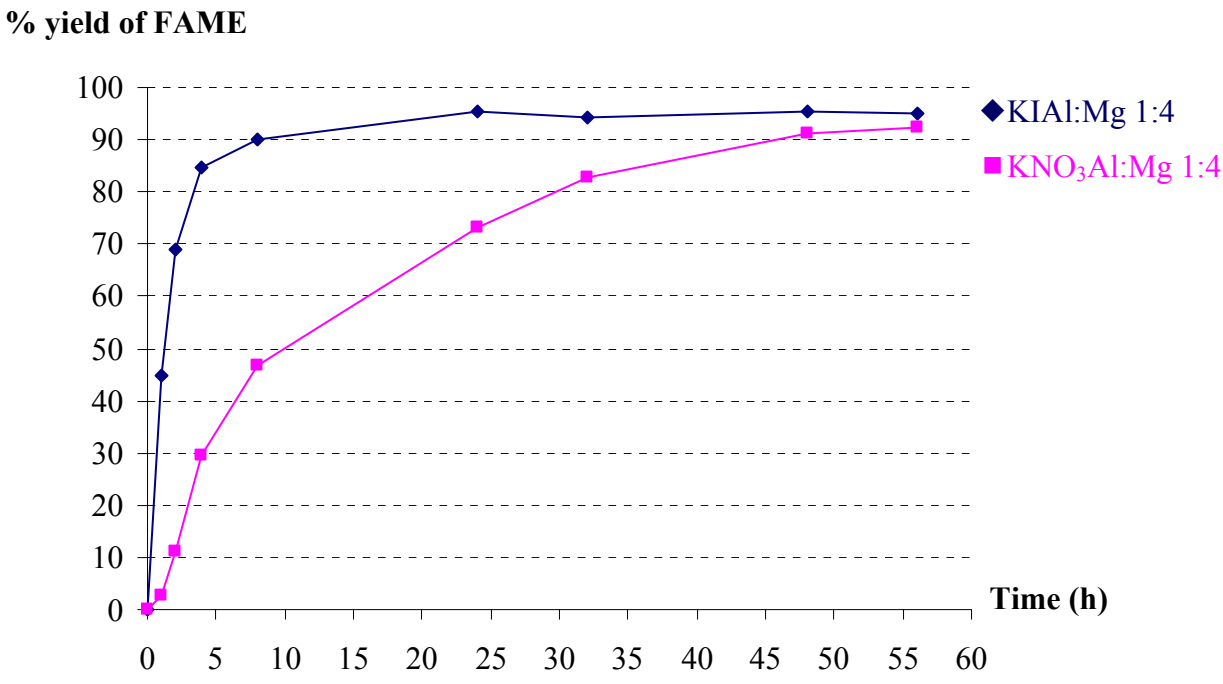

Figure 5.20 Influence of type of potassium salt doped Al-Mg mixed oxide at Al:Mg ratio of 1:4 on the percentage yield of FAME.

Figure 5.21 Leaching test of the calcined KI doped Al-Mg mixed oxide catalyst at Al:Mg ratio of 1:4. The catalyst was removed after 2 h and the transesterification was continued at 80 ^{o}C.

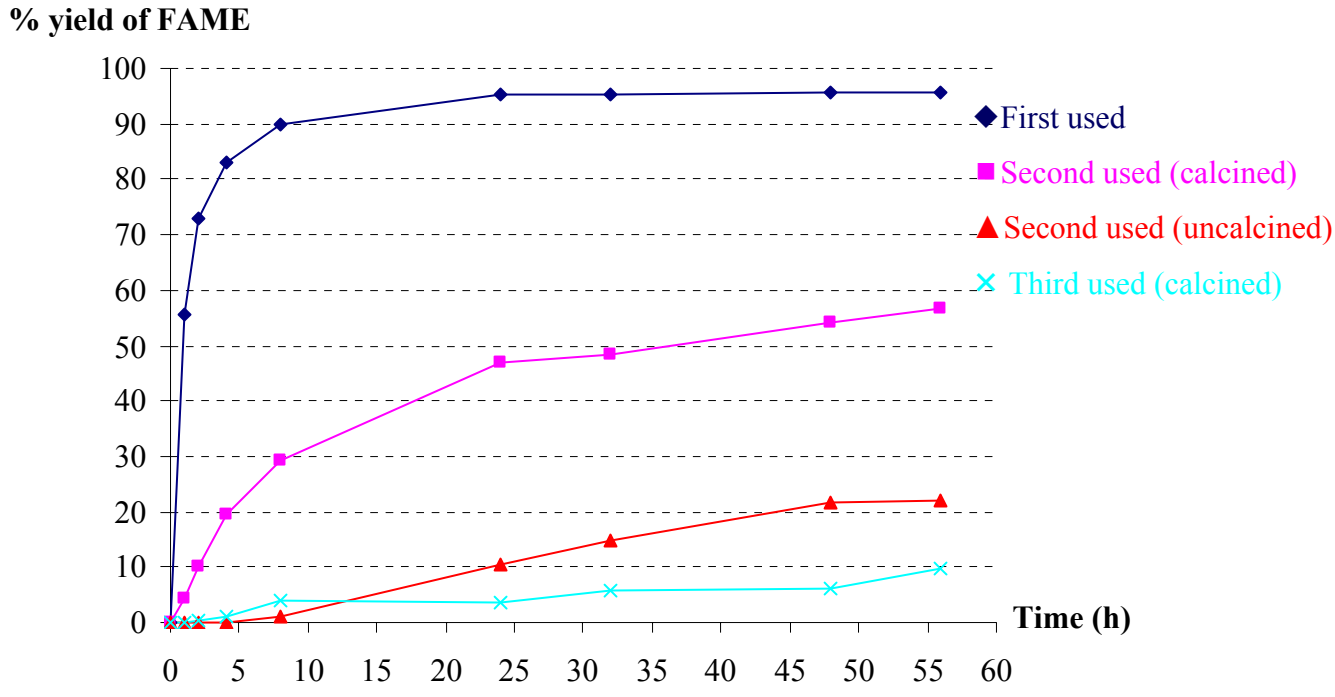

Figure 5.22 Reuse ability of the calcined KI doped Al-Mg mixed oxide at Al:Mg ratio of 1:4.

CHAPTER 6
CONCLUSION

The phases of the calcined alumina and the calcined magnesia were γ-Al_2O_3 and periclase, respectively. The phase of the calcined Al-Mg mixed oxides at Al:Mg ratios of 8:1, 4:1, and 2:1 were the mixture of γ-Al_2O_3 and periclase. On the other hand, the calcined Al-Mg mixed oxides at Al:Mg ratios of 1:1, 1:2, 1:3, 1:4, and 1:8 were the mixture of hydrotalcite ($Mg_6Al_2CO_3(OH)_{16}\cdot 4H_2O$) and periclase (MgO). The phases of all samples remained unchanged after doping with KI or KNO_3, except the additional appearance of KI and KIO_3 phases in the calcined KI doped samples and of KNO_3 and K_2O phases in the calcined KNO_3 doped samples.

The calcined alumina had mesoporous structure with tubular or ink-bottom pores. The calcined Al-Mg mixed oxides had capillary space between parallel plates or open slit-shaped capillary. The magnesia had only space among particles without mesopores in the material. The mesoporosity of the materials tended to decrease with the increasing magnesia content. BET surface area of alumina was 230 m^2g^{-1}. The calcined Al-Mg mixed oxides had BET surface areas varied between 127 and 266 m^2g^{-1}. The calcined Al-Mg mixed oxide at Al:Mg ratio of 1:4 had the highest BET surface area (266 m^2g^{-1}) and the calcined magnesia had the lowest BET surface area (96 m^2g^{-1}).

The base strength of the calcined alumina, the Al-Mg mixed oxides, and the magnesia increased with magnesia content.

The percentage yield of FAME using the calcined alkali doped alumina, Al-Mg mixed oxides, and the magnesia as catalyst were in range 5-90 % after 8 h of reaction. The calcined KI doped Al-Mg mixed oxide at Al:Mg ratio of 1:4 had the highest catalytic activity of approximately 90 % yield of FAME after 8 h and higher than the

calcined KNO_3 doped Al-Mg mixed oxide at the same ratio (47 %). Moerover, There was no catalytically active species leaching from the calcined Al-Mg mixed oxide at Al:Mg ratio of 1:4, indicating that this catalytic system was heterogeneous. Nevertheless, the reused catalysts were inactive, indicating that the catalysts might be deactivated or poisoned during the reaction.

SUGGESTION FOR THE FURTHER STUDY

1. The incipient wetness method for alkali doped Al-Mg mixed oxides may be used to increase dispersion of potassium species in their pores and their external surfaces and percentage weight of potassium salts should be varied to optimize the catalytic activity of the catalysts.

2. The catalytic conditions, such as soybean oil:methanol ratio, reaction temperature, and catalyst loading, should be studied to acheive maximum percentage yield of FAME.

3. The locally produced oils, such as palm oil and coconut oil may be used as a substrate in catalytic reaction to reduce the material cost.

REFERENCES

1. Wood CC. Kicking The Gasoline & Petro-Diesel Habit - A Business Manager's Blueprint For Action. 2008 [updated April 2008; cited 18 May 2008]; Available from: http://www.maccompanion.com/macc/archives/April2008/ Greenware/ KickingGasoline.htm.
2. (ATSDR) AfTSaDR. Toxicological profile for fuel oils. U.S. Department of Health and Human Services; 1995 [updated 1995; cited 18 May 2008]; Available from: http://www.atsdr.cdc.gov/toxprofiles/tp75-c3.pdf.
3. Srivastava A, Prasad R. Triglycerides-based diesel fuels. Renewable and Sustainable Energy Reviews. 2000; 4(2): 111-33.
4. Schlick ML, Hanna MA, Schinstock JL. Soybean and sunflower oil performance in a diesel engine. Transactions of the American Society of Agricultural Engineers. 1988; 31(5): 1345-9.
5. Schwab AW, Bagby MO, Freedman B. Preparation and properties of diesel fuels from vegetable oils. Fuel. 1987; 66(10): 1372-8.
6. Ziejewski M, Kaufman K, Schwab A, Pryde E. Diesel engine evaluation of a nonionic sunflower oil-aqueous ethanol microemulsion. Journal of the American Oil Chemists' Society. 1984; 61(10): 1620-6.
7. Sonntag NOV. Reactions of fats and fatty acids. Bailey's industrial oil and fat products. New York: John Wiley & Sons 1st ed.; 1979.
8. Ma F, Hanna MA. Biodiesel production: a review. Bioresource Technology. 1999; 70(1): 1-15.
9. Demirbas A. Biodiesel production via non-catalytic SCF method and biodiesel fuel characteristics. Energy Conversion and Management. 2006; 47(15-16): 2271-82.
10. Ghadge SV, Raheman H. Biodiesel production from mahua (Madhuca indica) oil having high free fatty acids. Biomass and Bioenergy. 2005; 28(6): 601-5.

11. Meher LC, Dharmagadda VSS, Naik SN. Optimization of alkali-catalyzed transesterification of Pongamia pinnata oil for production of biodiesel. Bioresource Technology. 2006; 97(12): 1392-7.
12. Sarin R, Sharma M, Sinharay S, Malhotra RK. Jatropha-Palm biodiesel blends: An optimum mix for Asia. Fuel. 2007; 86(10-11): 1365-71.
13. Sahoo PK, Das LM, Babu MKG, Naik SN. Biodiesel development from high acid value polanga seed oil and performance evaluation in a CI engine. Fuel. 2007; 86(3): 448-54.
14. Demirbas A. Comparison of transesterification methods for production of biodiesel from vegetable oils and fats. Energy Conversion and Management. 2008; 49(1): 125-30.
15. Christie WW. Gas chromatography and lipids: a practical guide. 1st ed. Dundee: The Oily Press; 1989.
16. Demirbas A. Biodiesel production from vegetable oils via catalytic and non-catalytic supercritical methanol transesterification methods. Progress in Energy and Combustion Science. 2005; 31(5-6): 466-87.
17. Haas MJO, PA, inventor The United States of America, as represented by the Secretary of (Washington, DC), assignee. Fuels as solvents for the conduct of enzymatic reactions. United States. 1997.
18. Thomson SJ. Heterogeneus Catalysis. T. L. Cottrell ed. London: Oliver & Boyd; 1968.
19. Swaddle TW. Inorganic Chemistry An Industrial and Environmental Perspective. California: Academic Press; 1990.
20. Remy H. Treatise in inorganic chemistry. J. Kleinberg 1st ed.: Elsevier publishing company; 1956.
21. Spinel. 2007 [updated 2007; cited 18 May 2008]; Available from: http://wikis.lib.ncsu.edu/index.php/Spinel.
22. Sohlberg K, Pantelides ST, Pennycook SJ. Surface Reconstruction and the Difference in Surface Acidity between γ- and η-Alumina. Journal of the American Chemical Society. 2001; 123(1): 26-9.
23. Civalleri B. Crystal geometry input. [cited 18 May 2008]; Available from: http://www.crystal.unito.it/tutojan2004/tutorials/A_geometry/geom_tut.html.

24. Mittelbach M. Lipase catalyzed alcoholysis of sunflower oil. Journal of the American Oil Chemists' Society. 1990; 67(3): 168-70.
25. Samukawa T, Kaieda M, Matsumoto T, Ban K, Kondo A, Shimada Y, et al. Pretreatment of immobilized Candida antarctica lipase for biodiesel fuel production from plant oil. Journal of Bioscience and Bioengineering. 2000; 90(2): 180-3.
26. Royon D, Daz M, Ellenrieder G, Locatelli S. Enzymatic production of biodiesel from cotton seed oil using t-butanol as a solvent. Bioresource Technology. 2007; 98(3): 648-53.
27. Du W, Xu Y, Liu D, Zeng J. Comparative study on lipase-catalyzed transformation of soybean oil for biodiesel production with different acyl acceptors. Journal of Molecular Catalysis B: Enzymatic. 2004; 30(3-4): 125-9.
28. Chen JW, Wu WT. Regeneration of immobilized Candida antarctica lipase for transesterification. Journal of Bioscience and Bioengineering. 2003; 95(5): 466-9.
29. Linko Y-Y, Linko M, Wu X, Uosukainen E, Seppälä, Linko P. Biodegradable products by lipase biocatalysis. Journal of Biotechnology. 1998; 66(1): 41-50.
30. Fukuda H, Kondo A, Noda H. Biodiesel fuel production by transesterification of oils. Journal of Bioscience and Bioengineering. 2001; 92(5): 405-16.
31. Ban K, Hama S, Nishizuka K, Kaieda M, Matsumoto T, Kondo A, et al. Repeated use of whole-cell biocatalysts immobilized within biomass support particles for biodiesel fuel production. Journal of Molecular Catalysis B: Enzymatic. 2002; 17(3-5): 157-65.
32. Fukuda Hideki KA, inventor Kansai Chemical Engineering Co., Ltd., assignee. Method for enhancing catalytic activity of cells. United States. 2003.
33. Hama S, Yamaji H, Kaieda M, Oda M, Kondo A, Fukuda H. Effect of fatty acid membrane composition on whole-cell biocatalysts for biodiesel-fuel production. Biochemical Engineering Journal. 2004; 21(2): 155-60.

34. Hama S, Tamalampudi S, Fukumizu T, Miura K, Yamaji H, Kondo A, et al. Lipase localization in Rhizopus oryzae cells immobilized within biomass support particles for use as whole-cell biocatalysts in biodiesel-fuel production. Journal of Bioscience and Bioengineering. 2006; 101(4): 328-33.
35. Panayiotou C. Solubility parameter revisited: an equation-of-state approach for its estimation. Fluid Phase Equilibria. 1997; 131(1-2): 21-35.
36. Kusdiana D, Saka S. Kinetics of transesterification in rapeseed oil to biodiesel fuel as treated in supercritical methanol. Fuel. 2001; 80(5): 693-8.
37. Kusdiana D, Saka S. Effects of water on biodiesel fuel production by supercritical methanol treatment. Bioresource Technology. 2004; 91(3): 289-95.
38. Rathore V, Madras G. Synthesis of biodiesel from edible and non-edible oils in supercritical alcohols and enzymatic synthesis in supercritical carbon dioxide. Fuel. 2007; 86(17-18): 2650-9.
39. Cao W, Han H, Zhang J. Preparation of biodiesel from soybean oil using supercritical methanol and co-solvent. Fuel. 2005; 84(4): 347-51.
40. Han H, Cao W, Zhang J. Preparation of biodiesel from soybean oil using supercritical methanol and CO_2 as co-solvent. Process Biochemistry. 2005; 40(9): 3148-51.
41. Lopez DE, Suwannakarn K, Bruce DA, Goodwin JJG. Esterification and transesterification on tungstated zirconia: Effect of calcination temperature. Journal of Catalysis. 2007; 247(1): 43-50.
42. Bonelli B, Cozzolino M, Tesser R, Di Serio M, Piumetti M, Garrone E, et al. Study of the surface acidity of TiO_2/SiO_2 catalysts by means of FTIR measurements of CO and NH_3 adsorption. Journal of Catalysis. 2007; 246(2): 293-300.
43. Lopez DE, Goodwin JJG, Bruce DA, Lotero E. Transesterification of triacetin with methanol on solid acid and base catalysts. Applied Catalysis A: General. 2005; 295(2): 97-105.
44. Furuta S, Matsuhashi H, Arata K. Biodiesel fuel production with solid superacid catalysis in fixed bed reactor under atmospheric pressure. Catalysis Communications. 2004; 5(12): 721-3.

45. Furuta S, Matsuhashi H, Arata K. Biodiesel fuel production with solid amorphous-zirconia catalysis in fixed bed reactor. Biomass and Bioenergy. 2006; 30(10): 870-3.

46. Jitputti J, Kitiyanan B, Rangsunvigit P, Bunyakiat K, Attanatho L, Jenvanitpanjakul P. Transesterification of crude palm kernel oil and crude coconut oil by different
solid catalysts. Chemical Engineering Journal. 2006; 116(1): 61-6.

47. Di Serio M, Cozzolino M, Tesser R, Patrono P, Pinzari F, Bonelli B, et al. Vanadyl phosphate catalysts in biodiesel production. Applied Catalysis A: General. 2007; 320: 1-7.

48. Sreeprasanth PS, Srivastava R, Srinivas D, Ratnasamy P. Hydrophobic, solid acid catalysts for production of biofuels and lubricants. Applied Catalysis A: General. 2006; 314(2): 148-59.

49. Gryglewicz S. Rapeseed oil methyl esters preparation using heterogeneous catalysts. Bioresource Technology. 1999; 70(3): 249-53.

50. Reddy C, Reddy V, Oshel R, Verkade JG. Room-Temperature Conversion of Soybean Oil and Poultry Fat to Biodiesel Catalyzed by Nanocrystalline Calcium Oxides. Energy & Fuels. 2006; 20(3): 1310-4.

51. Gelbard G, Vielfaure-Joly F. Polynitrogen strong bases as immobilized catalysts. Reactive and Functional Polymers. 2001; 48(1-3): 65-74.

52. Shibasaki-Kitakawa N, Honda H, Kuribayashi H, Toda T, Fukumura T, Yonemoto T. Biodiesel production using anionic ion-exchange resin as heterogeneous catalyst. Bioresource Technology. 2007; 98(2): 416-21.

53. Liu Y, Lotero E, Goodwin JJG, Lu C. Transesterification of triacetin using solid Bronsted bases. Journal of Catalysis. 2007; 246(2): 428-33.

54. Suppes GJ, Dasari MA, Doskocil EJ, Mankidy PJ, Goff MJ. Transesterification of soybean oil with zeolite and metal catalysts. Applied Catalysis A: General. 2004; 257(2): 213-23.

55. Xie W, Huang X, Li H. Soybean oil methyl esters preparation using NaX zeolites loaded with KOH as a heterogeneous catalyst. Bioresource Technology. 2007; 98(4): 936-9.

56. Yang Z, Xie W. Soybean oil transesterification over zinc oxide modified with alkali earth metals. Fuel Processing Technology. 2007; 88(6): 631-8.

57. Cantrell DG, Gillie LJ, Lee AF, Wilson K. Structure-reactivity correlations in MgAl hydrotalcite catalysts for biodiesel synthesis. Applied Catalysis A: General. 2005; 287(2): 183-90.

58. Xie W, Li H. Alumina-supported potassium iodide as a heterogeneous catalyst for biodiesel production from soybean oil. Journal of Molecular Catalysis A: Chemical. 2006; 255(1-2): 1-9.

59. Grosso D, Boissière C, Nicole L, Sanchez C. Preparation, treatment and characterisation of nanocrystalline mesoporous ordered layers. Journal of Sol-Gel Science and Technology. 2006; 40(2): 141-54.

60. Aguado J, Escola JM, Castro MC, Paredes B. Sol-gel synthesis of mesostructured γ-alumina templated by cationic surfactants. Microporous and Mesoporous Materials. 2005; 83(1-3): 181-92.

61. Misra C. Industrial Alumina Chemicals. 1987.

62. Cejka J. Organized mesoporous alumina: synthesis, structure and potential in catalysis. Applied Catalysis A: General. 2003; 254(2): 327-38.

63. Vaudry F, Khodabandeh S, Davis ME. Synthesis of Pure Alumina Mesoporous Materials. Chemistry of Materials. 1996; 8(7): 1451-64.

64. Yada M, Ohya M, Machida M, Kijima T. Synthesis of porous yttrium aluminium oxide templated by dodecyl sulfate assemblies. Chemical Communications. 1998(18): 1941-2.

65. Zhang Z, Pinnavaia TJ. Mesostructured gamma-Al_2O_3 with a Lathlike Framework Morphology. Journal of the American Chemical Society. 2002; 124(41): 12294-301.

66. Niesz K, Yang P, Somorjai GA. Sol-gel synthesis of ordered mesoporous alumina. Chemical Communications. 2005 ; 1986-7.

67. Saul Cabrera Jehjaabdbsbbdmpas. Surfactant-Assisted Synthesis of Mesoporous Alumina Showing Continuously Adjustable Pore Sizes. Advanced Materials. 1999; 11(5): 379-81.

68. Hammett LP, Deyrup AJ. A series of simple basic indicators. I. The acidity functions of sulfuric and perchloric acids with water. Journal of the American Chemical Society. 1932; 54(7): 2721-39.

69. Acid Value. 1989 [updated 1989; cited 18 May 2008]; Available from: http://www.iic.co.th/products/acid.htm.

70. Saponification value 1989 [updated 1989; cited 18 May 2008]; Available from: http://www.iic.co.th/products/sapon.htm.

71. Gelbard G, Brès O, Vargas R, Vielfaure F, Schuchardt U. 1H nuclear magnetic resonance determination of the yield of the transesterification of rapeseed oil with methanol. Journal of the American Oil Chemists' Society. 1995; 72(10): 1239-41.

72. Lopez T, Marmolejo R, Asomoza M, Sols S, Gomez R, Wang JA, et al. Preparation of a complete series of single phase homogeneous sol-gels of Al_2O_3 and MgO for basic catalysts. Materials Letters. 1997; 32(5-6): 325-34.

73. Yada M, Kuroki S, Kuroki M, Ohe K, Kijima T. Effect of Coexisting Anions on the Stabilization of Porous Alumina Templated by Dodecyl Sulfate Assemblies. Langmuir. 2002; 18(22): 8714-8.

74. Masson NC, Pastore HO. Synthesis and characterization of tubular aluminophosphate mesoporous materials containing framework magnesium. Microporous and Mesoporous Materials. 2001; 44-45: 173-83.

75. Ding Y, Zhang G, Wu H, Hai B, Wang L, Qian Y. Nanoscale Magnesium Hydroxide and Magnesium Oxide Powders: Control over Size, Shape, and Structure via Hydrothermal Synthesis. Chemistry of Materials. 2001; 13(2): 435-40.

76. S. J. Gregg KSWS. Adsorption, Surface Area and Porosity. London: Academic Press Inc.; 1967.

APPENDIX

APPENDIX A

THE CRYSTALLITE SIZE OF KI, KIO_3, KNO_3, AND K_2O OF Al-Mg MIXED OXIDES AND MAGNESIA

Table 1A The crystalline size of KI (200) and KIO_3 (220) of KI doped Al- Mg mixed oxides and magnesia**.**

Samples	Crystalline size (nm)	
	KI	**KIO_3**
KI doped Al-Mg mixed oxide at Al:Mg ratio of 8:1	-	55.67
KI doped Al-Mg mixed oxide at Al:Mg ratio of 4:1	-	45.50
KI doped Al-Mg mixed oxide at Al:Mg ratio of 2:1	-	24.69
KI doped Al-Mg mixed oxide at Al:Mg ratio of 1:1	89.96	71.19
KI doped Al-Mg mixed oxide at Al:Mg ratio of 1:2	96.57	112.83
KI doped Al-Mg mixed oxide at Al:Mg ratio of 1:3	2.20	2.69
KI doped Al-Mg mixed oxide at Al:Mg ratio of 1:4	37.58	41.91
KI doped Al-Mg mixed oxide at Al:Mg ratio of 1:8	40.50	101.86
KI doped magnesia	36.90	151.11

Table 2A The crystalline size of KNO_3 (111) and K_2O (200) of KNO_3 doped Al-Mg mixed oxide at Al:Mg ratio of 1:4.

Samples	Crystalline size (nm)	
	KNO_3	**K_2O**
KNO_3 doped Al-Mg mixed oxide at Al:Mg ratio of 8:1	31.95	38.89

APPENDIX B

TRANSMISSION ELECTRON MICROSCOPY (TEM)

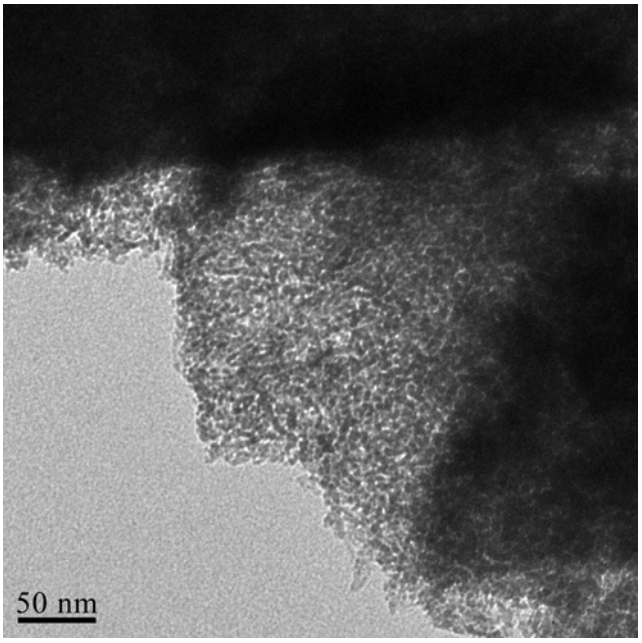

Figure 1B. TEM image of the alumina.

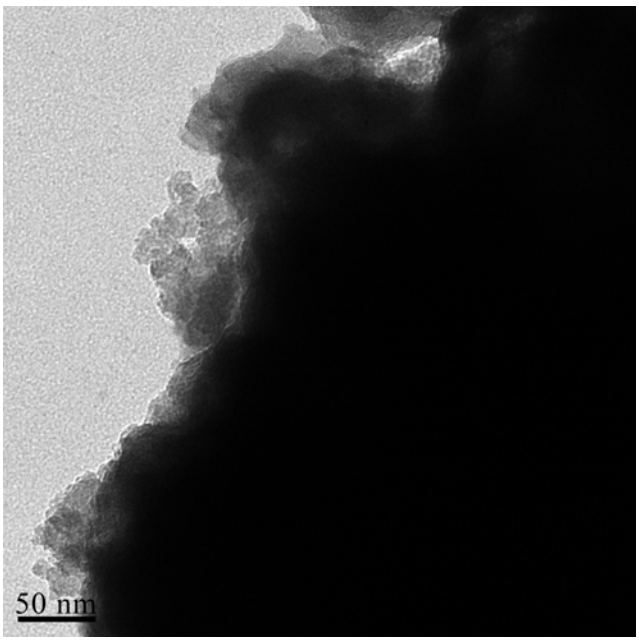

Figure 2B. TEM image of the Al-Mg mixed oxide at Al:Mg of 1:1.

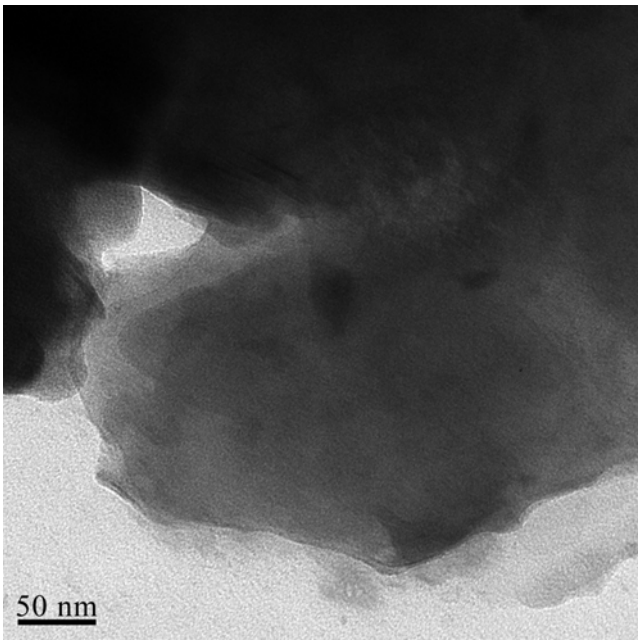

Figure 3B. TEM image of the KI doped Al-Mg mixed oxide at Al:Mg at of 1:1.

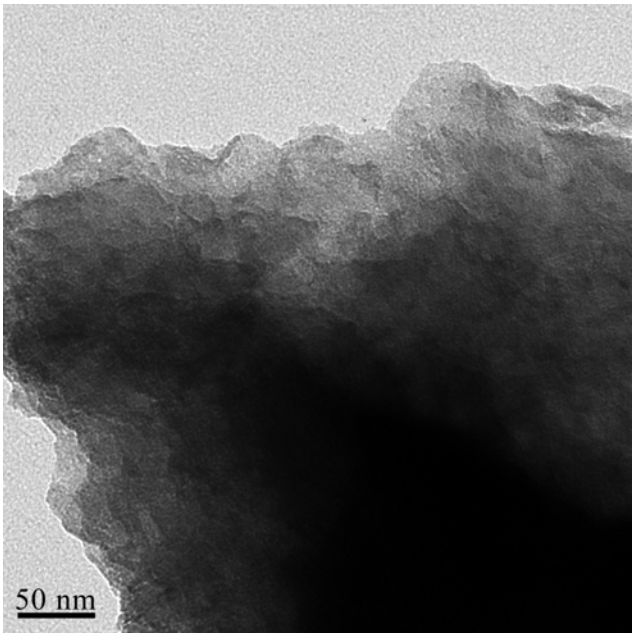

Figure 4B. TEM image of the Al-Mg mixed oxide at Al:Mg of 1:2.

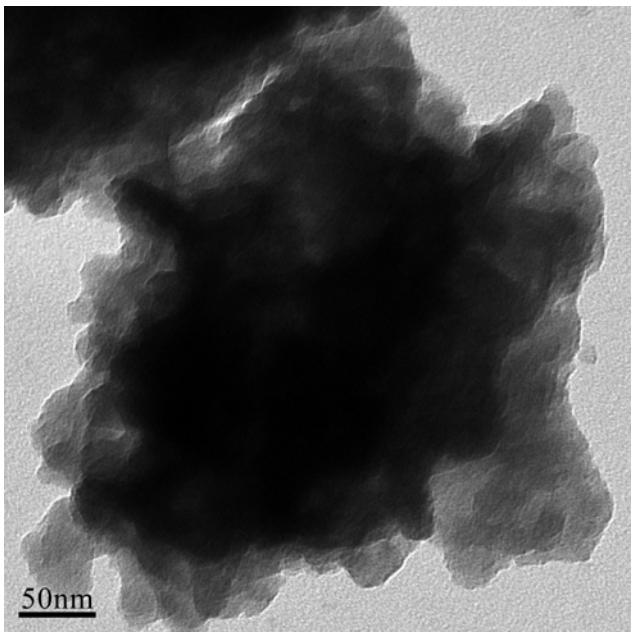

Figure 5B. TEM image of KI doped Al-Mg mixed oxide at Al:Mg of 1:2.

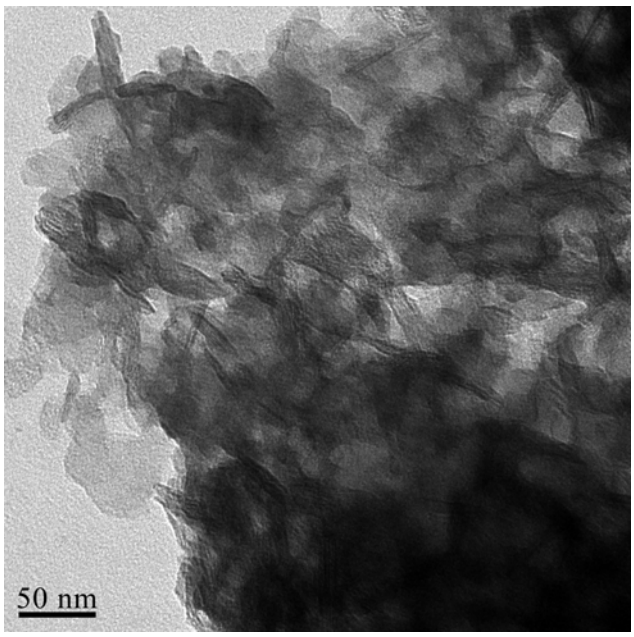

Figure 6B. TEM image of the Al-Mg mixed oxide at Al:Mg of 1:8.

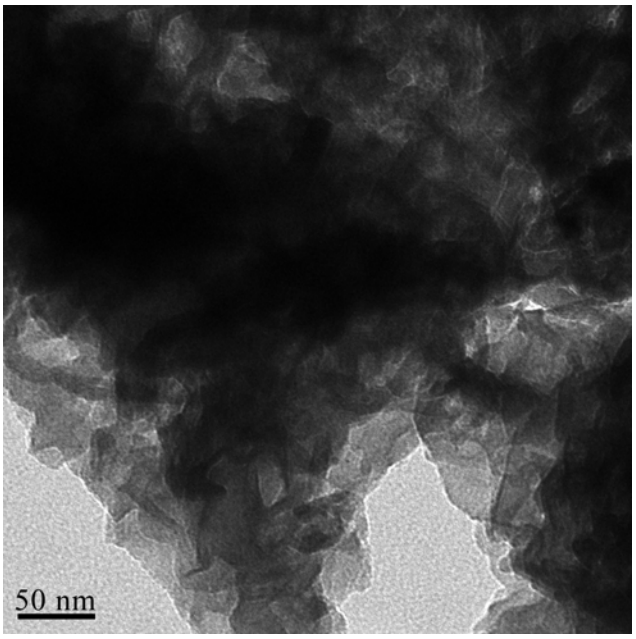

Figure 7B. TEM image of KI doped Al-Mg mixed oxide at Al:Mg of 1:8.

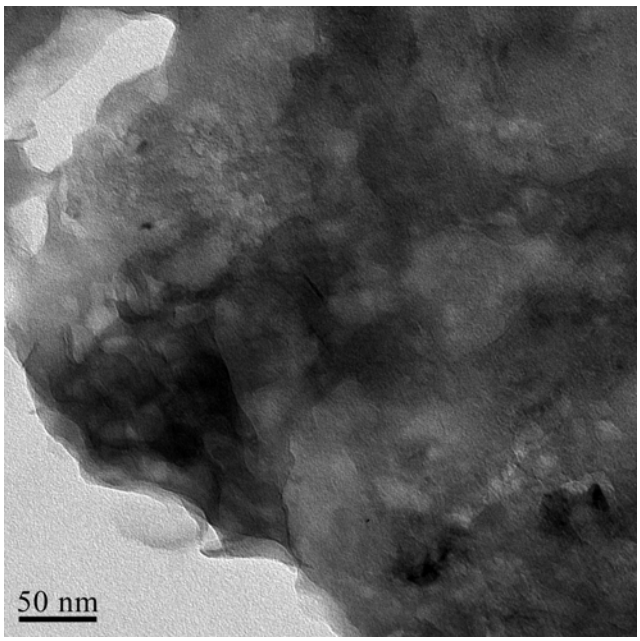

Figure 8B. TEM image of the magnesia.

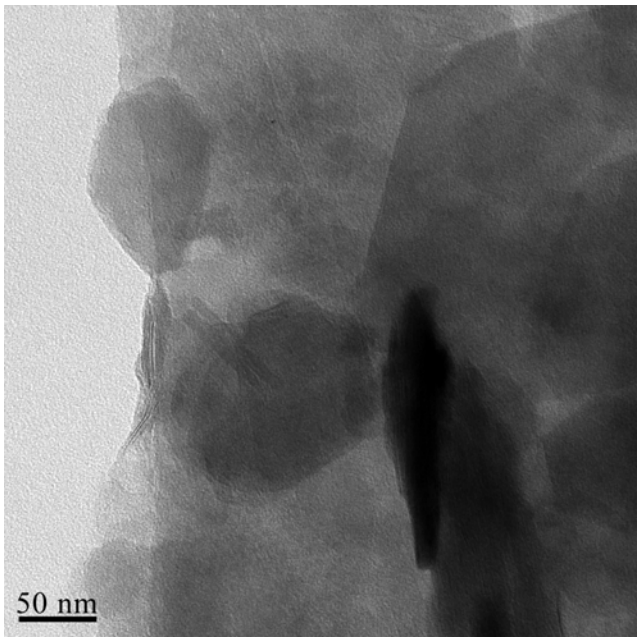

Figure 9B. TEM image of KI doped magnesia.

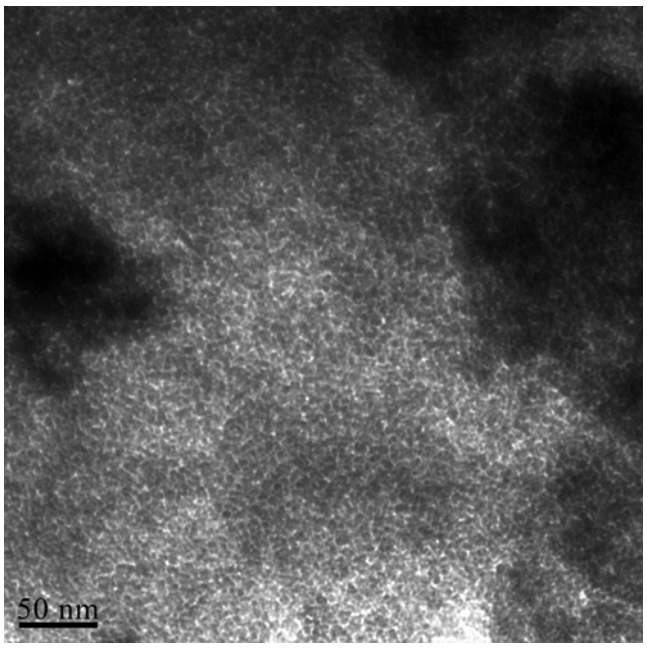

Figure 10B. TEM image of the Al-Mg mixed oxide at Al:Mg of 8:1.

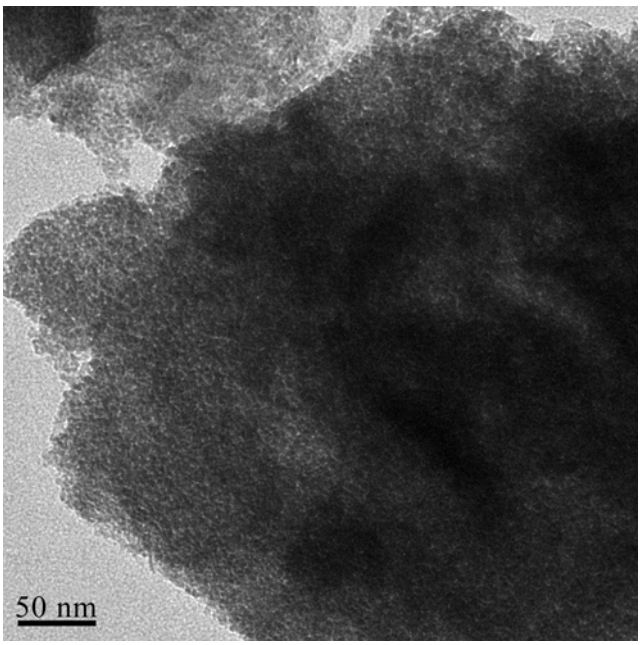

Figure 11B. TEM image of the Al-Mg mixed oxide at Al:Mg of 4:1.

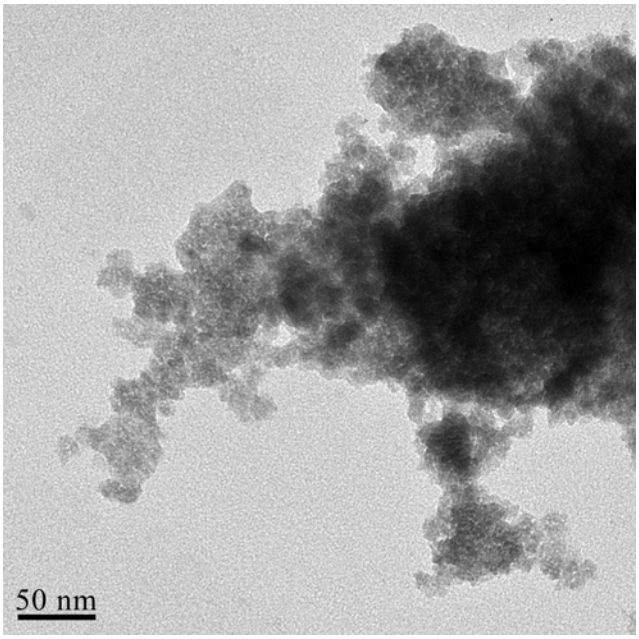

Figure 12B. TEM image of the Al-Mg mixed oxide at Al:Mg of 2:1.

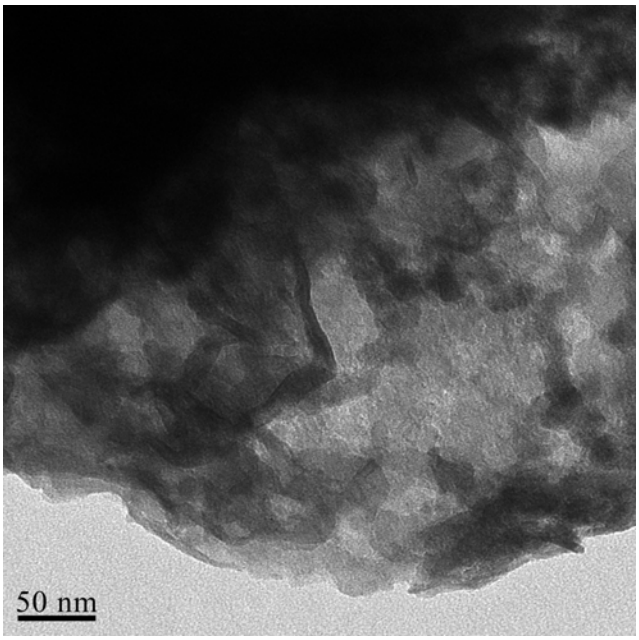

Figure 13B. TEM image of the Al-Mg mixed oxide at Al:Mg of 1:3.

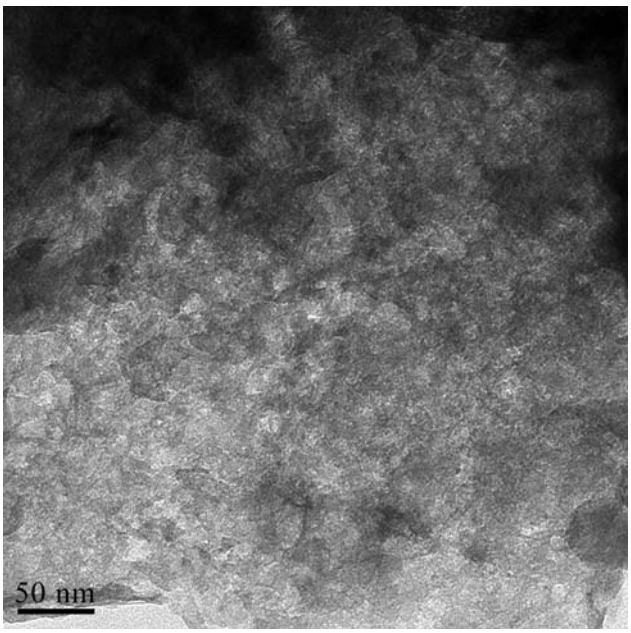

Figure 14B. TEM image of the Al-Mg mixed oxide at Al:Mg of 1:4.

APPENDIX C

BJH PORE SIZE DISTRIBUTION AND N_2 ADSOPRTION-DESORPTION ISOTHERM

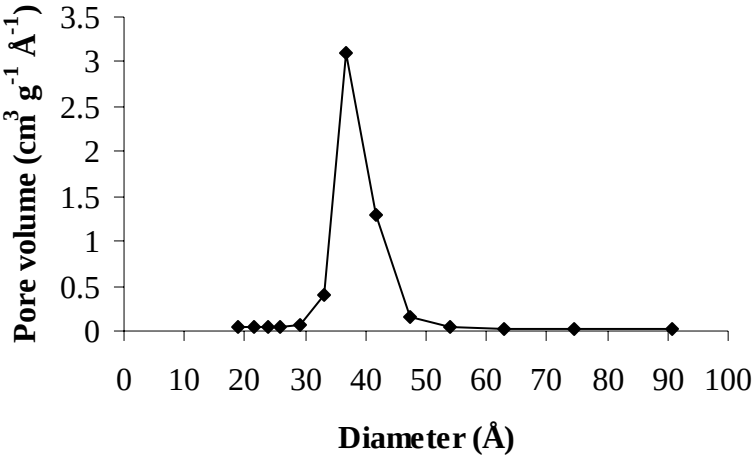

Figure 1C. BJH pore size distribution of alumina.

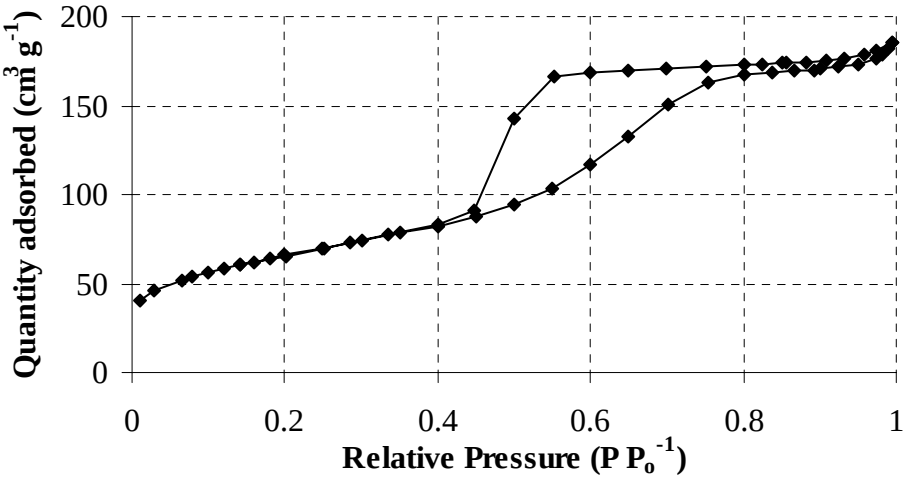

Figure 2C. N_2 adsorption-desorption isotherm of alumina.

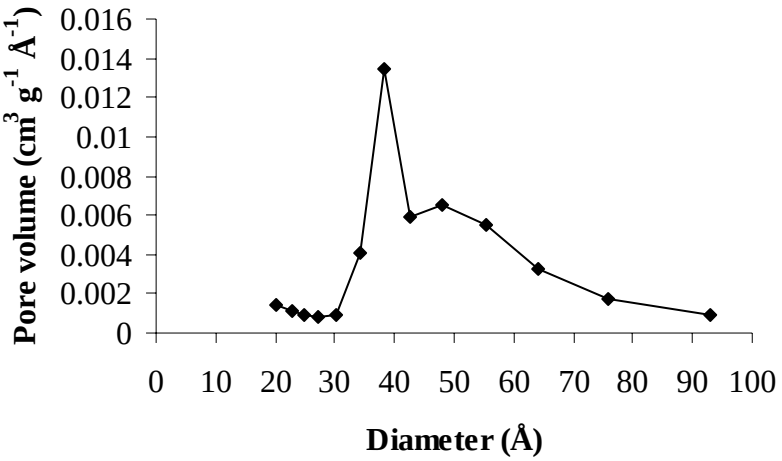

Figure 3C. BJH pore size distribution of Al-Mg mixed oxide at Al:Mg of 8:1.

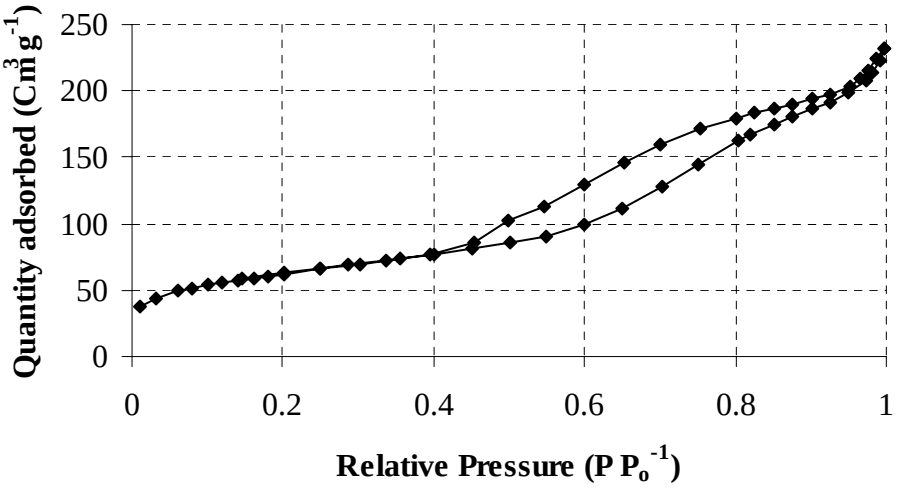

Figure 4C. N_2 adsorption-desorption isotherm of Al-Mg mixed oxide at Al:Mg of 8:1.

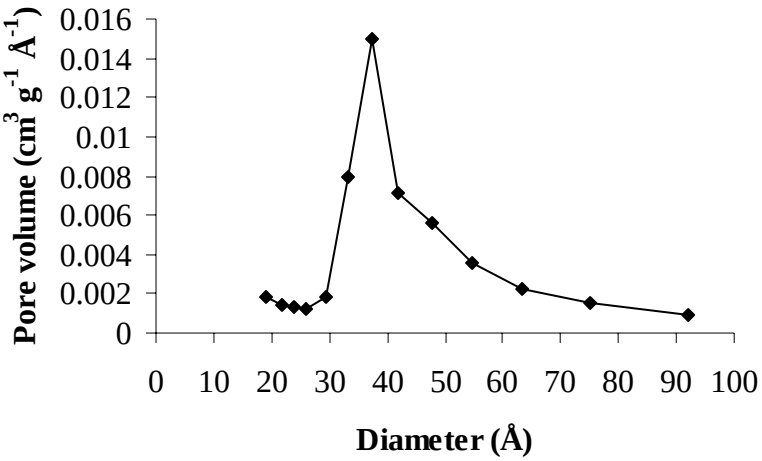

Figure 5C. BJH pore size distribution of Al-Mg mixed oxide at Al:Mg of 4:1.

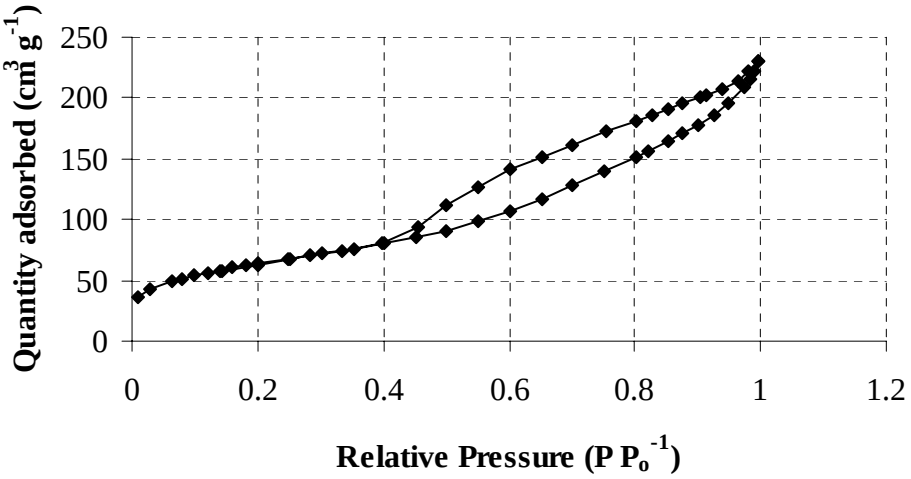

Figure 6C. N_2 adsorption-desorption isotherm of Al-Mg mixed oxide at Al:Mg of 4:1.

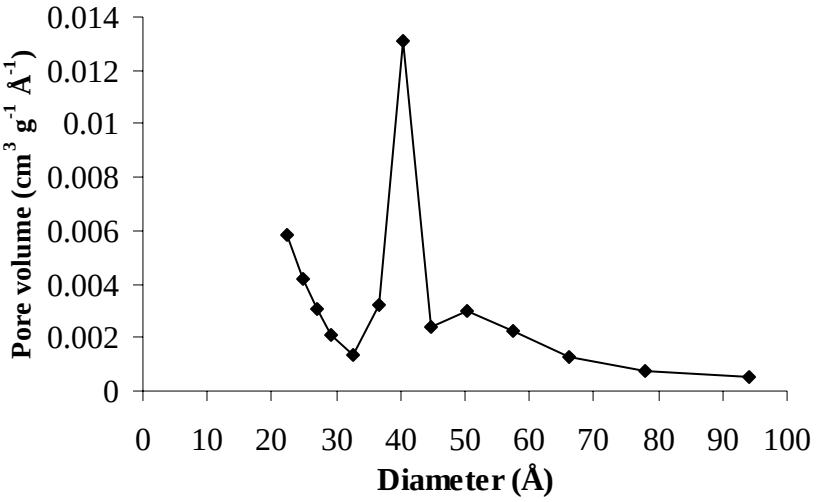

Figure 7C. BJH pore size distribution of Al-Mg mixed oxide at Al:Mg of 2:1.

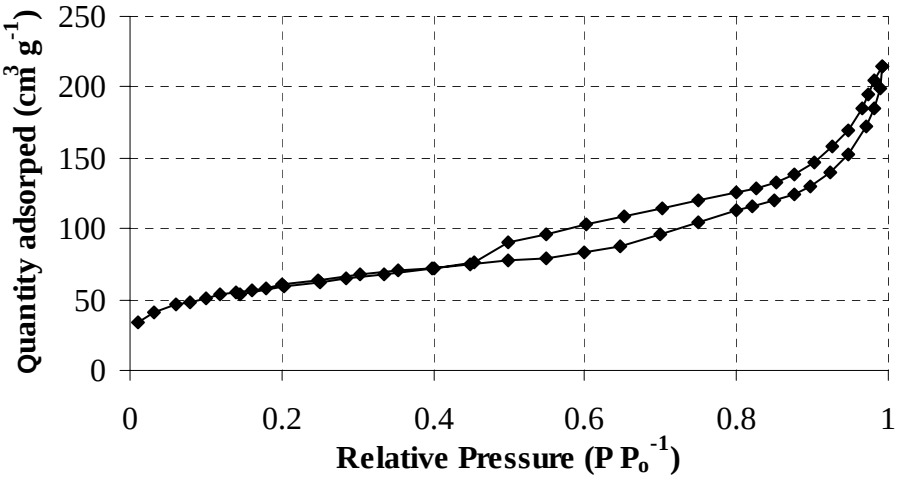

Figure 8C. N_2 adsorption-desorption isotherm of Al-Mg mixed oxide at Al:Mg of 2:1.

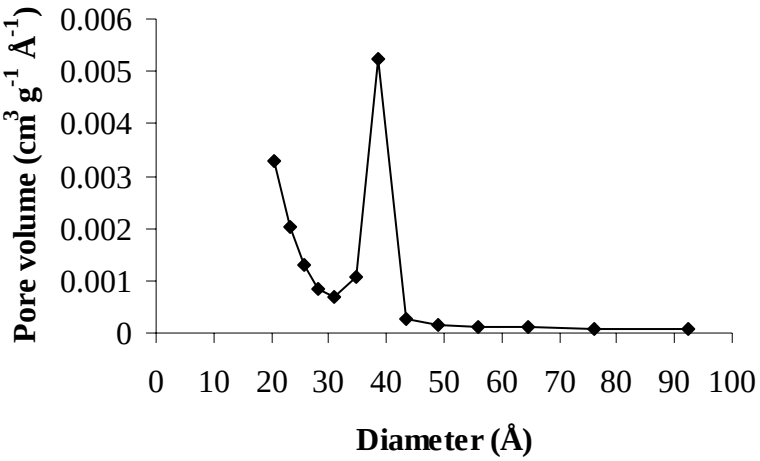

Figure 9C. BJH pore size distribution of Al-Mg mixed oxide at Al:Mg of 1:1.

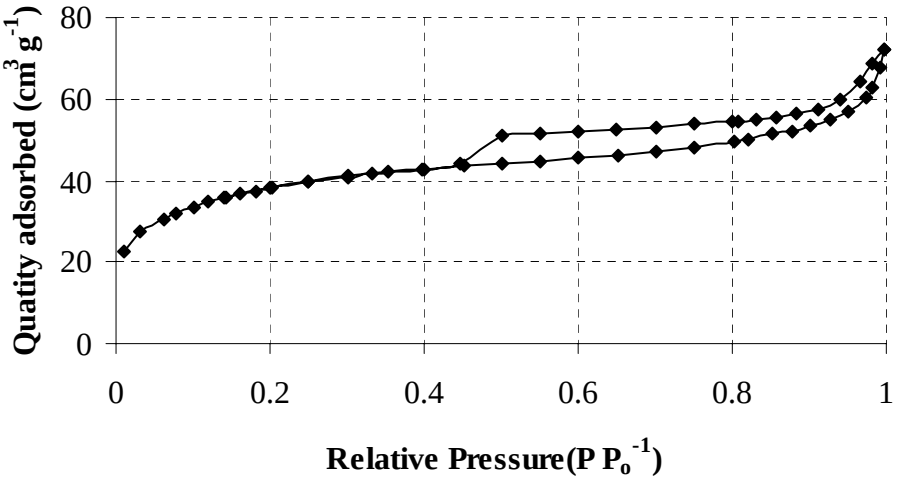

Figure 10C. N_2 adsorption-desorption isotherm of Al-Mg mixed oxide at Al:Mg of 1:1.

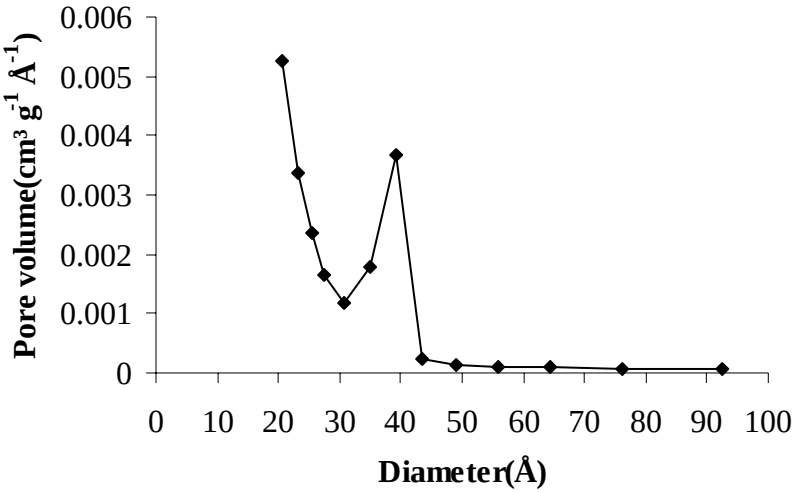

Figure 11C. BJH pore size distribution of Al-Mg mixed oxide at Al:Mg of 1:2.

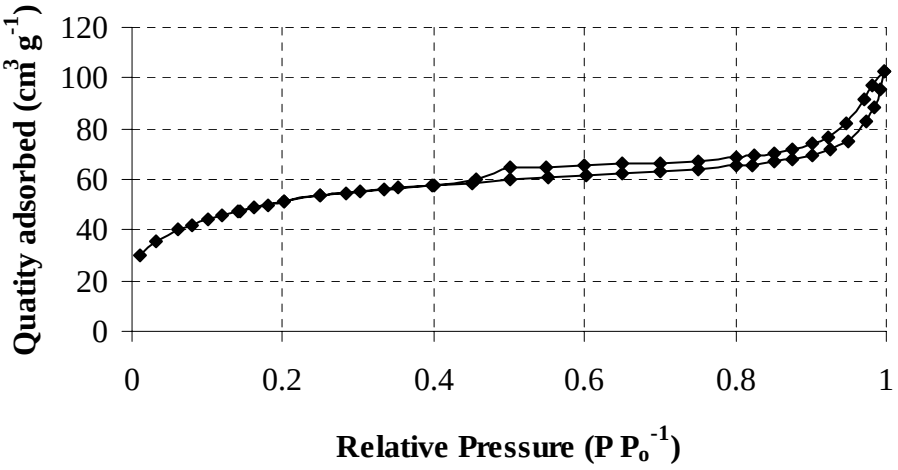

Figure 12C. N_2 adsorption-desorption isotherm of Al-Mg mixed oxide at Al:Mg of 1:2.

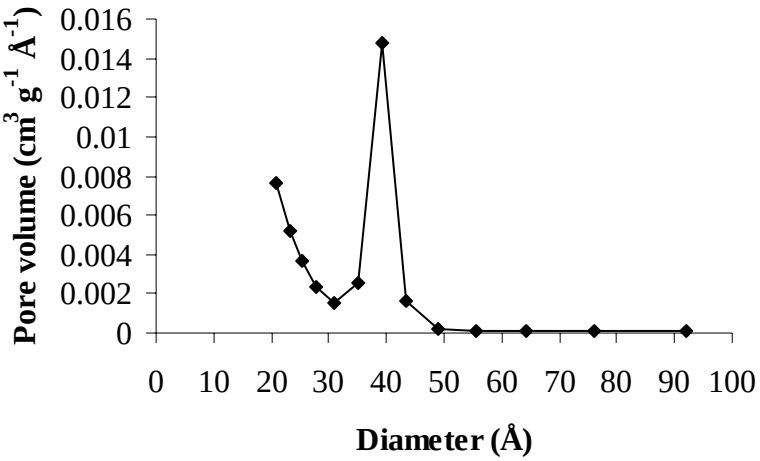

Figure 13C. BJH pore size distribution of Al-Mg mixed oxide at Al:Mg of 1:3.

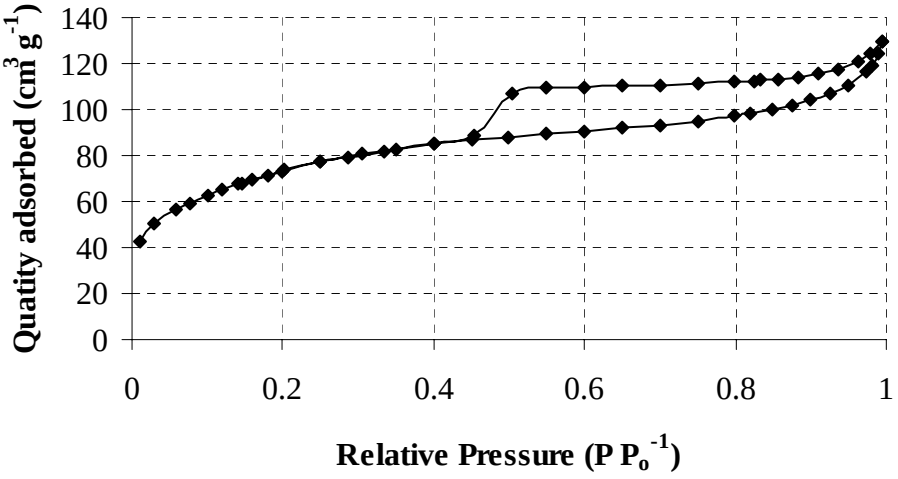

Figure 14C. N_2 adsorption-desorption isotherm of Al-Mg mixed oxide at Al:Mg of 1:3.

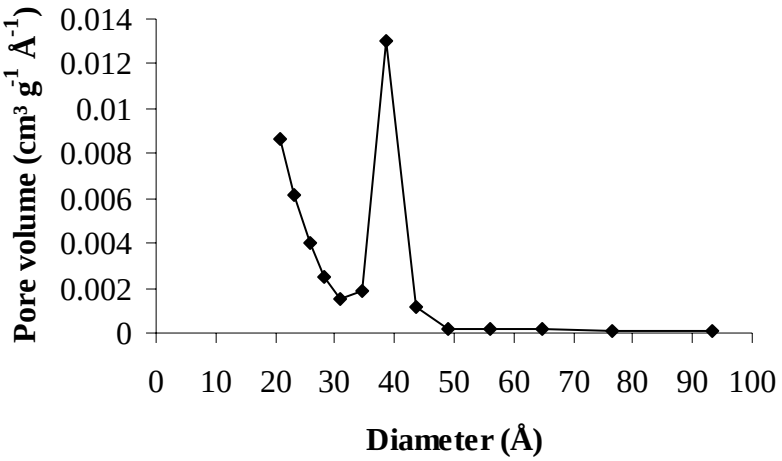

Figure 15C. BJH pore size distribution of Al-Mg mixed oxide at Al:Mg of 1:4.

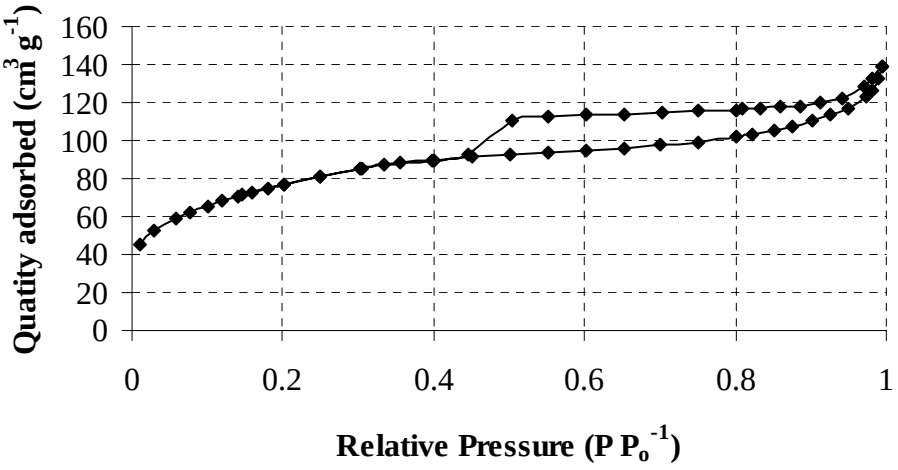

Figure 16C. BJH pore size distribution of Al-Mg mixed oxide at Al:Mg of 1:4.

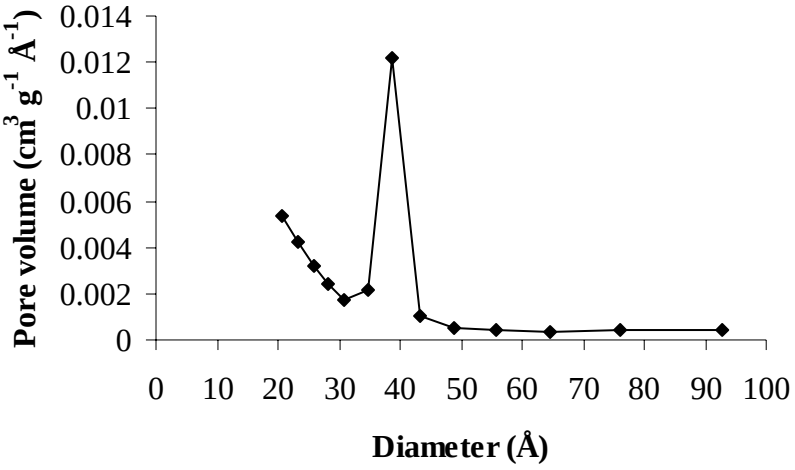

Figure 17C. BJH pore size distribution of Al-Mg mixed oxide at Al:Mg of 1:8.

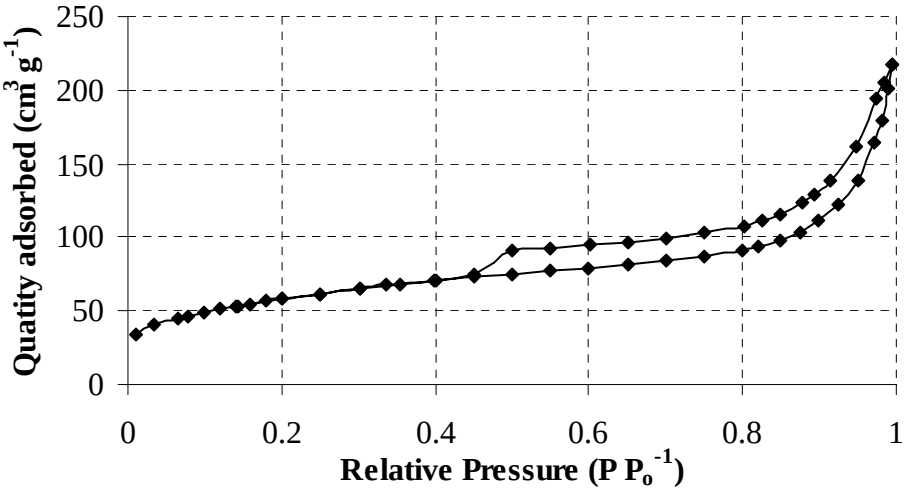

Figure 18C. BJH pore size distribution of Al-Mg mixed oxide at Al:Mg of 1:8.

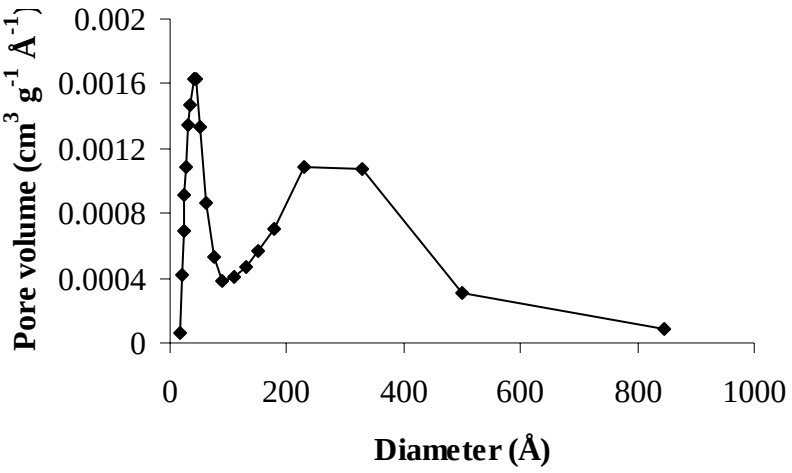

Figure 19C. BJH pore size distribution of magnesia.

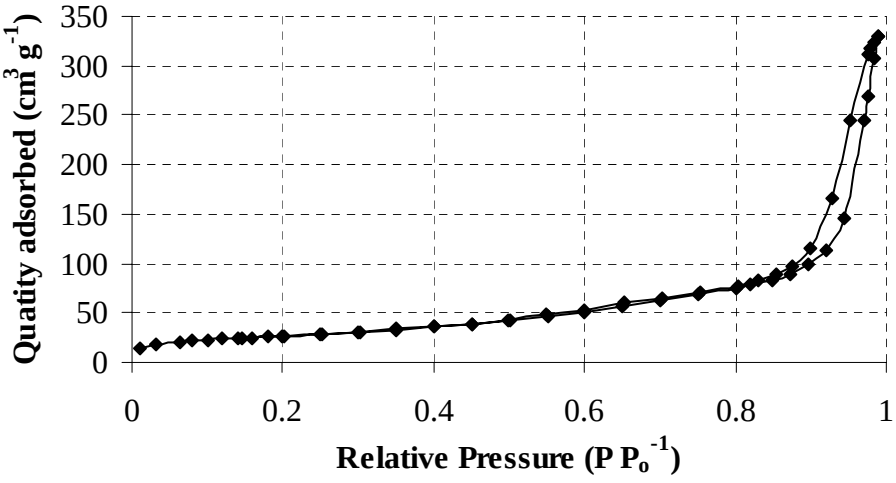

Figure 20C. BJH pore size distribution of magnesia.

APPENDIX D

MOLE OF Al AND Mg ATOMS IN THE Al-Mg MIXED OXIDES AND MOLE OF K ATOM IN THE K DOPED Al-Mg MIXED OXIDES

Table 1D mole of Al and Mg atoms in the Al-Mg mixed oxides 1g.

Al-Mg mixed oxide	Mole of Al atom (mmol)	Mole of Mg atom (mmol)
Al-Mg mixed oxide at Al:Mg ratio of 8:1	8.0	0.7
Al-Mg mixed oxide at Al:Mg ratio of 4:1	6.2	1.3
Al-Mg mixed oxide at Al:Mg ratio of 2:1	5.8	2.7
Al-Mg mixed oxide at Al:Mg ratio of 1:1	2.9	2.9
Al-Mg mixed oxide at Al:Mg ratio of 1:2	1.7	3.6
Al-Mg mixed oxide at Al:Mg ratio of 1:3	1.2	4.3
Al-Mg mixed oxide at Al:Mg ratio of 1:4	1.1	4.4
Al-Mg mixed oxide at Al:Mg ratio of 1:8	0.6	5.1

Table 2D mmole of K atom in the Al-Mg mixed oxides 1 g.

K doped Al-Mg mixed oxide	**Mole of K atom (mmol)**
KI doped Al-Mg mixed oxide at Al:Mg ratio of 8:1	1.9
KI doped Al-Mg mixed oxide at Al:Mg ratio of 4:1	1.8
KI doped Al-Mg mixed oxide at Al:Mg ratio of 2:1	1.8
KI doped Al-Mg mixed oxide at Al:Mg ratio of 1:1	1.6
KI doped Al-Mg mixed oxide at Al:Mg ratio of 1:2	2.0
KI doped Al-Mg mixed oxide at Al:Mg ratio of 1:3	2.0
KI doped Al-Mg mixed oxide at Al:Mg ratio of 1:4	1.5
KNO_3 doped Al-Mg mixed oxide at Al:Mg ratio of 1:4	1.6
KI doped Al-Mg mixed oxide at Al:Mg ratio of 1:8	1.8

APPENDIX E

PERCENTAGE YIELD OF FATTY ACID METHYL ESTER (FAME)

Table 1E Percentage yield of FAME from transesterification of soybean oil without catalyst.

Time (h)	% yield of FAME (%)
0	0
0	0
0	0
0	0
0	0
0	0
0	0
0	0
0	0

Table 2E Percentage yield of FAME from transesterification of soybean oil using Al-Mg mixed oxide at Al:Mg ratio of 1:4 as catalyst.

Time (h)	% yield of FAME (%)
0	0
1	0
2	0
4	0
8	0
24	0.53
32	0.94
48	1.67
56	2.09

Table 3E Percentage yield of FAME from transesterification of soybean oil using KI doped alumina as catalyst.

Time (h)	% yield of FAME (%)
0	0
1	1.91
2	5.97
4	16.71
8	36.20
24	79.32
32	86.65
48	91.61
56	92.57

Table 4E Percentage yield of FAME from transesterification of soybean oil using KI doped Al-Mg mixed oxide at Al:Mg ratio of 8:1 as catalyst.

Time (h)	% yield of FAME (%)
	0
1	0.95
2	2.68
4	6.71
8	19.91
24	59.45
32	67.31
48	75.16
56	76.50

Table 5E Percentage yield of FAME from transesterification of soybean oil using KI oped Al-Mg mixed oxide at Al:Mg ratio of 4:1 as catalyst.

Time (h)	% yield of FAME (%)
0	0
1	1.03
2	2.51
4	7.86
8	22.57
24	70.39
32	80.21
48	86.00
56	87.23

Table 6E Percentage yield of FAME from transesterification of soybean oil using KI doped Al-Mg mixed oxide at Al:Mg ratio of 8:1 as catalyst.

Time (h)	% yield of FAME (%)
0	0
1	0.95
2	2.68
4	6.71
8	19.91
24	59.45
32	67.31
48	75.16
56	76.50

Table 7E Percentage yield of FAME from transesterification of soybean oil using KI doped Al-Mg mixed oxide at Al:Mg ratio of 4:1 as catalyst.

Time (h)	% yield of FAME (%)
0	0
1	1.03
2	2.51
4	7.86
8	22.57
24	70.39
32	80.21
48	86.00
56	87.23

Table 8E Percentage yield of FAME from transesterification of soybean oil using KI doped Al-Mg mixed oxide at Al:Mg ratio of 2:1 as catalyst.

Time (h)	% yield of FAME (%)
0	0
1	2.29
2	5.14
4	10.69
8	26.57
24	63.92
32	74.22
48	81.29
56	80.49

Table 9E Percentage yield of FAME from transesterification of soybean oil using KI doped Al-Mg mixed oxide at Al:Mg ratio of 1:1 as catalyst.

Time (h)	% yield of FAME (%)
0	0
1	8.15
2	15.32
4	24.42
8	40.13
24	63.74
32	72.05
48	81.01
56	80.93

Table 10E Percentage yield of FAME from transesterification of soybean oil using KI doped Al-Mg mixed oxide at Al:Mg ratio of 1:2 as catalyst.

Time (h)	% yield of FAME (%)
0	0
1	35.89
2	47.23
4	54.93
8	62.23
24	74.52
32	76.73
48	79.87
56	81.38

Table 11E Percentage yield of FAME from transesterification of soybean oil using KI doped Al-Mg mixed oxide at Al:Mg ratio of 1:3 as catalyst.

Time (h)	% yield of FAME (%)
0	0
1	10.39
2	25.57
4	48.13
8	76.05
24	88.53
32	89.71
48	89.89
56	90.46

Table 12E Percentage yield of FAME from transesterification of soybean oil using KI doped Al-Mg mixed oxide at Al:Mg ratio of 1:4 as catalyst.

Time (h)	% yield of FAME (%)
0	0.19
1	44.76
2	68.91
4	84.69
8	89.89
24	95.53
32	94.16
48	95.43
56	94.86

Table 13E Percentage yield of FAME from transesterification of soybean oil using KI doped Al-Mg mixed oxide at Al:Mg ratio of 1:8 as catalyst.

Time (h)	% yield of FAME (%)
0	0
1	43.02
2	64.5
4	71.34
8	76.07
24	85.43
32	87.12
48	88.34
56	89.29

Table 14E Percentage yield of FAME from transesterification of soybean oil using KI doped magnesia.

Time (h)	% yield of FAME (%)
0	0
1	0.24
2	0.48
4	1.05
8	5.27
24	17.75
32	25.24
48	29.05
56	31.27

Table 15E Percentage yield of FAME from transesterification of soybean oil using KNO_3 doped Al-Mg mixed oxide at Al:Mg ratio of 1:4 as catalyst.

Time (h)	% yield of FAME (%)
0	0
1	2.69
2	10.98
4	29.53
8	46.71
24	73.00
32	82.84
48	91.37
56	92.31

Table 16E Percentage yield of FAME from transesterification of soybean oil using the first reused calcined KI doped Al-Mg mixed oxide at Al:Mg of 1:4 as catalyst.

Time (h)	% yield of FAME (%)
0	0
1	0.24
2	0.48
4	1.05
8	5.27
24	17.75
32	25.24
48	29.05
56	31.27

Table 17E Percentage yield of FAME from transesterification of soybean oil using the second reused calcined KI doped Al-Mg mixed oxide at Al:Mg ratio of 1:4 as catalyst.

Time (h)	**% yield of FAME (%)**
0	0
1	0.15
2	0.32
4	1.07
8	3.97
24	3.49
32	5.63
48	5.99
56	9.87

Table 18E Percentage yield of FAME from transesterification of soybean oil using the first reused uncalcined KI doped Al-Mg mixed oxide at Al:Mg ratio of 1:4 as catalyst.

Time (h)	**% yield of FAME (%)**
0	0
1	0
2	0
4	0
8	1.07
24	10.29
32	14.65
48	21.73
56	21.98

Table 19E Leaching test of the calcined KI doped Al-Mg mixed oxide catalyst at Al:Mg ratio of 1:4.

Time (h)	% yield of FAME (%)
0	0
1	37.56
2	55.88
3	56.82
4	57.55
5	57.03
6	57.41
7	57.71
8	57.73
24	58.59
25	57.32
26	59.65
27	57.11
28	56.66
29	57.37
30	58.05
48	54.59
56	53.62

BIOGRAPHY

NAME	Mr. Pannapat Chotmongkolsap
DATE OF BRITH	June 29, 1983
PLACE OF BIRTH	Bangkok, Thailand
INSTITUTIONS ATTENDED	Prince of Songkla University, 2001-2005 Bachelor of Science (Chemistry) Mahidol University, 2005-2008 Master of Science (Applied Analytical and Inorganic Chemistry)
RESEARCH GRANTS	The Center of Innovation in Chemistry: Postgraduate Education and Research Program in Chemistry (PERCH-CIC), 2005-2007 Teaching Assistant Scholarship Mahidol University, 2006
HOME ADDRESS	2, Raduthid Soi 24, Raduthid Rd., Hatyai, Songkhla 90110.